

FUEL ASSEMBLY SHAKER TEST SIMULATION

Fuel Cycle Research & Development

*Prepared for
U.S. Department of Energy
Used Fuel Disposition Campaign*

*Nicholas Klymyshyn
Scott Sanborn
Harold Adkins
Brady Hanson*

Pacific Northwest National Laboratory

*May 30, 2013
PNNL-22507*

FCRD-UFD-2013-000168



DISCLAIMER

This information was prepared as an account of work sponsored by an agency of the U.S. Government. Neither the U.S. Government nor any agency thereof, nor any of their employees, makes any warranty, expressed or implied, or assumes any legal liability or responsibility for the accuracy, completeness, or usefulness, of any information, apparatus, product, or process disclosed, or represents that its use would not infringe privately owned rights. References herein to any specific commercial product, process, or service by trade name, trade mark, manufacturer, or otherwise, does not necessarily constitute or imply its endorsement, recommendation, or favoring by the U.S. Government or any agency thereof. The views and opinions of authors expressed herein do not necessarily state or reflect those of the U.S. Government or any agency thereof.

Reviewed by:

PNNL Project Manager

Brady Hanson

SUMMARY

This report describes the modeling of a fuel assembly under dynamic shock loading in support of the Sandia National Laboratories (SNL) shaker test campaign. The focus of the test campaign is on evaluating the response of used fuel to shock and vibration loads that can occur during highway transport. Modeling began in 2012 using an LS-DYNA fuel assembly model that was first created for modeling impact scenarios. SNL's proposed test scenario was simulated through analysis and the calculated results helped guide the instrumentation and other aspects of the testing.

During fiscal year (FY) 2013, the fuel assembly model was refined to better represent the test surrogate. Analysis of the proposed loads suggested the frequency band needed to be lowered to attempt to excite the lower natural frequencies of the fuel assembly. Despite SNL's expansion of lower frequency components in their five shock realizations, pretest predictions suggested a very mild dynamic response to the test loading.

After testing was completed, one specific shock case was modeled, using recorded accelerometer data to excite the model. Direct comparison of predicted strain in the cladding was made to the recorded strain gauge data. The magnitude of both sets of strain (calculated and recorded) is very low, compared to the expected yield strength of the Zircaloy-4 material. The model was accurate enough to predict that no yielding of the cladding was expected, but its precision at predicting micro strains is questionable.

The SNL test data offer some opportunity for validation of the finite element model, but the specific loading conditions of the testing only excite the fuel assembly to respond in a limited manner. For example, the test accelerations were not strong enough to substantially drive the fuel assembly out of contact with the basket. Under this test scenario, the fuel assembly model does a reasonable job of approximating actual fuel assembly response, a claim that can be verified through direct comparison of model results to recorded test results. This does not offer validation for the fuel assembly model in all cases, such as high kinetic energy shock cases where the fuel assembly might lift off the basket floor to strike to basket ceiling. This type of nonlinear behavior was not witnessed in testing, so the model does not have test data to be validated against.

Looking forward to future applications of this detailed fuel assembly model, additional test data would be desirable to extend the validation range of the model. The SNL testing captured data for a certain range of fuel assembly dynamic response. Stronger excitations that cause significantly more rigid body motion of the assembly within its package structure may be of interest in the future. One current topic of interest to UFDC is the response of used fuel assemblies to rail car normal conditions of transport shock and vibration, which currently appear to have more potential for rigid body motion than the highway transport case. A further knowledge gap is the exact response of specific used fuel conveyance designs to highway excitation. This is more of a vehicle design and evaluation issue, but it is anticipated that the specific suspension system design of a conveyance could affect the fuel response in a manner that is beyond the scope of the SNL shaker test campaign.

Contents

SUMMARY	iv
ACRONYMS	ix
1.0 INTRODUCTION	1
2.0 FINITE ELEMENT MODEL DESCRIPTIONS	3
2.1 Baseline, Rev 0 (Sept. 2012 Progress Report)	3
2.2 Fuel Assembly Model Rev 1 (Pre-Test Model)	6
2.3 Fuel Assembly Model Rev 2 (Final Model of Study)	8
3.0 FUEL ASSEMBLY MODEL CHARACTERISTIC ANALYSIS	11
3.1 Modal Analysis Summary	11
3.2 Static Lateral Deflection Summary	12
4.0 SHOCK LOAD ANALYSIS	15
4.1 Shock Load Prediction Case (Rev 1 Model)	15
4.2 Half Sine Pulse	21
4.3 Post-Test Evaluation (Rev 2 Model)	25
4.4 Half Sine Pulse Evaluation (Rev 2 Model)	29
5.0 PRE-TEST PREDICTIONS	33
6.0 POST-TEST EVALUATION	35
6.1 Model Validation and Limitations	36
7.0 CONCLUSIONS	37
8.0 REFERENCES	39
Appendix A: Shaker Table Modeling Progress Report	40
Appendix B: Modal and Static Analysis of the Detailed Fuel Assembly Model	57

FIGURES

2.1	Grid Spacer (Shell Elements) and Cladding Sections (Beam Elements).....	5
2.2	Rev 0 Translational Spring Arrangement	5
2.3	Original Fuel Assembly and Test Fixture Model.....	6
2.4	Rev 1 Test Fixture Model	7
2.5	Rev 1 Test Fixture and Fuel Assembly Model with Basket Removed	7
2.6	Final Shaker Test Model.....	9
2.7	Final Shaker Test Model Felt Liner	9
2.8	Final Fuel Bundle with Three Zirc Rods	9
3.1	Static Lateral Deflection Model.....	12
4.1	Acceleration History of Shock Realization #1.....	16
4.2	Displacement History (in meters)	17
4.3	Motion of Fuel Assembly Relative to Shaker (+ is vertical separation).....	18
4.4	Velocity History.....	18
4.5	Fuel Assembly CG Acceleration	19
4.6	Shaker Acceleration.....	19
4.7	Acceleration Spectra (0-100 Hz)	20
4.8	Acceleration Spectra (100-700 Hz)	21
4.9	SDOF System Response (3% damping)	22
4.10	Half Sine Pulse Vertical Displacement. (A) is the End of the Pulse, (B) is the Beginning of Fuel Assembly Impact with the Top of the Basket.....	23
4.11	Half Sine Pulse Vertical Velocity. (A) is the End of the Pulse, (B) is the Beginning of Fuel Assembly Impact with the Top of the Basket.....	24
4.12	Half Sine Pulse Acceleration History	24
4.13	Shock Realization #2 Acceleration Response.....	26
4.14	Shock Realization #2 Acceleration Response (Frequency Domain)	26
4.15	Shock Realization #2, 0-100 Hz Response	26
4.16	Shock Realization #2, 0-20 Hz Response	27
4.17	Shock Realization #2 Relative Displacements (Fuel - Shaker)	27
4.18	Shock Realization #2 Vertical Displacement Contours (m)	28
4.19	Shock Realization #2 Maximum Strain Results at Three Cladding Locations.....	29
4.20	Rev 2 Half Sine Pulse Acceleration.....	30
A.1.	Grid Spacer (Shell Elements) and Cladding Sections (Beam Elements).....	42
A.2.	Shock Response Spectra	44

A.3. Shock6, Acceleration Time History	45
A.4. Shock7, Acceleration Time History	46
A.5. Shock9, Acceleration Time History	47
A.6. Shock6, Plastic Strain in Grids.....	48
A.7. Shock6, Cutaway View of Fuel Assembly in Basket.....	49
A.8. Shock6, Plastic Strain in Cladding.....	50
A.9. Shock6, Plastic Strain in Guide Tubes.....	50
A.10. Shock7, Plastic Strain in Cladding Locations	51
A.11. Shock9, Plastic Strain in Grid.....	52
A.12. Shock9, Cladding Plastic Strain.....	52
B.1. Scaled Vertical Participation Factor for Cases 3 and 4, Rev 1.....	61
B.2. Vertical Cumulative Mass Fraction for Case 3 and Case 4, Rev 1	62
B.3. The Six Modes Shapes with the Largest Vertical Participation Factor for Case 3, Rev 1	63
B.4. The Six Modes Shapes with the Largest Vertical Participation Factor for Case 4, Rev 1	63
B.5. Scaled Vertical Participation Factor for Cases 1 and 2, Rev 1.....	64
B.6. Vertical Cumulative Mass Fraction for Cases 1 and 2, Rev 1.....	65
B.7. The Six Modes Shapes with the Largest Vertical Participation Factor for Case 1, Rev 1	66
B.8. The Six Mode Shapes with the Largest Vertical Participation Factor for Case 2, Rev 1.....	66
B.9. Scaled Vertical Participation Factor for Cases 1, 3, 5, and 7, Rev 1.....	67
B.10. Vertical Cumulative Mass Fraction for Cases 1, 3, 5, and 7, Rev 1.....	68
B.11. The Six Mode Shapes with the Largest Vertical Participation Factor for Case 5, Rev 1.....	68
B.12. The Six Mode Shapes with the Largest Vertical Participation Factor for Case 7, Rev 1.....	69
B.13. The Six Mode Shapes with the Largest Vertical Participation Factor for Case 9, Rev 1.....	69
B.14. Scaled Vertical Participation Factor for Cases 1 and 11, Rev 1.....	70
B.15. Vertical Cumulative Mass Fraction for Cases 1 and 11, Rev 1.....	71
B.16. The Six Mode Shapes with the largest Vertical Participation Factor for Case 11, Rev 1	71
B.17. Scaled Vertical Participation Factor for Cases 5, 6, 13, and 14, Rev 1.....	72
B.18. Vertical Cumulative Mass Fraction for Cases 5, 6, 13, and 14, Rev 1.....	73
B.19. The Six Mode Shapes with the Largest Vertical Participation Factor for Case 13, Rev 1.....	73
B.20. The Six Mode Shapes with the Largest Vertical Participation Factor for Case 6, Rev 1.....	74
B.21. The Six Mode Shapes with the Largest Vertical Participation Factor for Case 14, Rev 1.....	74
B.22. Scaled Vertical Participation Factor for Cases 1 and 15, Rev 1.....	75
B.23. Vertical Cumulative Mass Fraction for Cases 1 and 15, Rev 1.....	76

B.24. The Six Mode Shapes with the Largest Vertical Participation Factor for Case 15, Rev 1.....	76
B.25. Scaled Vertical Participation Factor for Cases 5, 17, 18, and 19, Rev 1.....	77
B.26. Vertical Cumulative Mass Fraction for Cases 5, 17, 18, and 19, Rev 1.....	78
B.27. The Six Mode Shapes with the Largest Vertical Participation Factor for Case 17, Rev 1.....	78
B.28. The Six Mode Shapes with the Largest Vertical Participation Factor for Case 18, Rev 1.....	79
B.29. The Six Mode Shapes with the Largest Vertical Participation Factor for Case 19, Rev 1.....	79
B.30. Scaled Vertical Participation Factor for Cases 5, 18, and 20, Rev 1.....	80
B.31. Vertical Cumulative Mass Fraction for Cases 5, 18, and 20, Rev 1.....	81
B.32. The Six Mode Shapes with the Largest Vertical Participation Factor for Case 20, Rev 1.....	81
B.33. Scaled Vertical Participation Factor for Cases 21, 22, 23, and 24, Rev 2.....	83
B.34. Vertical Cumulative Mass Fraction for Cases 21, 22, 23, and 24, Rev 2.....	83
B.35. The Six Mode Shapes with the Largest Vertical Participation Factor for Case 21, Rev 2.....	84
B.36. The Six Mode Shapes with the Largest Vertical Participation Factor for Case 22, Rev 2.....	85
B.37. The Six Mode Shapes with the Largest Vertical Participation Factor for Case 23, Rev 2.....	85
B.38. Some of the Mode Shapes with the Largest Vertical Participation Factor for Case 24, Rev 2.....	86
B.39. Static Assembly Test Boundary Conditions.....	87
B.40. Displacement Along the Length of the Assembly for the Static Load Tests of all Copper with Density Adjusted, all Copper with Overlapping Beams, and all Zircaloy-4 with the Density Adjusted.....	88
B.41. Displacement Along the Length of the Assembly for the Static Load Test Varying the Rotational Spring Stiffness for a Zircaloy-4 Assembly.....	89
B.42. Displacement along the Length of the Assembly for the Static Load Test Varying the Rotational Spring Stiffness and Axial Spring Stiffness for a Zircaloy-4 Assembly.....	90
Figure B.43. Displacement along the Length of the Assembly for the Static Load Tests with the Rev 2 Modifications	91

TABLES

B.1. Modal Analysis Sensitivity Study Cases for Rev 1 Model	58
B.2. Modal Analysis Sensitivity Study Cases for Rev 2 Model	59
B.3. Nominal Material Properties	60

ACRONYMS

3D	three dimensional
CG	center of gravity
FEA	finite element analysis
Grms	root-mean-square value in units of multiples of gravity
ms	milliseconds
NRC	U.S. Nuclear Regulatory Commission
PNNL	Pacific Northwest National Laboratory
PWR	pressurized water reactor
SDOF	single degree of freedom
SNL	Sandia National Laboratories
UFDC	Used Fuel Disposition Campaign

FUEL ASSEMBLY SHAKER TEST SIMULATION

1.0 INTRODUCTION

The purpose of this modeling effort was to assist Sandia National Laboratories (SNL) with preliminary and post-test analysis of their shaker table testing of a pressurized water reactor (PWR) fuel assembly subjected to highway shock and vibration loading, performed under the Used Fuel Disposition Campaign (UFDC). The shaker testing was performed on April 30, 2013 on an extensively instrumented fuel assembly surrogate. Modeling of the test scenario began in 2012, and helped inform the testing as to desirable locations for strain gauges, accelerometers, and the best rod locations to place the limited number of Zircaloy-4 tubes (the majority of the surrogate fuel assembly tubes were made of copper because of the limited Zircaloy-4 availability). An existing, highly detailed finite-element model developed by Pacific Northwest National Laboratory (PNNL) for the U.S. Nuclear Regulatory Commission (NRC) formed the initial basis of the modeling effort. LS-DYNA, a commercially available finite element analysis (FEA) code, was used to model the assembly response to dynamic loading. The fuel assembly model was revised a number of times during this study to better resemble the test configuration and better match the anticipated response characteristics of a real fuel assembly. The final models represent a best estimate of one of the five shock tests, with a full set of transducer data for comparison.

This test represents a rare opportunity to validate a detailed fuel assembly model. Dynamic testing performed by vendors is often not available for this purpose. The SNL shock testing provoked a certain level of dynamic response from the fuel assembly and collected response data that can be compared against the finite element model calculated results. This provides the opportunity for direct comparison to determine the accuracy and precision of the finite element model. The applied loads proved to be relatively mild, which puts a practical limit on the range of the fuel assembly dynamic response that can be validated. For example, future use of the model in more energetic dynamic scenarios, like hypothetical accident scenarios, rail transportation loading, may prove to be outside the response range tested by SNL. This report will discuss the loads and the fuel assembly dynamic response to define the practical limits of the validation the shaker test series offers.

The finite element model of the fuel assembly is described in Section 2. An evaluation of the model characteristics is summarized in Section 3. Model results are discussed in Section 4. Pretest predictions, made prior to the SNL test campaign, are documented in Section 5. Post-test evaluation of the model is discussed in Section 6. Conclusions are listed in Section 7, with references following in Section 8. Appendix A includes a progress report written in September of 2012 and describes the Rev 0 model and results. Appendix B contains a significant amount of results data and discussion on the fuel assembly model characterization analysis, which was briefly summarized in Section 3.

2.0 FINITE ELEMENT MODEL DESCRIPTIONS

The detailed fuel assembly model used in this study was first created in the commercial explicit finite element analysis program LS-DYNA to analyze the potential damage to fuel assemblies during transportation package drop events. These nonlinear transient dynamic models were used to calculate impact response durations on the order of 100 milliseconds (ms). While this may seem like a relatively short amount of time to model, the explicit finite element method requires a certain minimum solution time step size for numerical stability, which depends on the model composition. Refining a given model to have more, smaller elements tends to decrease the minimum time step size and require additional computation time. This makes a delicate balance between total computation time and mesh composition. Refining just one region of a model can quickly lead to a doubling of computation time, so careful compromise is often needed to arrive at a viable model. One goal of this modeling study was to determine how adequate the existing model was for evaluating shock and vibration loads. A second goal was to determine what modifications to the existing model were needed to make the model more representative of the physical response, without becoming computationally intractable. These two modeling goals support the main goal of supporting the SNL shaker test campaign with predictive modeling and simulation.

The fuel assembly model underwent a number of alterations and input parameter variations at various stages in this study. The basic structure remained unchanged: beam elements representing the cladding and guide tubes, de-featured shell-element representations of the spacer grids, classic spring elements used at fuel/grid interaction points, and general contact that ensured all elements (beams, shells, and solids) accounted for physical contact with each other when deformed under applied loading.

The behavior of the model was tested a number of ways and compared against data found in the literature on fuel bundle stiffness and the first bending mode frequency expected for typical PWR fuel assemblies. Model variations considered the copper and lead wire fuel rod surrogates used in the shaker testing compared against the Zircaloy-4 cladding used in actual used fuel assembly configurations.

The three major model revisions are described in the following sections. The baseline model was used in the preliminary modeling effort captured in the September 2012 progress report, which is included in Appendix A. The Rev 1 model was updated based on the modeling experience between September 2012 and early May 2013, and represents a best-estimate model prior to receiving validation data from the shaker tests. The Rev 2 model represents the current best attempt to match the validation test data, as of late May 2013. Further revisions to the model are anticipated in the future, and the fuel assembly model currently being developed for the UFDC study of normal conditions of transport will have slightly different features.

2.1 Baseline, Rev 0 (Sept. 2012 Progress Report)

The baseline, or Rev 0 fuel assembly model is described in Appendix A. It was used in the first modeling effort of this study to estimate the shock test response and to guide the placement of accelerometers and the location of the limited number of Zircaloy-4 cladding tubes available for testing. At the time, the exact loading time histories of the test were not known, so PNNL created three different synthetic shock

test cases based on SNL's specified frequency response spectrum. At the time, the proposed test fixture also had a different configuration and composition.

An existing PNNL LS-DYNA finite element model of a Westinghouse WE 17x17 PWR fuel assembly was used directly as the Rev 0 model. The model represented each fuel rod as a series of beam elements. The beam elements had a hollow circular cross section with an outer and inner diameter set equal to the cladding dimensions. The fuel inside the cladding was not included in the geometry, but the density of cladding material was adjusted upwards to accurately account for the missing mass. This method of representing the fuel in the cladding was a carryover from the existing models, but is a reasonable assumption for the surrogate geometry for which there is a significant gap between the lead 'fuel' and copper 'cladding' and is expected to underpredict the structural contribution of fuel as a conservative measure.

The control rod guide tubes were also modeled with beam elements and their ends are connected to end plates that were modeled with shell elements. Grid spacers were also modeled with shell elements in a simplified box structure. Figure 2.1 shows a subsection of a grid structure. The spacer grid is composed of shell elements of uniform thickness, with the outer shells thicker to represent the outer strap thickness. The cladding beams have a circular outer cross section shape, but LS-DYNA represents them with a faceted prism for visualization.

One key feature of the model was the translational springs used to model fuel pin-to-spacer grid interaction. Figure 2.2 shows a sketch of the arrangement of the fuel pin to the spacer grid wall. Each face of the spacer grid comprised four shell elements sharing a common central node. Spring elements connected the four faces of the surrounding spacer to the central beam node. These springs were meant to represent in a simplified manner, the typical leaf spring and dimple contact to the fuel cladding. The structure and fuel-to-spacer interaction in a realistic fuel assembly design are actually much more complex and could be represented in much more rigorous detail, but then the model would have been too computationally expensive to solve loading conditions of a practical duration. The 3D spring elements used in Rev 0 provided supporting forces that acted to resist the motion of point C (Figure 2.2) from the relative center of the spacer grid compartment. The forces acted in all three directions, including axially (along the fuel cladding's central axis), and divided the reaction force among the four spacer face nodes.

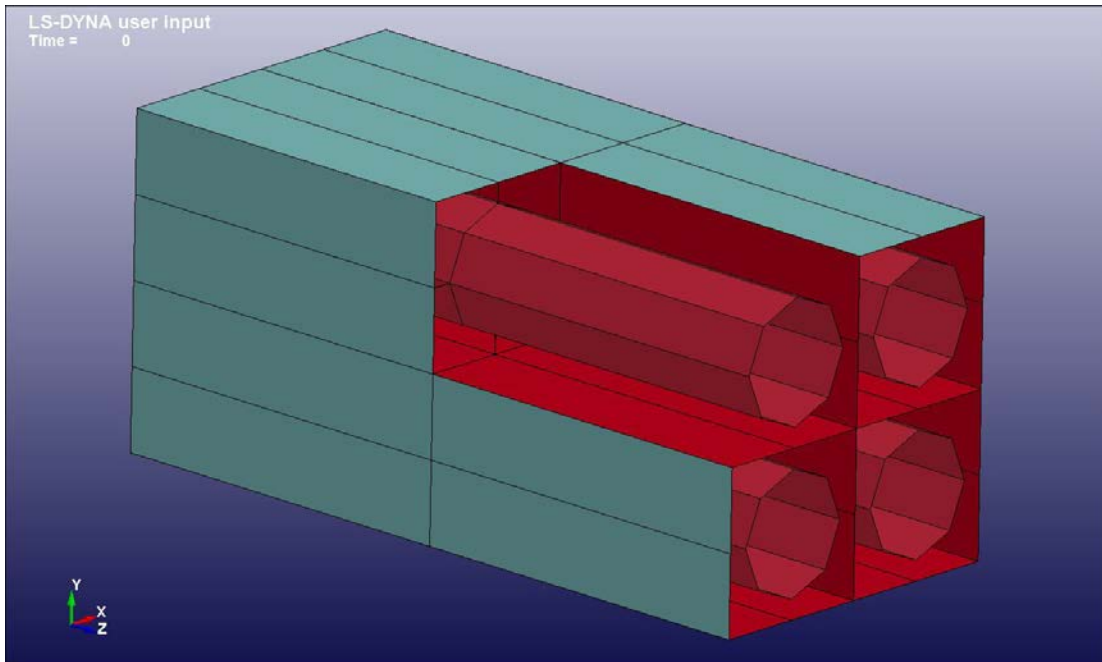


Figure 2.1. Grid Spacer (Shell Elements) and Cladding Sections (Beam Elements)

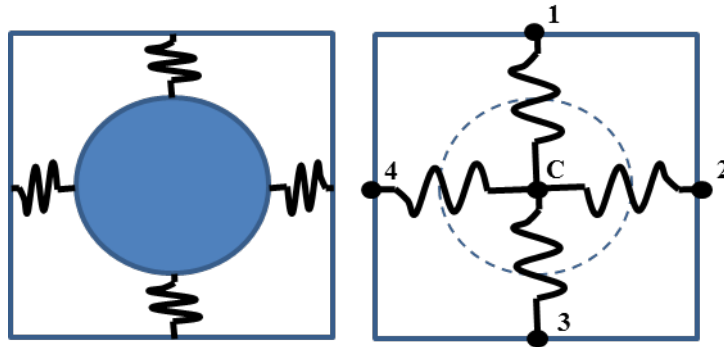


Figure 2.2. Rev 0 Translational Spring Arrangement (Conceptual [left] and Finite Element [right])

Contact between components is a major model feature in all revisions of the model. LS-DYNA's automatic general contact definition was used because it accounted for beam-to-beam contact, which was a physically necessary feature of the model. The fuel assembly structural response to dynamic loading can result in cladding-to-cladding contact between adjacent fuel rods if the applied loading is strong enough. Cladding can also deflect in any direction, stretching into any available void space, diagonal to the regular rows and columns of the fuel assembly array.

The Rev 0 model had some carryover geometry and features from the WE 17x17 optimized fuel assembly (OFA) that did not agree with the specific fuel assembly surrogate used by SNL for shaker testing. The conclusions of the September 2012 progress report (Appendix A) are not expected to be significantly affected by the differences, but the Rev 1 and Rev 2 models included revisions that were made to make the PNNL fuel assembly model match the planned SNL test configuration.

The Rev 0 fuel assembly model and a cutaway view of the original test fixture design are plotted in Figure 2.3. The figure shows a deformed geometry that resulted from a relatively strong hypothetical shock pulse in the vertical direction. Permanent deformation (racking) in the grids is visible. The hypothetical shock pulses used at the time covered a range of weak, medium, and strong pulse cases because the testing shock time histories were not available. This level of damage was not expected to occur in testing because of the relatively weaker shock time history ultimately used.

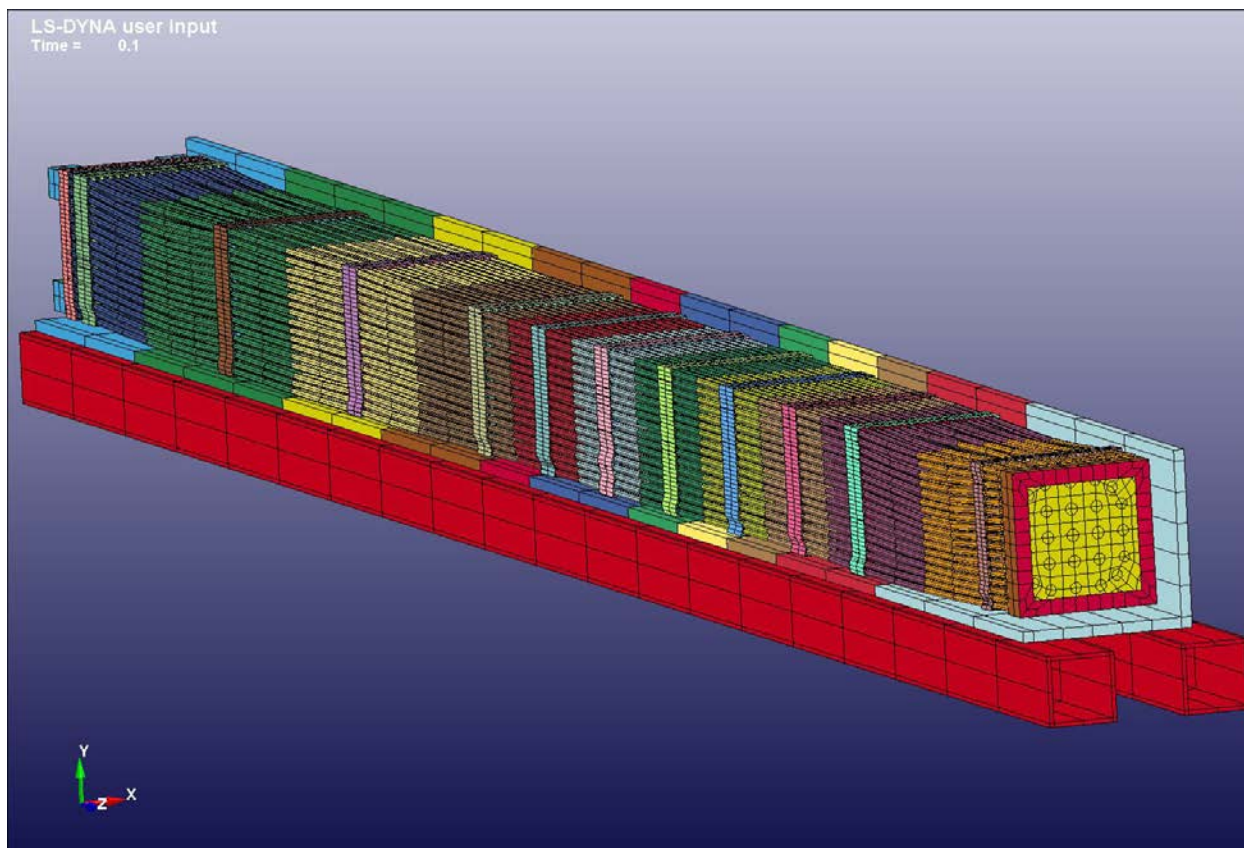


Figure 2.3. Original Fuel Assembly and Test Fixture Model

2.2 Fuel Assembly Model Rev 1 (Pre-Test Model)

SNL's test plan was revised in March 2013, and the revised document included drawings of the actual test assembly with spacer grid span distances defined. The test fixture was also altered from the initial design to provide a more rigid connection of the basket to the shaker table. The fuel assembly and test fixture models were adjusted to match the test plan configuration as closely as possible. This required some changes from the Rev 0 model, including grid locations, grid sizes, and the actual length of the copper and Zircaloy-4 cladding used in the test surrogate. The Rev 1 model also changed the tie plate components to be solid elements instead of shell elements. This was done to correct a modeling issue with beam-to-shell penetrations at the bottom tie plate.

Figure 2.4 shows the final test fixture model and Figure 2.5 shows the test fixture with the basket removed to show the fuel assembly model. Acceleration history loads were applied to the bottom of the expander head (the large red plate at the bottom of the model), which was directly bolted to the shaker table. Connected to the expander head were a number of springs and damper elements that were only used in the half sine pulse cases to arrest the motion of the test fixture after the short pulse was complete. The half sine pulse case was not one of the anticipated test cases, but it offered an interesting comparison to the shock test cases.

17 X 17 Assembly with Basket on Shaker Table Setup

- Assembly 1
 - FEM Parts
 - Geom Parts
 - Part 1

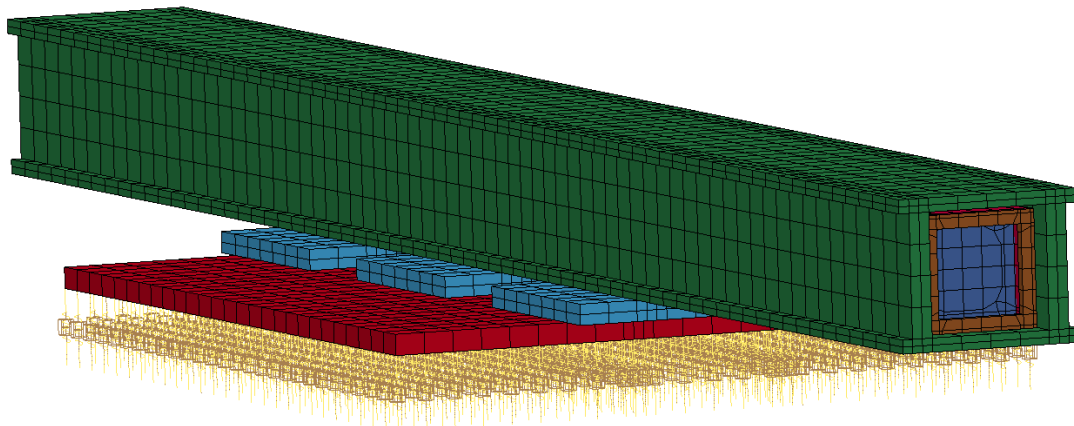


Figure 2.4. Rev 1 Test Fixture Model

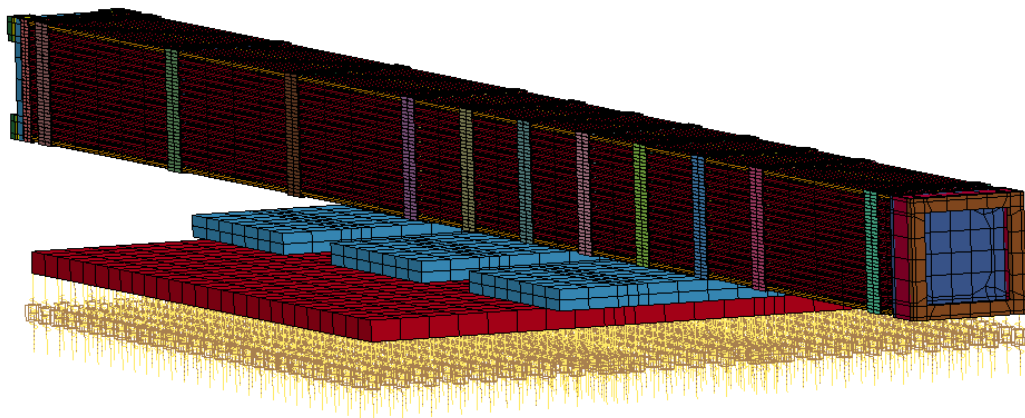


Figure 2.5. Rev 1 Test Fixture and Fuel Assembly Model with Basket Removed

The Rev 1 fuel assembly model was also evaluated separately using modal and static structural analyses to help characterize the model behavior. This allowed for comparison against existing fuel assembly test data in the literature (such as lateral deflection tests in Preumont et al. 1982). This also provided insight to the effects of different fuel assembly configurations, such as the differences in behavior between a fuel assembly surrogate composed of copper cladding and lead wire versus realistic Zircaloy-4 cladding. The modal and static structural analyses of the fuel assembly model were also used to compare the effects of

model features and spring stiffness values on the overall bundle stiffness and modal behavior. This fuel assembly characterization analysis will be discussed in the next section. In general, the Rev 1 fuel assembly model appeared to be more compliant and have a lower first mode frequency than expected. This observation led to some of the Rev 2 model changes, which led to a response that is more consistent with expectations based on the stiffness of the rods.

The Rev 1 finite element model used the same translational spring scheme to model cladding-to-grid interaction as described in the Rev 0 case (see Figure 2.2). It was expected that the validation data would suggest refinement of this area of the model would be necessary, but the pre-test model characterization studies did not suggest such detail was necessary for the Rev 1 model.

2.3 Fuel Assembly Model Rev 2 (Final Model of Study)

Rev 2 is the final model revision of this study. The test fixture model was changed slightly to better represent the test configuration. The springs and dampers previously modeled at the base of the expander head were removed (Figure 2.6). All excitation loads for the model come from prescribed motion of the expander head. A felt liner was also added to the basket inside surfaces to match the final test setup (Figure 2.7). SNL test facility management required the felt liner to prohibit direct metal-to-metal contact between the assembly and basket. The felt liner was modeled as a linear elastic material, with the intention to explore more complex material models in the future. Initial results suggested the thin felt layer had little effect on the results at the tested excitation magnitudes.

Based on the Rev 1 static model results (presented in Appendix B) it was determined that increasing the stiffness properties of the translational springs (see Figure 2.2) and/or adding rotational springs linking the fuel rods to the spacer grids would never increase the overall assembly stiffness enough to bring the static behavior in the range of available experimental results from the literature. The deformed shape of the static model indicated that the connections between the guide tubes and the spacer grids and the guide tube and the end caps were likely allowing too much rotation. For each guide tube at each spacer grid, the Rev 1 model had only a single node-to-node 'spot weld' (the spot weld is an LS-DYNA numerical method to provide a rigid fixation between two nodes in the model). The Rev 2 model changed this spot weld to group the four nodes on each side of the guide tube for each of the three rows of nodes per spacer grid; i.e., a total of 12 spacer grid nodes were welded to a total of 3 guide tube nodes. In addition to this spot-weld modification, the guide tubes were also extended into the end cap plates to overcome the lack of rotational resistance at the guide tube-end cap connection. This extended portion of the guide tubes shared nodes with the plate, meaning that however the end cap plates rotated, the guide tubes would essentially rotate the same at the ends. These modifications better represent the stiff mechanical connections of the assembly's support skeleton. The Rev 2 fuel bundle is shown in Figure 2.8, with the end structures removed.

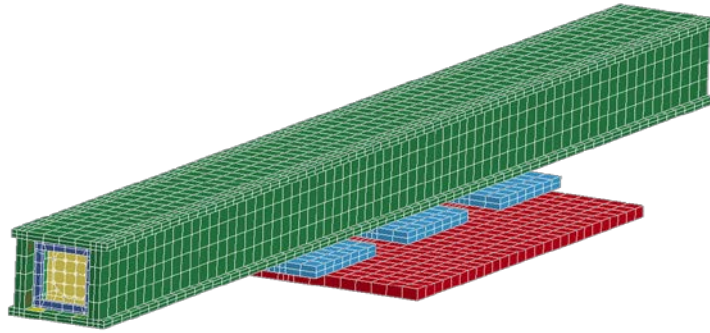


Figure 2.6. Final Shaker Test Model

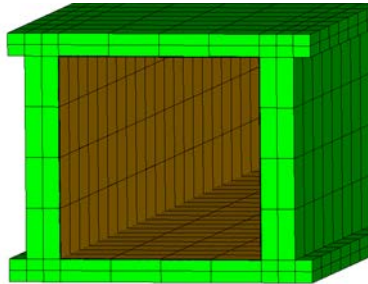


Figure 2.7. Final Shaker Test Model Felt Liner

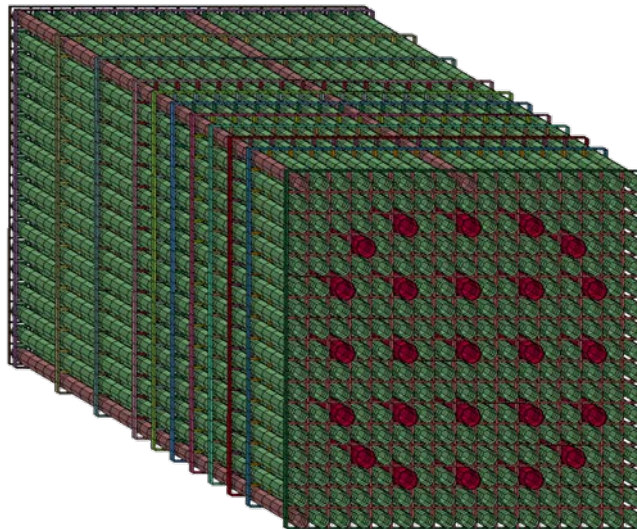


Figure 2.8. Final Fuel Bundle with Three Zircaloy-4 Rods

3.0 FUEL ASSEMBLY MODEL CHARACTERISTIC ANALYSIS

The Rev 1 detailed fuel assembly model was evaluated using modal and static structural analysis methods, in order to understand its expected dynamic response characteristics. It was also needed to predict the effect of altering assembly model parameters, such as translational spring stiffness, or changing the copper tubing of the test surrogate to actual irradiated zirconium alloy material. It also served as a further check of the detailed model against known fuel assembly characteristics, either documented in the literature or known to the analysts from prior experience.

The modal and static structural analyses are described in more detail in Appendix B. The results are summarized here.

3.1 Modal Analysis Summary

Modal analysis identifies the natural frequencies of vibration for the assembly and the relative deformed shape (mode) of the vibration response at those frequencies. Fuel assembly designs typically undergo significant physical testing to establish their first few vibration modes (roughly, the first ten). The first mode lateral bending frequency and often the third mode frequency are used by vendors in their seismic analysis of the fuel assemblies in the core. While this information is often not publicly available, an estimate of the typical first mode frequency for typical fuel assemblies at end of life is roughly 3-6 Hz.

Modal analysis was performed extensively on the Rev 1 fuel assembly during its development and to support the development of the final Rev 2 model. This was done in ANSYS, another commercially available finite element code. This required adjustments to the model, and some of the nonlinear features of the LS-DYNA fuel assembly model, like contact between components, had to be simplified. The same types of elements are available in ANSYS and LS-DYNA, so conversion from one code to another was generally straightforward. The linear ANSYS modal analysis is expected to provide a reasonable assessment of the fundamental frequencies of the nonlinear LS-DYNA fuel assembly model, but some interpretation of the results is necessary to identify legitimate mode shapes from the ones that are not physically realistic. Appendix B discusses this issue in more detail.

For the case of the fuel assembly surrogate used in testing, the detailed Rev 1 model has a first lateral bending mode at 1.9 Hz. This is below the expected range, and below the SNL shock test's frequency content range (3-600 Hz). The all-zirconium alloy cladding cases have lower first mode frequencies of 1.30 and 1.35 Hz for zero stiffness contribution of the fuel pellets and a 10 percent stiffness contribution of the fuel pellets, respectively. These observations suggest that the Rev 1 fuel assembly model is more compliant than it should be (stiffer bundles lead to higher frequencies). This is a reasonable conclusion because the dynamic behavior of fuel assemblies is known to depend heavily on the fuel cladding-to-grid interaction. The modal analysis highlights the importance of cladding-to-grid interaction by demonstrating that changes to the stiffness of the cladding material or slight stiffening to account for the fuel pellets has very little effect on the first-bending-mode frequency of the model. Pellet-to-cladding interaction could potentially have a more significant stiffness effect in a real fuel assembly, but this was not explored in this study beyond considering a 10 percent increase in stiffness. Ongoing research for the UFDC involving cladding bend tests is expected to help quantify the contribution of fuel pellets for future modeling.

The Rev 2 fuel assembly model had increased stiffness because of a change in the way the guide tubes were attached to the grid spacers. This increased stiffness contributed to somewhat higher modal frequencies. The dominant Rev 2 mode shapes are different from the dominant Rev 1 shapes, but looking at the cumulative mass participation of mode shapes shows that significant modal frequencies exist below 10 Hz, with some strong mode shapes that appear similar to the first lateral bending mode shapes determined for Rev 1 near 5 Hz.

To summarize, the modal analysis provided insight into the Rev 1 model behavior and led to the Rev 2 refinement of the model. Further evaluation of the Rev 2 model using modal analysis indicates that it has significant mode frequencies below 10 Hz, which could potentially be excited by low frequency loads.

3.2 Static Lateral Deflection Summary

The Rev 1 fuel assembly model was subjected to a lateral load at the middle grid to compare its deflection behavior with available fuel assembly design data. This physical test is often used on new fuel assembly prototype designs to characterize the lateral stiffness of a fuel assembly. Seismic fuel assembly models are often benchmarked to these lateral stiffness tests.

For a given lateral force load the Rev 1 fuel assembly was predicted to deflect significantly more than a comparison case from Preumont et al. (1982). Figure 3.1 shows a sketch of the model and the deflection results at each grid elevation. A force of 30 kgf causes a maximum lateral deflection of about 23 mm in the copper cladding cases and about 28 mm in the Zircaloy-4 case. Preumont et al. (1982) showed a beginning-of-life PWR fuel assembly laterally deflects about 2 mm for that same load, an order of magnitude difference. The Preumont et al. (1982) paper is not a precise match to the fuel assembly used by SNL, an undisclosed 14x14 PWR design versus the specific WE 17x17 used in testing, but based on this reference and experience it is estimated that the Rev 1 model is likely to be a factor of 3 to 6 too compliant.

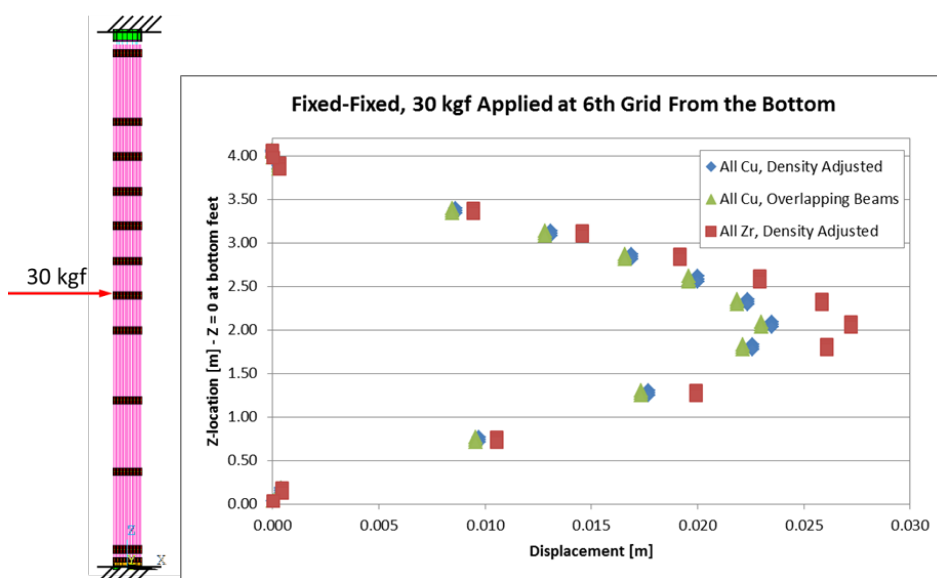


Figure 3.1. Static Lateral Deflection Model

Additional lateral stiffness analysis of the Rev 2 model demonstrated that the stiffening adjustment made to the guide tube to grid spacer connection brought the fuel assembly stiffness much closer to the expected stiffness range. See Appendix B for the full details

4.0 SHOCK LOAD ANALYSIS

The shock load cases of SNL's shaker test campaign are of primary interest because they represent the high magnitude and short duration loading events that would be expected to be more severe than random vibration loading. The three shock cases modeled and discussed in the September 2012 progress report (Appendix A) had a very different character than the cases ultimately defined in the test plan. SNL's September 2012 test plan clearly defined the time history accelerations they intended to apply in the shock testing, and they were all of much longer duration than originally expected. Those test cases were on the order of 4 seconds in duration, while typical shock tests are short pulses of 100 ms or shorter. The three PNNL Rev 0 model shock cases explored the frequency response target range specified by SNL, but did not anticipate the lengthy shock duration SNL intended to apply in testing. An additional surprise was the lack of frequency content below 10 Hz in SNL's initial test description. SNL clearly identified that their intended target range began at 10 Hz, but PNNL did not expect their intention was to cut out all frequency content below 10 Hz. This led to a large difference between the PNNL model predictions for the Rev 0 cases and the results calculated by applying the actual SNL proposed shock time history to the Rev 1 models.

Interaction between PNNL and SNL led to a further change of SNL's test plan in March 2013. The shock realizations were adjusted to have defined frequency content in the 3-10 Hz range, in an attempt to capture the first mode frequency response of the fuel assembly. This led to five new shock realizations. A shock realization is a specific time history derived to meet a frequency response spectrum. The five shock realizations have slight differences but appeared to be similar enough that PNNL only needed to study one in detail.

Section 4.1 describes the Rev 1 model results of SNL's Shock Realization #1, and it represents the best pre-test predictions. Section 4.2 describes a comparison analysis of the Rev 1 model subjected to a half sine shock pulse excitation. NUREG/CR-0128 recommended this as a simplified shock load to represent highway shocks. Its duration is only 59 milliseconds, and seems to fit the typical expectations for shock testing.

Section 4.3 compares the Rev 2 model results of SNL's Shock Realization #2 to actual test data. At the time of this writing, PNNL only has access to the Shock Realization #2 data.

Section 4.4 considers the half sine shock pulse from NUREG/CR-0128 applied to the Rev 2 model.

4.1 Shock Load Prediction Case (Rev 1 Model)

SNL created five time history realizations of the shock response spectrum based on the combination of a number of decaying sinusoids. The basic format for each individual frequency component is $A \cdot \text{sine}(\omega(t + \text{delay})) \cdot e^{-k\omega t}$, with A, delay, and k selected for roughly 50 evenly spaced frequencies (ω) over the range of 3 to 600 Hz. Adding these components together creates a unique acceleration time history (Figure 4.1), which represents the expected vertical motion of the shaker table. In the LS-DYNA models, this acceleration history is applied to the bottom of the expander plate that is bolted to the shaker table. The fuel assembly is free to move as the system rises and falls, within the confines of its basket compartment.

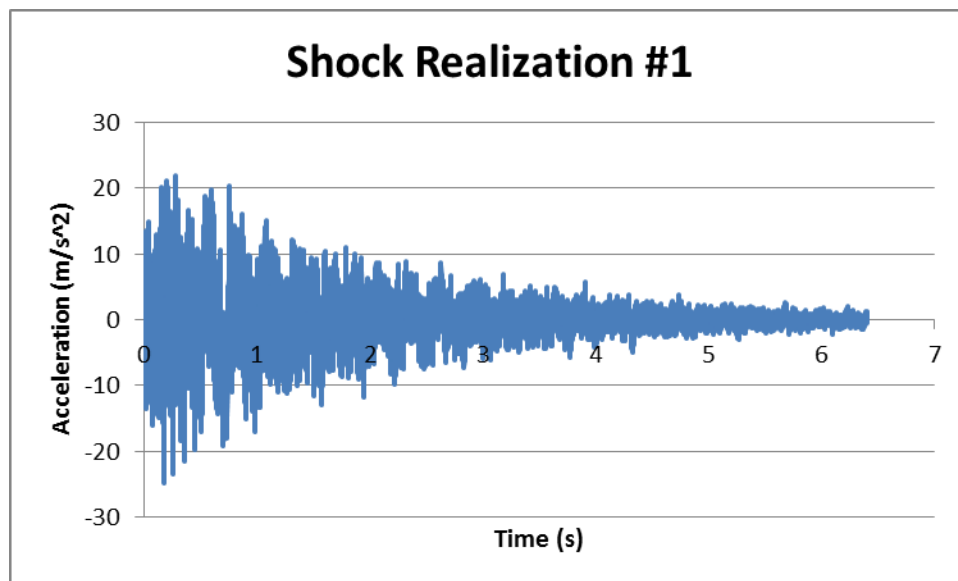


Figure 4.1. Acceleration History of Shock Realization #1

SNL's five shock realizations are all very similar, so just the first (Shock Realization #1) was modeled. The exceptionally long duration (about 6.4 seconds) makes this a challenge to analyze numerically because the explicit FEA method requires a very small time step (about 1 ms) that must remain constant throughout the analysis. With roughly one million solution steps required per second of model time, it is computationally expensive to run the full 6.4 seconds. Using four central processing units (CPUs), this would take about 48 hours per second of model time on PNNL's normal LS-DYNA platform, or 13 days of constant run time to compute all 6.4 seconds of model time. This is for a single-precision solution; PNNL prefers double precision for severe impact models using the detailed fuel assembly model because it was shown to make a difference in stress and strain calculations in cases with large deformation. For the shock test cases single precision solutions were generated as standard to speed up the computation time. In the Rev 2 modeling, a direct comparison of single and double precision results was made and will be discussed in Section 4.3.

Note the tapering shape of the acceleration time history in Figure 4.1. A practical way to reduce the modeled shock duration is to focus on the high-amplitude time period. MIL-STD-810F is a U.S. Department of Defense test method standard for evaluating equipment for environmental effects, including vibration and mechanical shock loads. In the mechanical shock section, MIL-STD-810F defines effective shock duration as the time period that includes all acceleration amplitudes that are 33 percent of the peak magnitude or higher. This criterion would reduce the effective duration to 2.7 seconds. Numerical model results were halted at 1.8 seconds and evaluated. By 1.8 seconds, all peaks of 50 percent and higher in the shock realization have completed.

The 1.8-second results provide valuable insight into the fuel assembly response to the shaker input. The motion of the center of mass of the fuel assembly and of the shaker (expander head) can easily be extracted from LS-DYNA and can provide the rigid body response of the two bodies. In the model, the shaker table acceleration is directly applied to the expander head, and the center of gravity (CG) of that plate makes a convenient point of reference. The whole test assembly (expander head, basket, and mounting brackets) is nearly rigid, with the basket CG tracking the expander head CG within +/- 0.1 mm.

Figure 4.2 shows the calculated displacement history, and Figure 4.3 shows the relative motion of the fuel assembly, in relation to the shaker.

Figure 4.2 shows that the motion of the two bodies is very similar, with the fuel assembly often moving slightly lower than the shaker. This is because of the settling of the fuel assembly against the relatively rigid basket floor, a large component of which comes from the drooping of unsupported fuel rod spans between spacers. Gravitational acceleration is imposed at time zero and the first few milliseconds of the solution represent the fuel assembly reacting to that load.

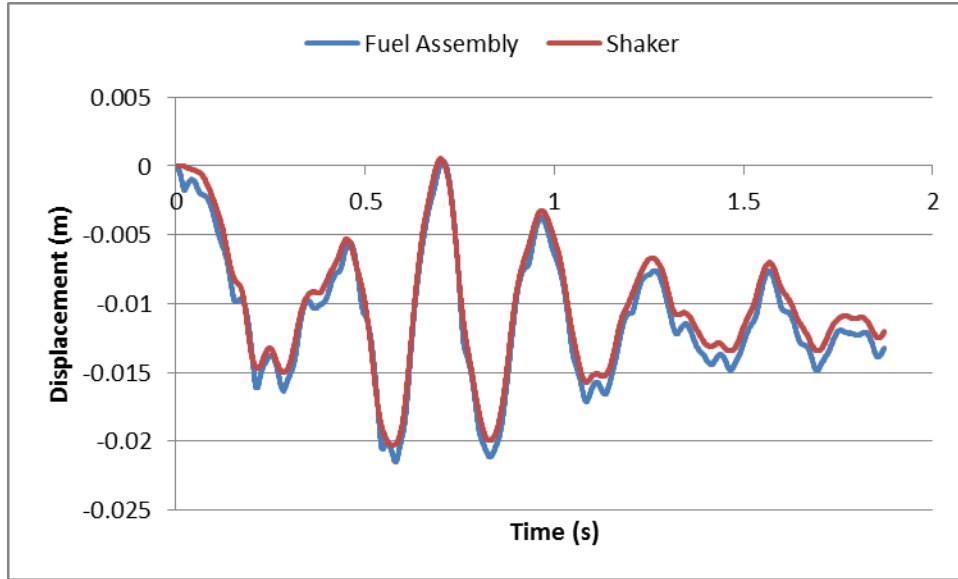


Figure 4.2. Displacement History (in meters)

Figure 4.3 shows that most of the relative motion is below 0, which is an indication of contact between the fuel assembly and basket floor. The few peaks above 0 indicate fuel assembly liftoff from the basket floor. These peaks are all less than 1 mm, and the vertical clearance with the top basket surface is about 10 mm, so the liftoff is not enough to permit an impact with the ceiling of the basket compartment. Because this is only considering the CG of the fuel assembly, additional evaluation of the results was made to confirm that the fuel assembly does not significantly bend. The maximum difference in vertical displacement between the top and bottom tie plates was less than 1.5 mm. This is an indication that the fuel assembly maintained a relatively flat, horizontal response to the excitation. Looking at the local end response, the bottom end separated a maximum of about 2.5 mm from the shaker while the top end rose up a maximum of about 1.25 mm from the shaker. Both of these local separations occurred in roughly 50-ms spikes within the first quarter of a second of the excitation history.

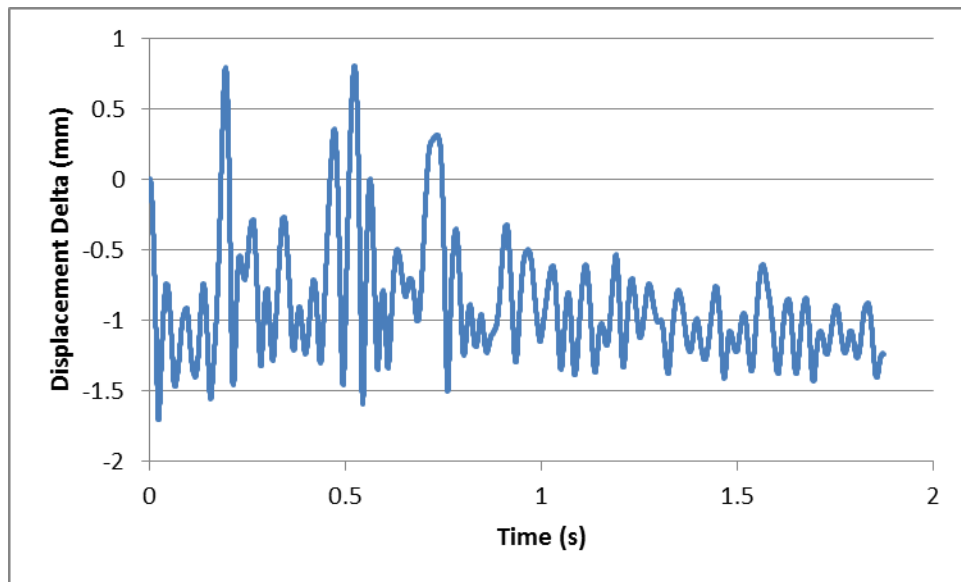


Figure 4.3. Motion of Fuel Assembly Relative to Shaker (+ is vertical separation)

The velocities show a trend that is similar to the displacement. Figure 4.4 shows a time period that contains the peak velocities and the maximum mismatch. Note that the maximum velocity the fuel assembly reaches is about 0.4 m/s. For a 30-foot drop scenario, impact velocity is about 13 m/s. For a 1-foot handling drop, the impact velocity is about 2.4 m/s. In comparison, the kinetic energy and potential impact velocities are very small for this shock test case. In this case, the only impact is with the bottom of the basket, and the maximum relative impact velocity is about 0.2 m/s.

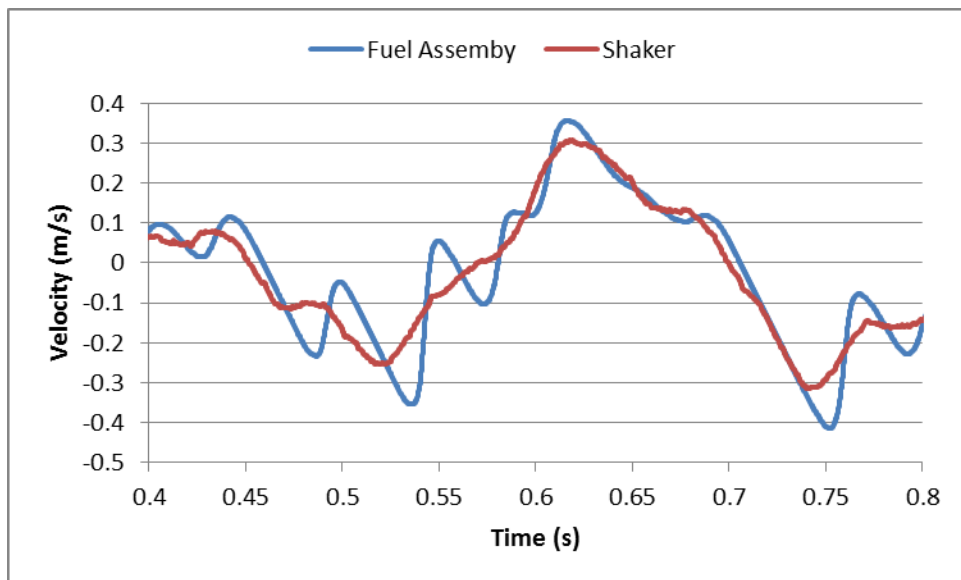


Figure 4.4. Velocity History

The acceleration of the fuel assembly CG is plotted in Figure 4.5. It shows a few short duration acceleration spikes of less than 9 g on the positive vertical direction. The negative accelerations have a floor of 1 g, which represents moments of “freefall,” when the basket moves downward and gravity acts

to pull the fuel assembly back into contact. The positive accelerations represent forces transmitted to the fuel assembly from the basket floor, but as the relative displacement plot of Figure 4.3 showed, these impulses do not amount to any significant separation between the fuel assembly and the basket. For reference, the shaker acceleration is plotted in Figure 4.6. It is not significantly different than the shock realization plotted in Figure 4.1 (note that the time scales are different).

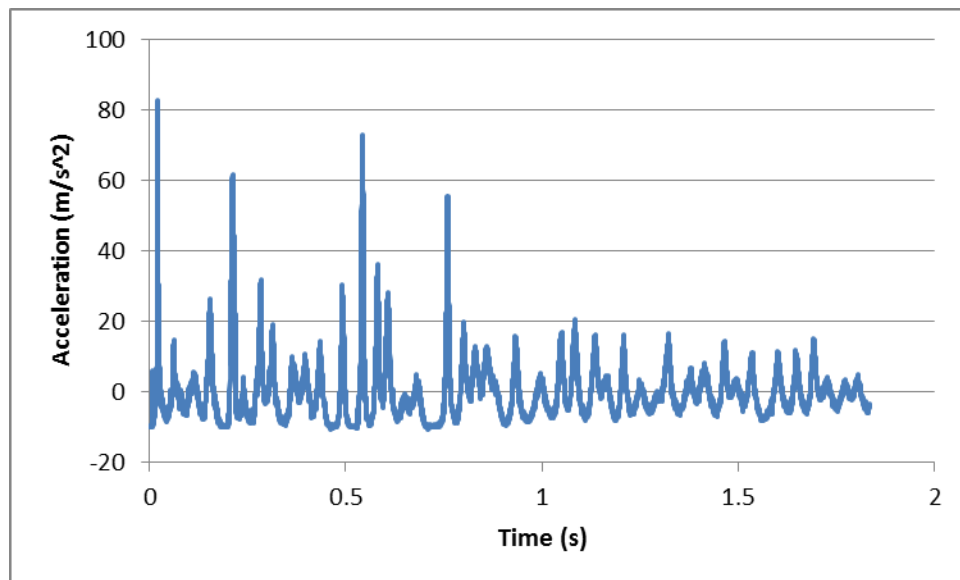


Figure 4.5. Fuel Assembly CG Acceleration

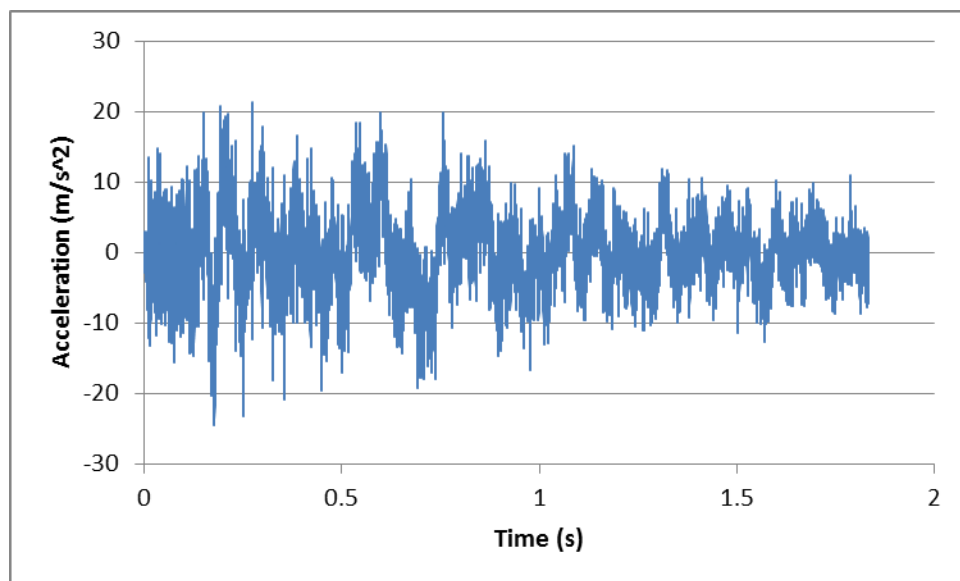


Figure 4.6. Shaker Acceleration

Viewing the acceleration data in the frequency domain reveals some interesting qualities of the shock realization and the fuel assembly response. Figure 4.7 shows the fast Fourier transform (FFT, performed in LS-Prepost) of the acceleration histories for the fuel assembly and shaker for frequencies up to 100 Hz. Figure 4.8 shows the acceleration spectra from 100 to 700 Hz. In both plots, the shaker excitation shows clear peaks at evenly spaced intervals, which correspond to the frequencies chosen to construct the artificial time histories. The two figures show that the fuel assembly response is strongest in a range up to about 150 Hz; beyond 150 Hz the shaker excitation is not significantly echoed in the fuel assembly response. Below 10 Hz, the shaker and fuel assembly respond nearly identically, possibly because the excitation is not strong enough to cause enough separation between the basket and fuel assembly. The fuel assembly first mode lateral bending frequency is expected to be below 10 Hz, but the low amplitude of the low frequency content in the shaker test scenario would not necessarily allow that mode shape to develop. The strongest response of the fuel assembly is in the 10-150 Hz range, with the strongest relative response to the input excitation in the 10-60 Hz range. Because the excitation is not continuous in the frequency domain, it is difficult to draw conclusions about the full frequency range response characteristics.

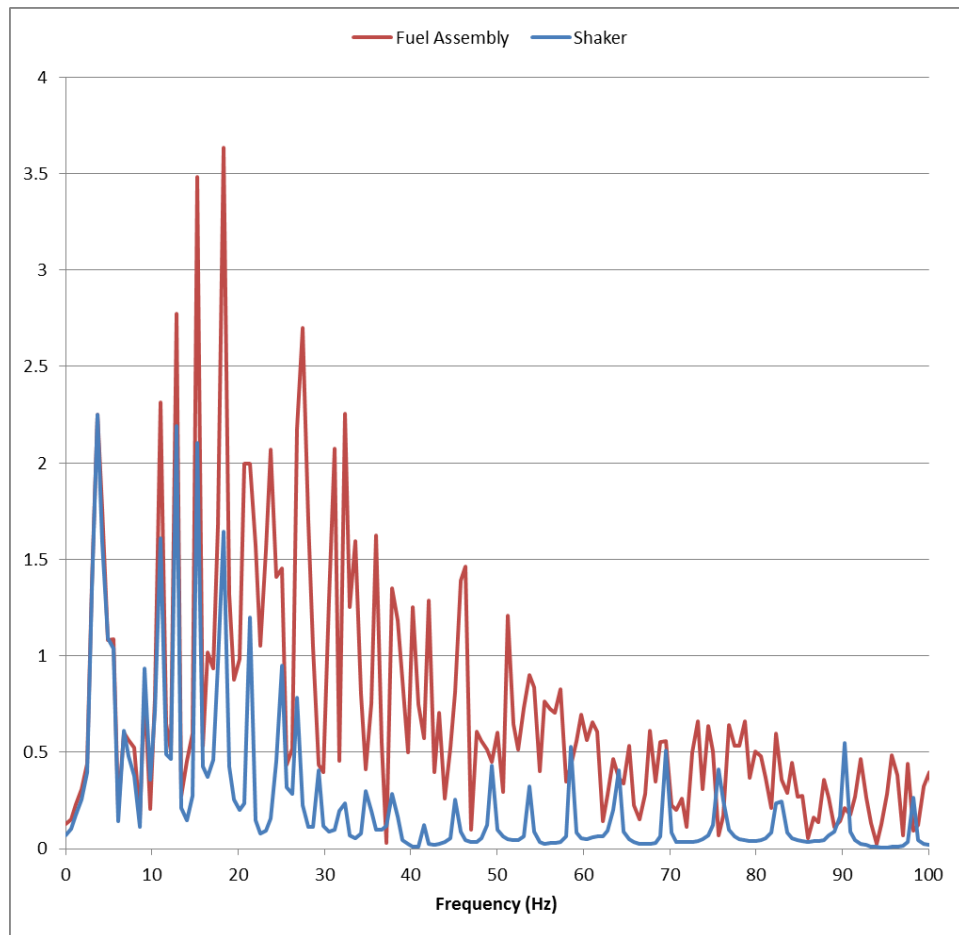


Figure 4.7. Acceleration Spectra (0-100 Hz)

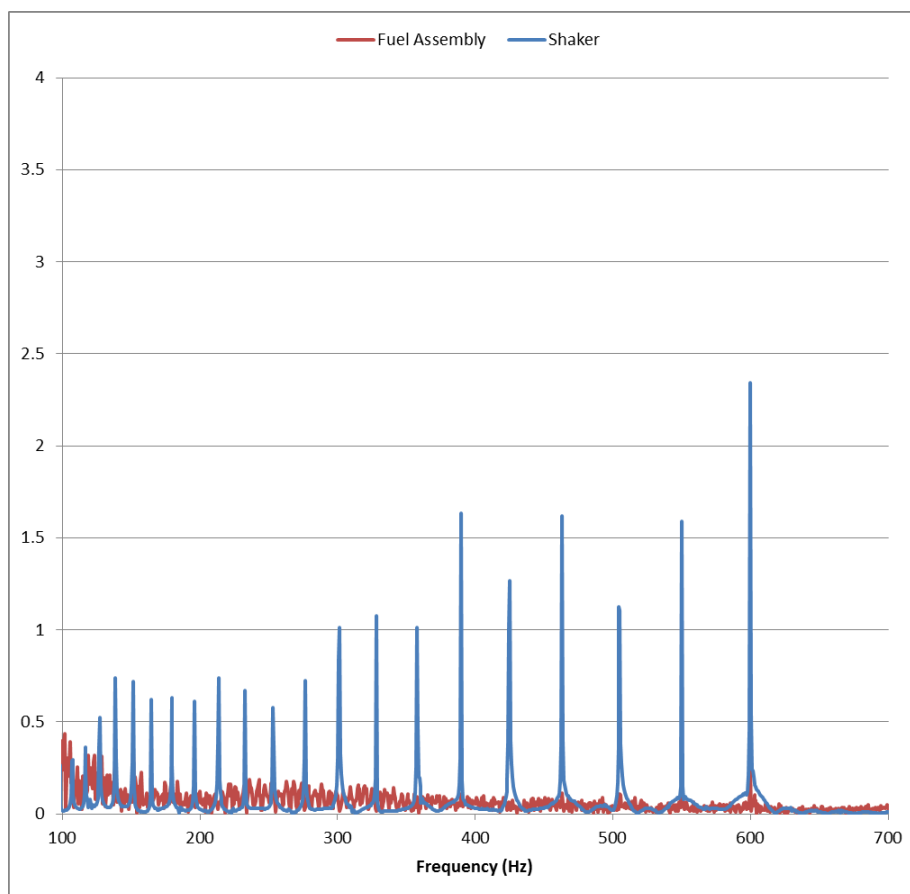


Figure 4.8. Acceleration Spectra (100-700 Hz)

Based on the CG dynamics, this loading scenario appears to be a low-energy case with little chance of damaging the fuel assembly or any of its components. No plastic strains are predicted in the grid spacers, guide tubes or the Zircaloy-4 cladding. Small plastic strains up to 0.0023 mm/mm are predicted at the ends of the copper cladding, where they are believed to make brief contact with the tie plates. These small plastic strains in the copper are not expected to be significant in terms of safety of the test or even enough to alter the dynamic response of the fuel assembly.

The actual test response is expected to be similar to the model response, but one goal of the modeling study is to validate the model using collected test data. Fuel assemblies are complex, and while PNNL's detailed fuel assembly model is also complex, its grid-to-cladding contact behavior is known to be highly simplified. SNL's shock realizations appear to offer a safe, non-destructive test bed for studying the fuel assembly dynamic response. Accelerometer data from the shaker bed will provide precise information regarding the shaker input. Accelerometer data from points in the fuel assembly will offer direct comparison points for tuning the model to most accurately match the experimental results.

4.2 Half Sine Pulse

NUREG/CR-0128 describes a vertical half sine shock pulse that conservatively represents the shock loads recorded during the highway transport study. The sources of these shock pulses are noted to be potholes, cattle guards, bridge approaches, and railroad crossings, traversed at speeds of 42-88 km/hr. The half sine

pulse is 59 ms in duration, reaching a peak acceleration of 2.9 g. The method of determining the pulse characteristics was not documented, but evaluating the pulse numerically with single-degree-of-freedom spring and damper systems suggests that the pulse fully envelopes the target response spectrum at 3 Hz and above. The objective of this evaluation is to provide a reasonable comparison between SNL's test plan and the recommended pulse from NUREG/CR-0128.

An analysis of single degree of freedom (SDOF) system response was performed using a spring, mass, and damper model in LS-DYNA. Time history base acceleration was applied to SDOF systems with natural frequencies of from 1 Hz to 99 Hz, in 1 Hz increments. Figure 4.9 shows how the SNL Shock Realization #1 and the half sine pulse compare against the target spectrum from NUREG/CR-0128. Absolute maximum (+ or -) instantaneous acceleration of the mass in each SDOF system is plotted against its natural frequency. The plot shows that both response spectra envelop the target at 5 Hz and higher, but not in the lower frequency range. The SNL test excitation drops off quickly below 3 Hz. The half sine pulse excitation misses the local peak between 1 and 3 Hz, but otherwise envelopes the target response. The half sine pulse was analyzed for direct comparison against SNL's test excitation, using the same LS-DYNA FEA model.

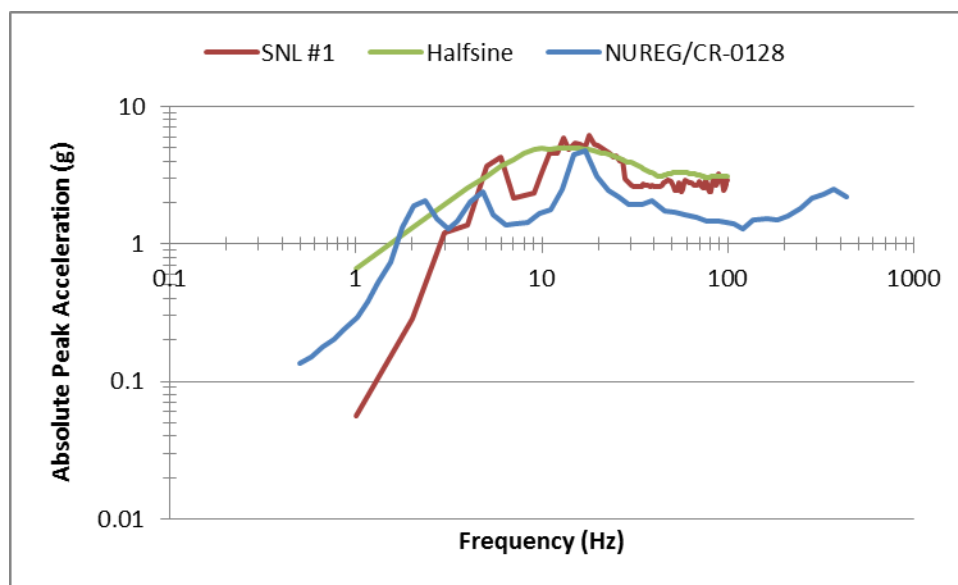


Figure 4.9. SDOF System Response (3% damping)

The half sine excitation, by definition, is a brief acceleration pulse. This is easy to define numerically, but in a physical test setup the pulse would lead to a net positive change in velocity and vertical location. A real physical system would be expected to return to its starting location, causing essentially two discrete loading phases: the specified pulse and the settling period after the pulse. The model was adjusted to add springs and dampers to the bottom of the expander head to arrest the vertical motion and damp the resulting vibrational response. Arbitrary spring and damper constants were chosen bring the test fixture to a gentle halt over a longer period of time than the initial pulse.

The post-pulse behavior of the system is nearly as important as the initial pulse because there is enough rigid-body motion caused by the pulse that the fuel assembly could potentially impact the top of the basket structure. In this case the shaker was not returned to its initial position after the pulse, but forced

to settle at its location at the end of the defined pulse. This treatment still results in an impact of the fuel assembly with the top of the basket, but the impact is relatively gentle. More extreme cases could be devised, but the point of this evaluation is to provide a reasonable comparison between SNL's test plan and the recommended pulse from NUREG/CR-0128.

Figure 4.10 shows the displacements of the center of mass of the shaker and fuel assembly, using the same methods and terminology discussed in the previous section. The acceleration pulse ends at 59 ms (A) when the displacement of both bodies is about 30 mm. At 60 ms, the springs and dampers are engaged to provide resistance to the upward motion. The shaker displacement curve can be seen to begin to flatten. At about 80 ms (B) the fuel assembly impacts the basket, and the momentum drives the test fixture upward. Both bodies then settle into a downward trend, meeting and starting to move together around 150 ms. The relatively loose springs allow them to drop below 30 mm (which is the zero-force reference for the springs) and the system would tend to oscillate around this vertical value. Eventually, the system would come to a halt, though gravity would cause the final vertical location to be some value less than 30 mm, depending on the spring constant and mass of the system.

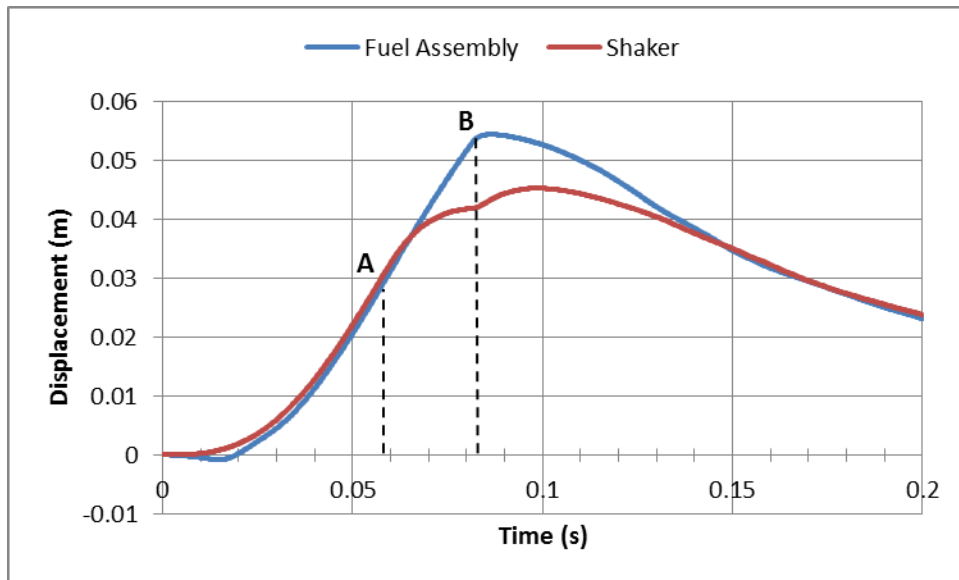


Figure 4.10. Half Sine Pulse Vertical Displacement. (A) is the End of the Pulse, (B) is the Beginning of Fuel Assembly Impact with the Top of the Basket

The velocity plot, Figure 4.11, shows the same events from a velocity perspective. The acceleration pulse ends at A, after which the shaker has 1 ms of constant velocity before the springs and dampers engage. The fuel assembly velocity continues to rise slightly because of stored elastic energy. Between 60 and 80 ms the shaker velocity is sharply reduced because of the action of the base springs and dampers, while the fuel assembly velocity falls more gently because only gravity is acting on it. Impact between the fuel assembly and the basket (transmitted nearly rigidly to the expander head/shaker) occurs at B. Settling of the fuel assembly against the basket can be seen early in the 0-30 ms time period before the two bodies start to move in unison. After the impact at B, the fuel assembly rebounds and its direction of motion is reversed (crosses zero). It moves faster than the shaker until it makes contact with the bottom of the basket around 130 ms. By the end of the analysis, the fuel assembly and shaker are moving together again.

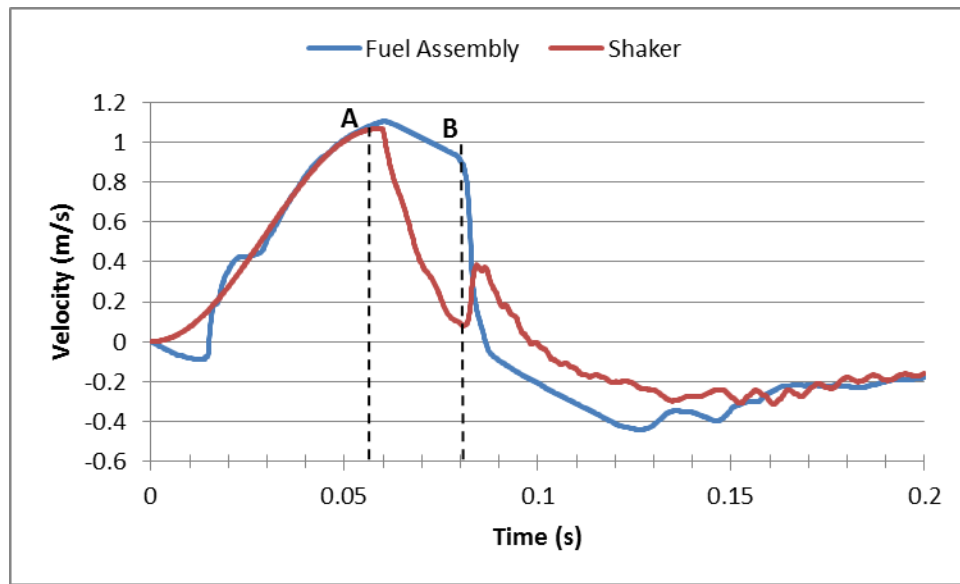


Figure 4.11. Half Sine Pulse Vertical Velocity. (A) is the End of the Pulse, (B) is the Beginning of Fuel Assembly Impact with the Top of the Basket.

The acceleration history of the shaker during this analysis is plotted in Figure 4.12. The first 60 ms are driven by an acceleration pulse (59 ms of sine plus 1 ms of zero acceleration). After 60 ms the springs and dampers at the base of the expander header are engaged to bring the system to rest. The sharp acceleration spike near 80 ms is the response of the test fixture to the impact of the fuel assembly with the top of the basket. The choice of spring and damper constants directly affects the system response after the defined 60 ms of pulse. Stronger springs could have led to higher relative impact velocities and a higher chance for fuel assembly damage.

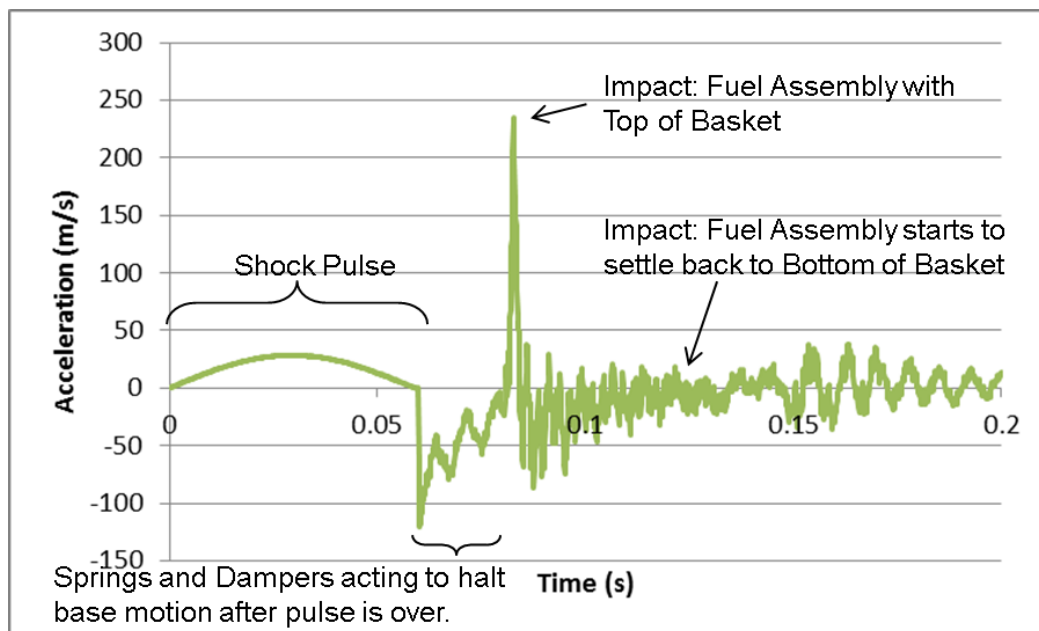


Figure 4.12. Half Sine Pulse Acceleration History

Despite the higher velocities and secondary impacts of the half sine pulse case, no significant damage to the fuel assembly is predicted. Slight plastic strains in the copper fuel cladding were noted at the ends of the fuel, presumably caused by interaction with the upper and lower tie plates. The magnitude of these plastic strains was below 0.1 percent. Given the low yield strength of copper, this type of minor localized yielding could reasonably be expected, and might go unnoticed in testing. The Zircaloy-4 cladding had no plastic strains at all, and neither did the guide tubes or grids.

It can be concluded from this case that the potential shock response of a fuel assembly undergoing highway transport could be significantly different than the SNL test cases, from a dynamics standpoint. Structurally, the dynamics differences did not cause a significant difference in damage prediction, but the assumptions of the surrounding basket motion had an influence. The major difference is the amount of rigid body motion, and in a realistic environment it could potentially have a more damaging effect than under laboratory test conditions.

4.3 Post-Test Evaluation (Rev 2 Model)

The shaker testing collected a total of 40 channels of accelerometer and strain gauge data, for each of 13 tests. Shock Realization #1 was the excitation set that was used for preliminary testing, but it was not the best candidate for post-test evaluation because of an issue with the experiment. Shock Realization #1 may have bottomed-out the shaker test fixture. It was adjusted and run a second time with slightly different frequency components.

Shock Realization #2 was selected by SNL as a representative case. PNNL was provided base accelerometer data for this case relatively soon after the testing. The full set of accelerometer and strain gauge data for Shock Realization #2 was supplied later, about 2 weeks before this report's due date. Given the time constraints, the strain gauge data for the largest span are the focus of the model-to-test data comparison. The other recorded data for Shock Realization #2 was not comprehensively reviewed, and PNNL does not yet have access to the other five sets of shock realization data. These factors make this post-test evaluation very limited in its scope, but some significant conclusions can be made.

Figure 4.13 shows the shaker acceleration history compared to the fuel assembly acceleration response. The shaker excitation period represents a subset of the full acceleration history, selected to include the peak acceleration. The fuel response is the calculated motion of the center of mass of the fuel assembly. Figure 4.14 shows the same response in the frequency domain, as calculated through an FFT. Similar to Figures 4.7 and 4.8, the discrete frequencies composing the shaker excitation are visible. Comparing the difference in amplitudes between the shaker excitation and the fuel response, Figure 4.15 and Figure 4.16 show the largest region of frequency amplification is roughly in the 10-60 Hz range. This is an indication that the fuel assembly response is susceptible to resonance or dynamic amplification to cyclical excitation in the 10-60 Hz range. Below 10 Hz, there is little to no amplification. This is an indication that the fuel assembly is either not responsive below 10 Hz, or the test did not excite its lower frequency modes. Based on the fuel assembly characterization presented in Appendix A, a stronger response in the 2-9 Hz range would be expected. The lack of low frequency response appears to be explained by the amount of relative motion between the fuel and the basket.

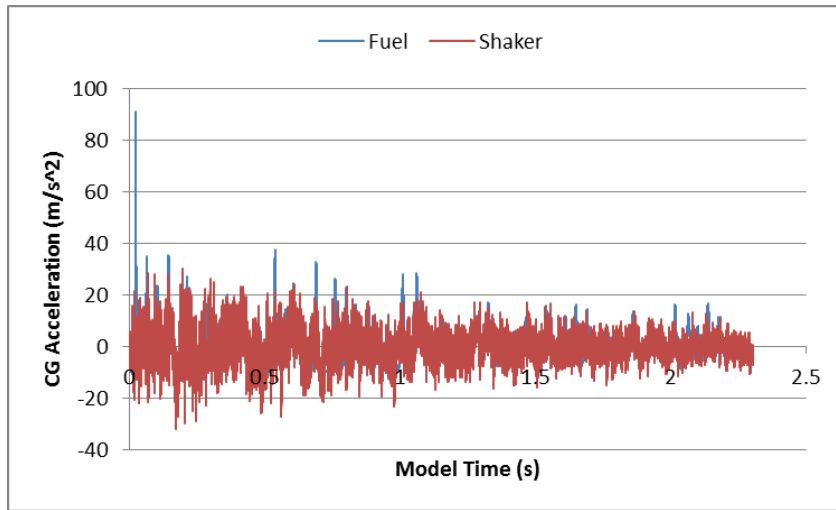


Figure 4.13. Shock Realization #2 Acceleration Response

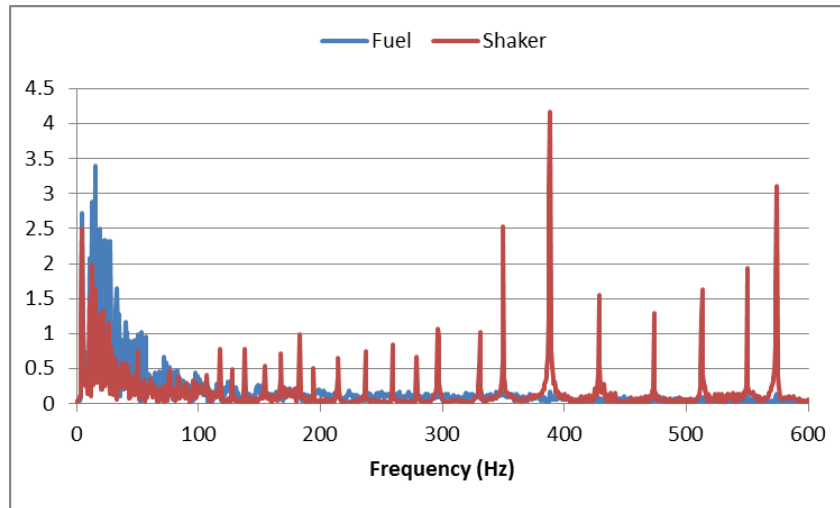


Figure 4.14. Shock Realization #2 Acceleration Response (Frequency Domain)

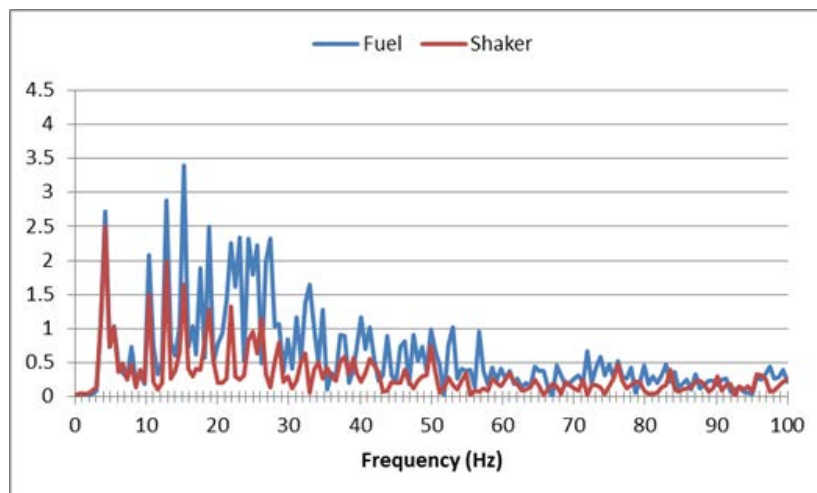


Figure 4.15. Shock Realization #2, 0-100 Hz Response

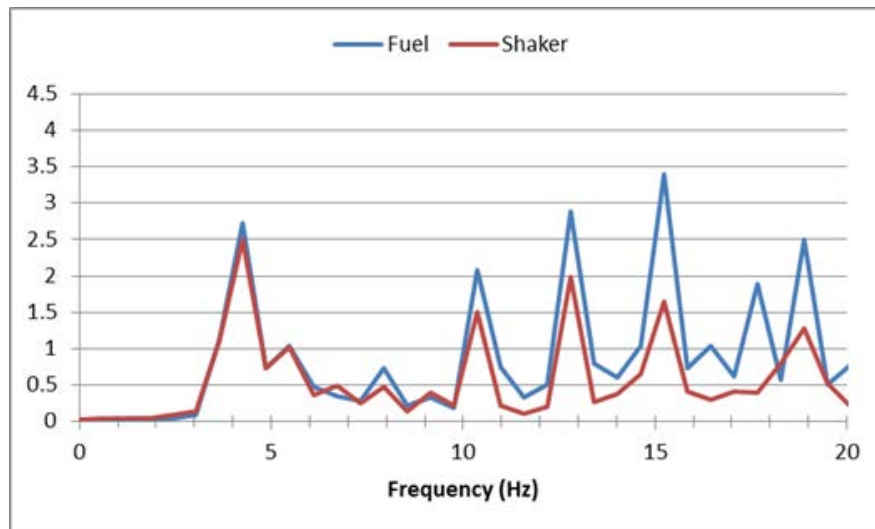


Figure 4.16. Shock Realization #2, 0-20 Hz Response

The fuel response to the test environment seems to be very limited, because of a lack of separation from the basket floor. Figure 4.17 plots the relative displacement of the fuel assembly center of mass compared to the shaker table excitation history. Negative values indicate compression of the fuel assembly. Positive values indicate separation from the basket floor. With the felt liners included in the model, the fuel assembly has about 8 mm of clearance with the ceiling of the basket. With a maximum separation of about 1.25 mm, the fuel is not close to striking the basket ceiling. In fact, it spends most of its response time compressed against the basket floor. This assessment is based on the motion of the center of mass. Figure 4.18 shows contours of vertical displacements of the spacer grids, and the ends are rising higher than the middle. This is one of the strongest bowed fuel assembly shapes, but the maximum difference between the end displacements and middle displacements is less than 1 mm. This makes the center of mass motion highly indicative of the fuel assembly motion in this case.

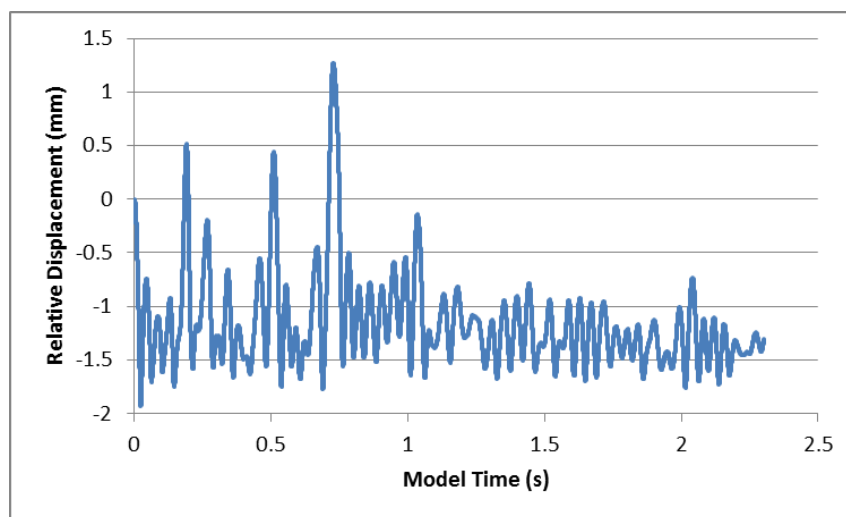


Figure 4.17. Shock Realization #2 Relative Displacements (Fuel - Shaker)

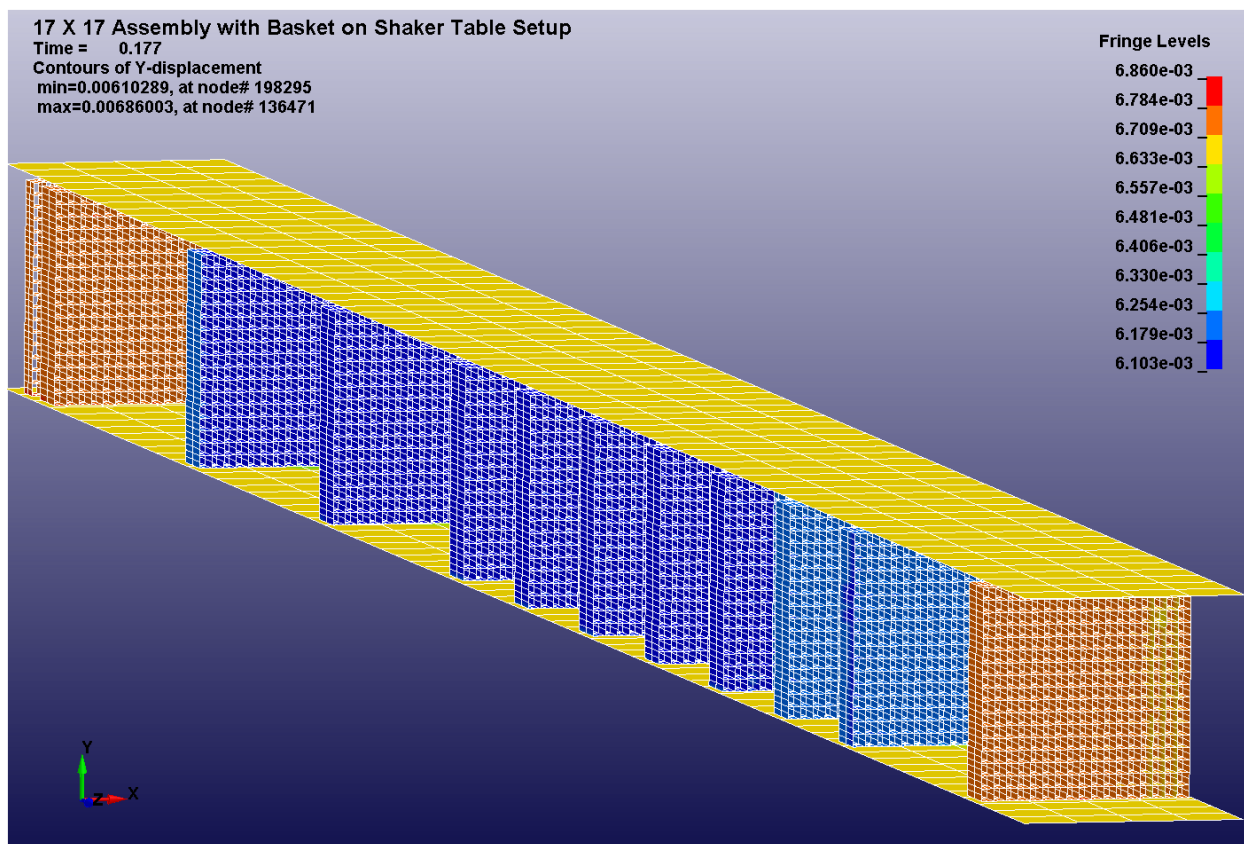


Figure 4.18. Shock Realization #2 Vertical Displacement Contours (m)

Evaluating the dynamic response of the fuel assembly to the test case, it seems apparent that the fuel assembly does not have the freedom to vibrate or respond at the lower frequency range. The fuel assembly is essentially riding along with the shaker table motion, with some response in the 10-60 Hz range, probably corresponding to the natural frequency of individual spans. The first lateral bending mode of the fuel assembly would involve more bowing than is predicted by the model. The modal analysis shows that the fuel assembly modal frequencies change according to the boundary conditions (Free-Free, Fixed-Fixed) which is to be expected. The choice of excitation history applies effective boundary conditions to the fuel assembly response. The assembly has the geometric freedom to leave the floor of the basket, but unless it does it remains constrained by the basket floor surface. Therefore, the rod response will depend on the amplitude of these lower frequency excitations.

The Zircaloy-4 cladding strains recorded in the testing are on the order of 200 μs (micro strains, equal to $1\text{E-}6$ mm/mm). The strains calculated by the Rev 2 model are on the order of 700 μs , using the LS-DYNA single precision solver. An assessment of the effect of using single precision versus double precision at specific strain gauge locations through time suggests the average strain error is ± 10 μs , with a maximum instantaneous error of ± 480 μs . The average error confirms single precision offers a reasonable estimate of the double precision results, but the instantaneous peak error suggests the confidence in calculating the peak strain from a single precision model is relatively low, compared to the magnitude of strains expected.

Directly from the model, Figure 4.19 shows element integration point maximum axial stress values for three locations that approximately coincide with strain gauges in the longest span. A is the bottom end, B is the top end, and C is the mid span. This is for the top-center Zircaloy-4 fuel cladding. Maximum strains are plotted, and they can represent any location around the circumference of the cladding. Of these three locations, the peak strain gauge result was $150 \mu\text{s}$, or 0.00015 m/m . Compared to the peak model-calculated strain of approximately $725 \mu\text{s}$, and the potential instantaneous error of $\pm 480 \mu\text{s}$, the model is within reasonable agreement with such small numbers. A better comparison for the model would be if the cladding was loaded closer to its yield limit ($6,800 \mu\text{s}$) during testing, which would provide a better indication of the model accuracy and precision near a more significant stress or strain level.

The best that can be concluded at this point is that the shaker test causes relatively insignificant stresses and strains in the fuel assembly, and the model calculates insignificant stresses and strains that are only slightly higher in peak magnitude.

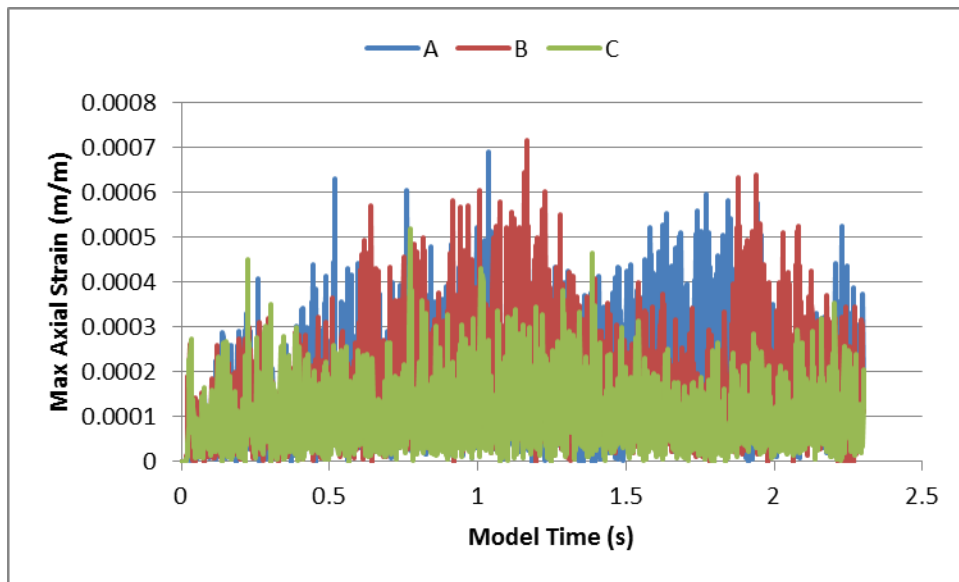


Figure 4.19. Shock Realization #2 Maximum Strain Results at Three Cladding Locations

4.4 Half Sine Pulse Evaluation (Rev 2 Model)

The Rev 2 model was loaded with the half sine pulse described in Section 4.2, with a change to the post-pulse behavior. In Section 4.2, the end of the pulse was constrained by springs and dampers that halted the movement of the system somewhat abruptly and caused it to settle to a damped vibration response. In this case, the pulse accelerates the basket vertically until it reaches a velocity of about 1.1 m/s , then after the pulse, the basket is subject to constant deceleration because of gravity (9.81 m/s) until the upward velocity reaches 0. This is intended to be a very gentle treatment of the post-pulse dynamics.

Figure 4.20 shows the acceleration history of the shaker (B, green) compared to the fuel assembly center of mass (A, red). The first few microseconds shows the fuel assembly is being compressed by gravity against the basket floor. At the first major spike, the fuel assembly gets ahead of the pulse, resulting in a dip in acceleration near 25 ms. By the end of the 59 ms pulse, the fuel assembly is moving with the

basket floor. Between 75 and 150 ms both the fuel assembly and basket are in free fall. Around 175 ms, when the basket is brought to a halt, the fuel assembly impacts the basket floor gently.

In this load case, the peak strains in the three strain gauge locations are predicted to reach just 600 μs , which is less than the Shock Realization #2 model results. Comparative peak strains from the Rev 1 model case reached 1200 μs , which is probably because of the assumed post-pulse behavior, but may also be because of the difference in fuel assembly model or potentially the lack of felt. The significant point of this analysis is that the half sine shock pulse itself is not particularly damaging to the fuel assembly, and causes a similar amount of strains to the Shock Realization #2 case. The difference is in the post-pulse behavior of the shaker system. Any practical implementation of a half sine pulse will have a post-pulse response to bring the system back to rest. The pulse is expected to cause the fuel assembly to reach a velocity of about 1.1 m/s, and the corresponding amount of kinetic energy will need to be dissipated at the end of the test. How this energy is dissipated will determine how much stress, strain, and potential damage the fuel assembly may experience.

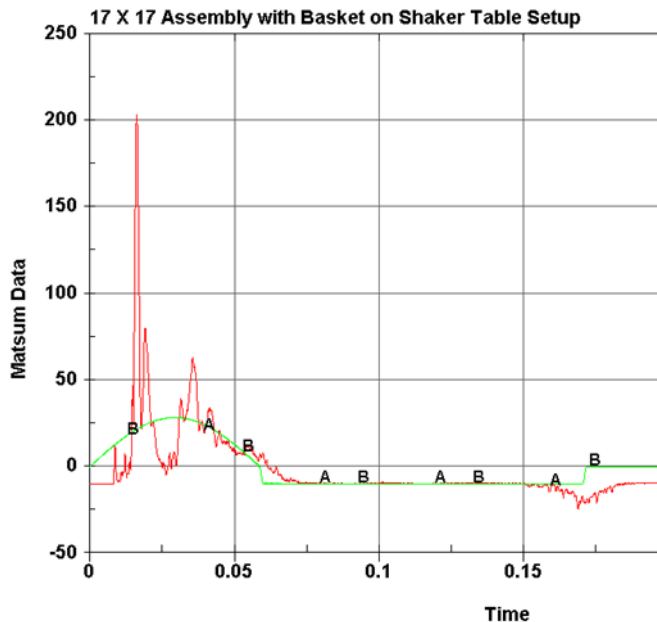


Figure 4.20. Rev 2 Half Sine Pulse Acceleration

The relevance of the half sine pulse to this study is its relation to the basis of SNL's shock realizations. SNL used the frequency response curve from NUREG/CR-0128 to guide the choice of a number of damped sinusoids to construct five specific time history curves. The half sine pulse is an alternative representation of the same data. Both types of load are purely artificial. NUREG/CR-0128 mentions that the basis of the data is a loaded truck, crossing potholes, railroad tracks, cattle guards, and other road surface disruptions. The report does not provide actual recorded time histories of the events that caused the shock loading. Because of this, we do not have any practical insight into the actual fuel assembly response that might be expected, for example, when the truck crosses a railroad track. The shock realizations all eliminate low-frequency shock components that could contribute to realistic rigid body motion. The half sine pulse causes significant rigid body motion, and accumulated velocity potentially

resulting in impact with the basket ceiling, but the amount of potential stress, strain, and damage to the fuel assembly will depend on what happens after the pulse.

For both of these shock loading approaches, an understanding of the actual dynamic response that would be witnessed in the field is missing. A used fuel package conveyance crossing a railroad track will have some measurable dynamic response. The data in NUREG/CR-0128 do not provide a complete definition of what that response might be. Even if the recommended half sine pulse was implemented as a load in a shaker test scenario, the practical fuel assembly response would largely depend on what happens after the pulse, and to estimate what this would be in a practical situation crosses into vehicle dynamics territory. The suspension system of the specific conveyance design is likely to determine what realistic loads a fuel assembly will witness under transport conditions, and this goes beyond the scope of SNL's test campaign, and beyond the basis of their loads, NUREG/CR-0128.

5.0 PRE-TEST PREDICTIONS

The primary purpose of this work was to assist SNL with analysis of the test scenario. The early phases of the modeling work (using the Rev 0 model) informed SNL's decisions on the placement of strain gauges and accelerometers on the surrogate fuel assembly. The Rev 1 model was used prior to testing to estimate the fuel assembly response. The earliest Rev 1 model results drove the suggestion to SNL to lower the low end frequency range of their shock realizations to attempt to excite the lower fuel assembly modes. SNL altered their shock realizations to include frequencies as low as 3 Hz.

The final use of the Rev 1 models was to make pretest predictions of the fuel assembly response under test conditions, to advise SNL of any potential problems and generally estimate the fuel assembly response. Shortly before testing commenced, PNNL was advised that the test fixture would include a felt liner between the fuel assembly surrogate and the basket walls. PNNL did not have enough time to incorporate felt into the model, but it is expected that the felt will have a noticeable effect on the shaker test results. The potential effect of felt will be discussed with each prediction.

Rigid Body Motion. Based on the modeling, the fuel assembly surrogate is expected to generally move with the shaker table, with negligible liftoff. The ends of the fuel assembly might locally lift up more than the center, but to a maximum of 2 mm, leaving plenty of clearance with the ceiling of the basket. The presence of felt is expected to soften the contact interface and result in even less liftoff than was predicted in Figure 4.3.

Copper Cladding. No plastic deformation in the copper cladding is expected. If plastic strains are observed, it will likely be close to the grid contact points, caused by bending. The copper cladding could make contact with the felt or with neighboring cladding.

Zircaloy-4 Cladding. No plastic deformation is expected. Contact with neighboring cladding is possible, as is contact with the felt for cladding near the bottom surface.

Grid Spacers. No permanent deformation of the grids is expected based on the modeling. Typical grids can experience significant impact forces without causing any perceptible permanent deformation. There are exceptions, where some grid designs will plastically deform prior to reaching their buckling limit, but these tend to be very small deformations on the order of 0.1 mm. The model is not expected to be able to predict this level of grid deformation accurately. No major impact forces are expected, and no significant grid deflection is expected. The presence of felt is expected to soften impact forces.

6.0 POST-TEST EVALUATION

Comparison of the model to test results show that the Rev 2 finite element model of the fuel assembly offers a reasonable agreement with the observed test response, as discussed in Section 4.3. The model precision does not seem to be high enough to match strains at the micro-strain magnitude, but it is accurate enough to predict that no significant strains in the cladding were to be expected from the test excitation magnitudes. There are a few additional considerations that might bring the model results closer to test data.

- **Gravity.** The PNNL model applies gravity as an acceleration load that begins at time = 0. It was done this way to save time associated with calculating a preload step at time < 0. Future analyses will have this preload step built in. The strain gauge data do not include the effect of gravity because the gauge was applied to the fuel assembly in a gravity-relaxed state. This would add approximately 50 μs to the reported strain gauge value.
- **Coarse Mesh Effects.** The PNNL assembly model has a relatively coarse mesh that does not precisely align with the strain gauge locations. The two end-of-span locations include local high stress/strain concentrations that may be artificially high because of a single-point contact rather than the multi-point spring-and-dimple contact occurring in a realistic spacer-grid geometry. Photos of the test geometry also show the strain gauges are slightly offset from the edge of the grids, whereas the cladding elements reported in the model are fully within the grids. This means the comparison is with slightly different locations.
- **Maximum vs. Local Strains.** The PNNL model results are reported as the maximum around the cladding circumference. The test's strain gauge data are fixed to one point on the cladding surface. It is not known if the strain gauges experienced any rotation during the testing, but any rotation away from the peak bending stress location (towards the neutral bending axis) would lead to less-than-maximum strain measures.
- **Strain Gauge Sensitivity.** It is not clear what the accuracy of the strain gauges are, or how sensitive they are to low strains. Strains are so small they might have trouble accurately identifying them. This issue was not evaluated; it is just listed as a potential source of difference between the recorded data and the model predictions.
- **Fuel Stiffness Modeling.** In all versions of the model, the lead wire within the cladding was not modeled as having any stiffness effect on the cladding. Adjusting cladding stiffness to account for this, or modeling overlapping beams to represent the lead wire would probably help reduce the amount of stresses and strains.

The fact that the model predicts higher strains than the test case might simply be because of simplifications inherent to the finite element model. In particular, the cladding-to-spacer grid interaction is modeled in such a way that no energy losses occur, unless the cladding makes contact with the grid shell structure. In a realistic fuel assembly, the cladding would make contact with springs or dimples, and any axial motion would cause energy losses because of friction. These losses would be small, but the strains are also very small. One test case was modeled with a small amount of global mass damping applied to the model. Mass-proportional damping acts against rigid body motion, but the coefficient was chosen to cause a relatively small amount of energy loss compared to the total kinetic energy of the

system. This test case resulted in reduced cladding strains (from 700 to 300 μs) but it affected the character of the strain response in a way that made it questionable compared to the recorded strain gauge data. Adding selective damping at the grid to cladding interaction locations might be a reasonable approach, but this is something to be considered for future applications of the model.

6.1 Model Validation and Limitations

The test data offer a real-world example for comparison against model results. This can be used to validate the model, to a certain extent. The single test case data to which we have access is relatively limited in scope. The test had a limited magnitude and limited frequency content. As discussed in Section 4.3, the greatest excitation of the fuel assembly is in the 10-60 Hz range, and this seems likely to be the result of the low magnitudes of acceleration and the lack of low-frequency components in the excitation. The test case did not drive the fuel assembly to separate from the basket floor, as might have happened with a different choice of excitation history. With this limited excitation, the validation of the model is limited to a response range that is similar to what was witnessed in testing.

The validation range does not cover cases with significant opportunity for free vibration, i.e., cases where the fuel assembly lifts off from the basket floor. Nor does it cover cases with dominant excitation in the less than 10 Hz range. An example of this is in rail transport applications, where the railcar suspension system has a strong natural frequency near 2 Hz and considerable potential for vertical travel (on the order of 6 inches [150 mm]). Additional validation would be needed when implementing this detailed fuel assembly model in cases with higher excitation.

The validation might not even apply to all highway transportation scenarios, when vehicle dynamics and suspension systems are considered. As discussed in Section 4.4, the half sine pulse offers an alternative way of defining a shock time history that is still based on the NUREG/CR-0128 data set. The key difference between the half sine pulse and SNL's shock realizations is the amount of rigid body motion they cause in the fuel assembly and shaker system. The half sine pulse introduces significantly more kinetic energy to the system than the SNL shock realizations. Depending on the dynamic response of the conveyance, the half sine pulse might prove to be significantly more damaging than the test cases run by SNL. This points to an important knowledge gap: Example time histories tied to specific on-road events, such as crossing railroad tracks for specific conveyance designs, are not documented in NUREG/CR-0128 and are not readily available. Their exact nature will determine the loads a realistic used fuel assembly will see in practice. This kind of evaluation was beyond the scope of the SNL test campaign, but should be considered for future study.

7.0 CONCLUSIONS

PNNL modeling of a fuel assembly shaker test was able to assist SNL in its conduct of the experiments. Model results helped to guide the placement of strain gauges and accelerometers, helped identify the best locations to use a limited number of Zircaloy-4 claddings, and made sure that the test scenario would not likely damage the fuel assembly.

Pre-test predictions based on modeling were found to be accurate: no perceptible damage occurred to the fuel assembly during testing. Very little separation with the basket floor occurred. It was predicted to be a very mild excitation of the fuel assembly, and that proved to be the case.

Directly comparing model results to one test case, the model predicted somewhat higher strains, though they were still far from the material yield strength. The magnitude of the error was comparable to the potential error because a single precision solver was used instead of a more computationally expensive double-precision solver. A number of issues were identified that might contribute to a closing of the gap between the model and the recorded test data. The main conclusion was that the model did a reasonable job of predicting fuel assembly behavior as a whole, but had difficulty precisely matching the low strains witnessed in testing.

The validation range of the model was limited because the test conditions limited the range of response. Response validation was probably best in the 10-60 Hz range, because that was the range where the fuel response was amplified relative to the excitation. Below 10 Hz the low-frequency range was not well exercised because there was little to no separation with the basket floor. The fuel assembly had geometric freedom to separate from the basket floor, but the chosen load history did not cause that to happen. If alternate loading conditions were used, more separation from the basket and a different response range would be possible.

This leads to an important knowledge gap for highway transportation of used fuel. It is not clear what dynamic response range actual transported fuel will fall into when details like specific conveyance designs and precise on-road events are considered: the low-kinetic energy, low separation, linear response range tested by SNL's shaker test, or a higher energy, highly nonlinear response range that is suggested by the half sine pulse loading described in NUREG/CR-0128. This may be a vehicle dynamics problem that will depend largely on the design of the conveyance and its suspension system.

8.0 REFERENCES

MIL-STD-810F. 2000. *Department of Defense Test Method Standard for Environmental Engineering Considerations and Laboratory Tests.*

NUREG/CR-0128. 1978. *Shock and Vibration Environments for Large Shipping Container During Truck Transport (Part II).* CF Magnuson. SAND78-0337, Sandia Laboratories, Albuquerque, New Mexico.

Preumont A, P Thomson, and J Parent. 1982. "Seismic Analysis of PWR-RCC Fuel Assemblies." *Nuclear Engineering and Design.* 71:103-119.

Appendix A: Shaker Table Modeling Progress Report

By Nicholas Klymyshyn, Pacific Northwest National Laboratory

September 2012

Author's Note (May 2013): Appendix A contains a report provided to the Used Fuel Disposition Campaign team to document progress on the modeling in September 2012. The report captured the state of the simulation work in September 2012. It was not prepared as a milestone deliverable; its purpose was merely to communicate preliminary results to the team.

The progress report used the Rev 0 model, which was incrementally improved in Rev 1 and Rev 2 to better match the expected fuel assembly dynamic response characteristics. Even so, the Rev 0 model seems to offer a reasonable approximation of nonlinear fuel assembly dynamics.

The three shock loads applied in this progress report turned out to be non-representative of the actual loads Sandia National Laboratories (SNL) applied in their testing. The random pulse of Shock7 was closest to the actual SNL loads and caused similarly mild results, but it only lasted for 0.1 seconds while the SNL shock realizations were on the order of 6.0 seconds. This disconnect in loading speaks to the knowledge gap discussed in the body of the report in Section 6.2. When the loading is defined only by a response spectrum, an infinite number of time histories can be synthesized to meet or envelope the spectrum. The five SNL shock cases represent one family of curves that all have an absence of low-frequency components. In order to predict what happens to the fuel during transport, what is still needed is an understanding of the actual time history response of the conveyance, which may be heavily influenced by the specifics of the conveyance design.

These results showed the potential range of response of the fuel assembly, with some uncertainty in the magnitudes of loads. The instrumentation recommendations were helpful in ensuring sufficient validation data was collected, but, because of the low excitation magnitudes, potentially interesting phenomena like grid crushing did not take place.

A-1. Introduction

This modeling effort seeks to use a detailed Pacific Northwest National Laboratory (PNNL) fuel assembly finite element model of a WE 17x17 to inform Sandia National Laboratories' (SNL's) upcoming shaker table experiment series. The testing is slated to evaluate a full-scale fuel assembly under U.S. highway vibration and shock loads resulting from normal truck transport. The modeling serves two purposes: it will help inform the instrumentation decisions prior to the shaker table testing, and after testing is complete, it will be used to predict the behavior of irradiated used fuel after the modeling methodology has been validated. The instrumentation decisions are critical because only a limited amount of data can be captured during the experiments, and accelerometers and strain gauges need to be placed where they can provide the best insight into the fuel assembly behavior under these transport conditions. An additional issue to address is that SNL has a limited budget and can only afford a small number of Zircaloy-4 cladding tubes, and most of the fuel rods in the assembly will need to be represented by copper and a lead wire core. One of the pre-test concerns is where in the assembly to put the Zircaloy-4 rods for the best results. The post-test use of the model is critical to relate the experimental results from the laboratory setting to used fuel in the actual field state. The adjustments will include modifications to the material model plus an accounting for the elevated temperature of the fuel within the package.

This report will describe the modeling progress to date, note some key preliminary results, and detail the main steps that still need to be completed. This report concludes with an initial set of recommendations for instrumentation, based on the modeling work completed to date. It is recommended that a few more cases be run before the test plan is finalized.

A-2. Initial Modeling

An existing PNNL LS-DYNA finite element model of a WE 17x17 was used as the basis of this study. The model represents each fuel rod as a long line of beam elements. The beam elements have a hollow circular cross section with an outer and inner diameter set equal to the cladding dimensions. The fuel inside the cladding is not included in the geometry, but the density of cladding material is adjusted upwards to accurately account for the missing mass. This method of representing the fuel in the cladding is a carryover from the existing models and is expected to underpredict the structural contribution of fuel as a conservative measure until refinements can be made. The intention with the current model is to run the models with an adjusted copper material modulus to reflect the stiffness contribution of the lead wire within the copper cladding, but the current models still represent the old conservative cladding modeling method. The adjusted cladding modulus will be implemented in follow-up work.

The control rod guide tubes are also modeled with beam elements and their ends are connected to end plates that are modeled with shell elements representing the tie plates. Grid spacers are also modeled with shell elements in a simplified box structure. Figure A.1 shows a subsection of a grid structure. The spacer grid is composed of uniform thickness shell elements, with the outer shells thicker to represent the outer strap thickness. The cladding beams have a circular outer cross section shape, but LS-DYNA represents them with a faceted prism for visualization.

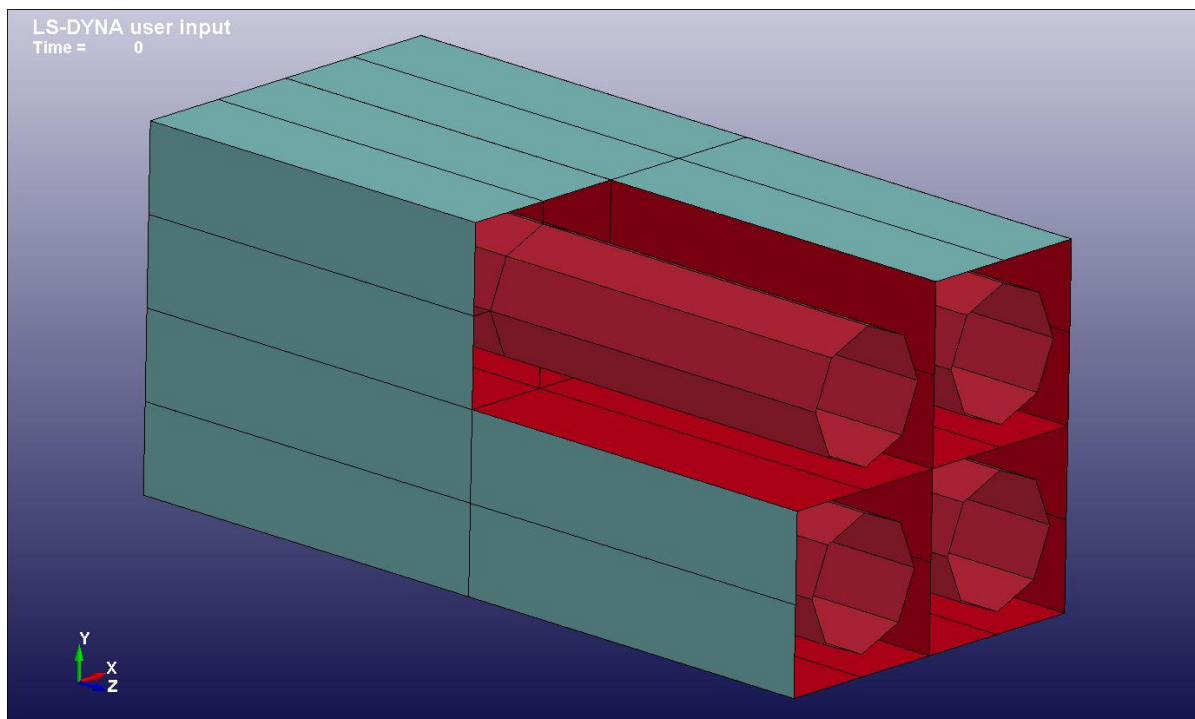


Figure A.1. Grid Spacer (Shell Elements) and Cladding Sections (Beam Elements)

Contact between components is a major model feature. LS-DYNA's automatic general contact definition is used because it accounts for beam-to-beam contact, which is a physically necessary feature of the model. The fuel assembly structural response to dynamic loading can result in cladding-to-cladding contact if loading is strong enough. Cladding can also deflect in all three dimensions, stretching into any available void space, diagonal to the regular rows and columns of the fuel assembly array.

The initial model was developed to represent an irradiated WE 17x17 optimized fuel assembly (OFA). The model had three elevated temperature zones (top, middle, and bottom) and assumed irradiated Zircaloy-4 material properties with appropriately increased yield strength and lowered ductility. The base model had to be adjusted to represent the particular WE 17x17 geometry that is to be tested at SNL. Room temperature material properties were implemented and the grid spacer locations had to be shifted to match drawings provided by SNL.

In addition, the shaker testing is intended to be carried out within a mocked-up fuel basket compartment of steel plate walls with open ends. The plate basket structure is mounted on two beams that are attached to the shaker table surface. These test items had to be included in the LS-DYNA model to provide accurate loading and interaction with the assembly. Since fuel compartment geometry could have an important effect on the shock results, it is recommended that the later phases of this analytical task include a sensitivity study based on fuel compartment geometry.

A-3. Shaker Table Loading (Excitation)

The shaker table will be used for two types of loads: random vibration and mechanical shock. The mechanical shock loading was the focus of this study because it represents the greatest chance of damaging the fuel assembly structure because of elevated acceleration loads. A shaker table input loading spectrum was provided by SNL (see the Target curve, Figure A.2) which comes from the report, "Shock and Vibration Environments for Large Shipping Container During Truck Transport (Part II)," NUREG/CR-0128, August 1978. The spectrum provides significant information about the character of the excitation but does not completely define the intended loading history. Each point on the figure describes the response the random excitation would cause to a single-degree-of-freedom system (SDOF) with a particular natural frequency. For example, a classic spring and mass system with a natural frequency of 10 Hz would respond to the random shock load with a peak acceleration of 2.7 times the acceleration of gravity. This method of describing shock loading is common, but it is not sufficient information to predict exactly what the excitation load will be in the time domain or how much total energy is imparted to the dynamic system during the shock pulse. For the later phases of this work, the actual excitation time history will be recorded and the model can be evaluated precisely for the recorded input. Various base acceleration histories were artificially generated and applied to the model for the current phase of simulation. The goal in this type of analysis is to come up with an excitation load history that closely matches the desired response spectrum. This can be done by using a recorded, similar shock history and making any necessary adjustments to it, or it can be done using purely numerical means, involving random number generation and frequency band adjustments. Three distinct excitation load cases are discussed in this letter report, designated Shock6, Shock7, and Shock9. The response spectra of these excitation load histories are plotted in Figure B.2 for comparison. Figure B.2 was generated using a separate SDOF spring-mass-damper model for each frequency in LS-DYNA. Each of the three excitation loads was applied to the SDOF models and the absolute peak response for each frequency is plotted. Each excitation load case will be discussed in more detail below.

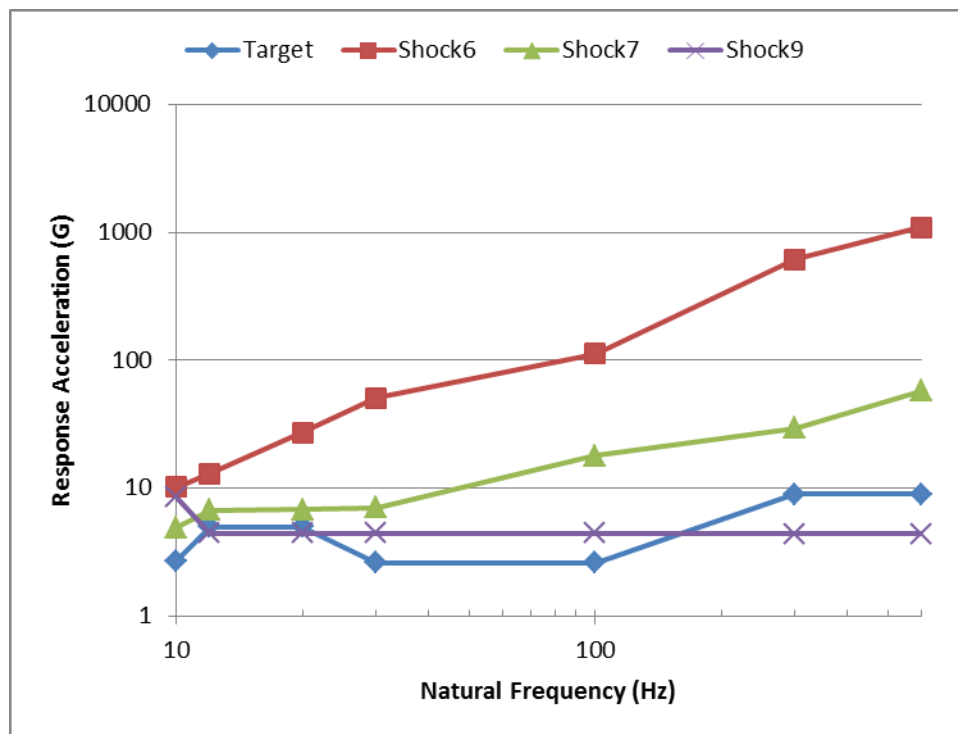


Figure A.2. Shock Response Spectra

The time history of the Shock6 acceleration pulse is plotted in Figure A.3. This case is based on a uniformly distributed random series with the higher frequency components filtered out using an 8-pole Butterworth filter with a cutoff frequency of 600 Hz. The removal of the high-frequency band gives the load curve a strong, distinct shape with clearly defined peaks. The 20 millisecond (ms) duration was chosen based on suggested effective shock durations listed in Table 516.5-I of MIL-STD-810F, pertaining to functional and crash hazard testing for flight and ground equipment. The 20-ms duration may not be applicable to the specific shock testing intended for the fuel assembly, but it represents a relatively short duration, high magnitude shock that exceeds the response spectrum target at every defined frequency point (see Figure A.2). The target shock response spectrum also provides information related to the shock magnitude, which was calculated to be 11.2 Grms (root-mean-square value in units of multiples of gravity). The Grms value defines the magnitude of the excitation, but not the sign because the root mean square (RMS) operation turns all negative numbers positive. This is one area where the target response spectrum does not provide sufficient information to determine a time history excitation load. Shock6 has a comparable RMS value, but greatly exceeds the target at some frequencies. As will be discussed in the next section, Shock6 causes significant plastic deformation of the grids, localized plastic deformation in the guide tubes, and some plastic deformation in the cladding. This is the most generally damaging of the three load cases. While the high frequency components appear to be orders of magnitude higher than the target, these higher frequencies are not expected to be a major cause of damage. The effective first mode frequency of the fuel assembly is expected to be in the 3-5 Hz range, so that is below the lowest target frequency, and high frequency excitation like 600 Hz is not expected to be very significant. However, modes and mode shapes represent a linear view of the fuel assembly. Actual fuel assemblies have significant nonlinear characteristics, and the models and loading conditions are nonlinear and attempt to

represent the realistic response. The models are solved with such small time steps they can capture shock wave propagation and physical frequency responses above 10 kHz. It is not clear what effect high-frequency components will have on the fuel assembly impact with the basket. For testing, the frequency range of interest should be as high as it is practical to measure.

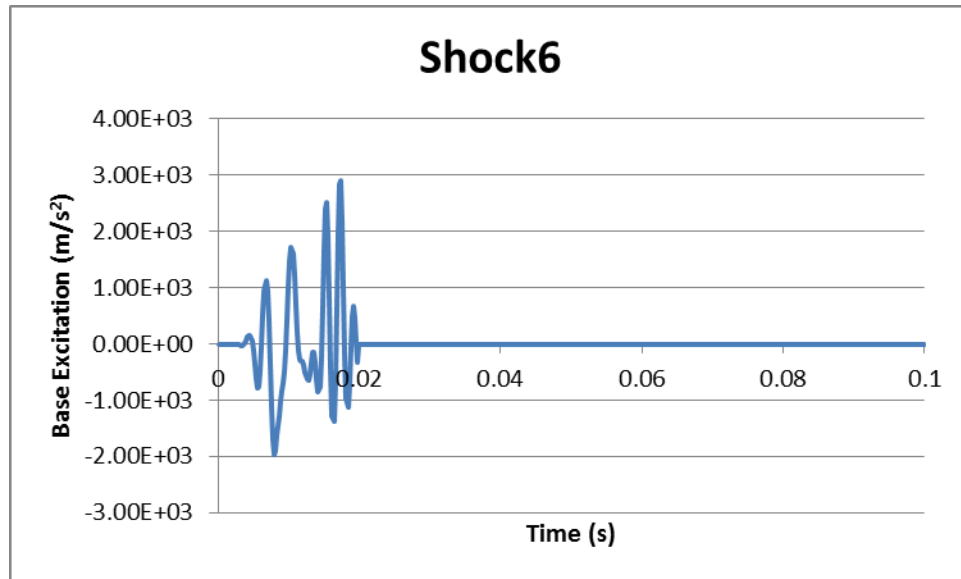


Figure A.3. Shock6, Acceleration Time History

Shock7 assumes a random uniform distribution over 100 ms with no frequency filtering applied (see Figure A.4). The time period of the pulse was lengthened to the period of 10 Hz sine wave, based on the fact that 10 Hz is the lowest frequency of interest. The random signal was amplified to match the 11.2 Grms target. The lower magnitude, longer duration, and continual oscillation between positive and negative acceleration values lead to a load case that causes little deformation or damage to the fuel assembly. It does cause some plastic strain in the cladding, but is overall the least damaging case.

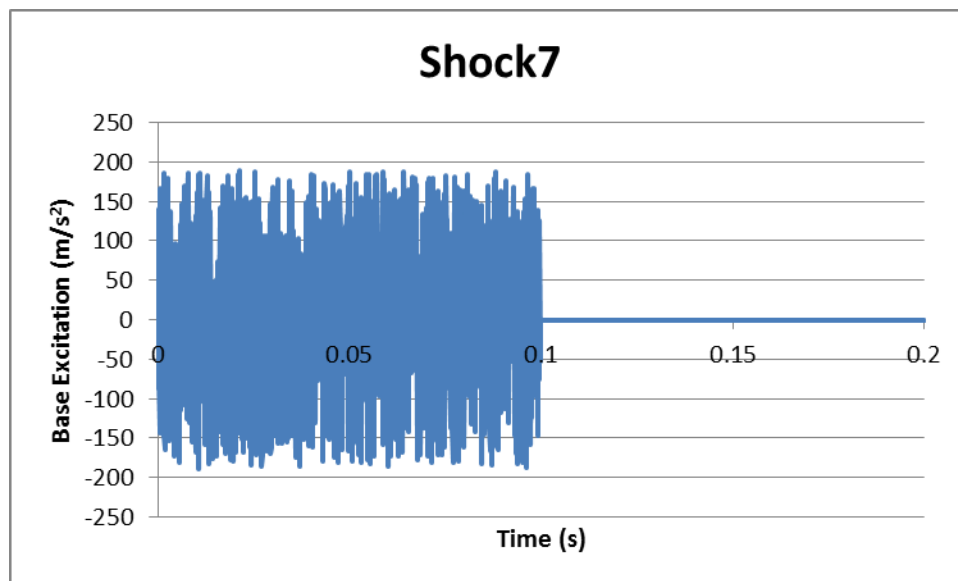


Figure A.4. Shock7, Acceleration Time History

Shock9 is simply a square pulse with a 100-ms duration and an amplitude that was chosen to flatten out the frequency response in Figure A.2 and bring it closer to the target. That goal was largely achieved, with the exception being the 10 Hz data point. Figure A.5 plots the Shock9 excitation curve. It has a much lower peak magnitude than Shock7, but its average pulse value is 18 m/s² while Shock7 is essentially zero. The Grms value of Shock9 is only 1.8, so it is significantly lower than the target of 11.2. Still, this pulse causes plastic deformation of the grids and cladding. While its frequency response is lower than some of the target frequencies (see Figure A.2) Shock9 is the middle ground in terms of permanent deformation of the fuel assembly components. Shock9 is most below the target response amplitude at 300 Hz and 600 Hz, and this seems to suggest that these higher frequency components are not a determinant of plastic deformation. Shaker test results should help determine the importance of including these higher-frequency ranges in modeling.

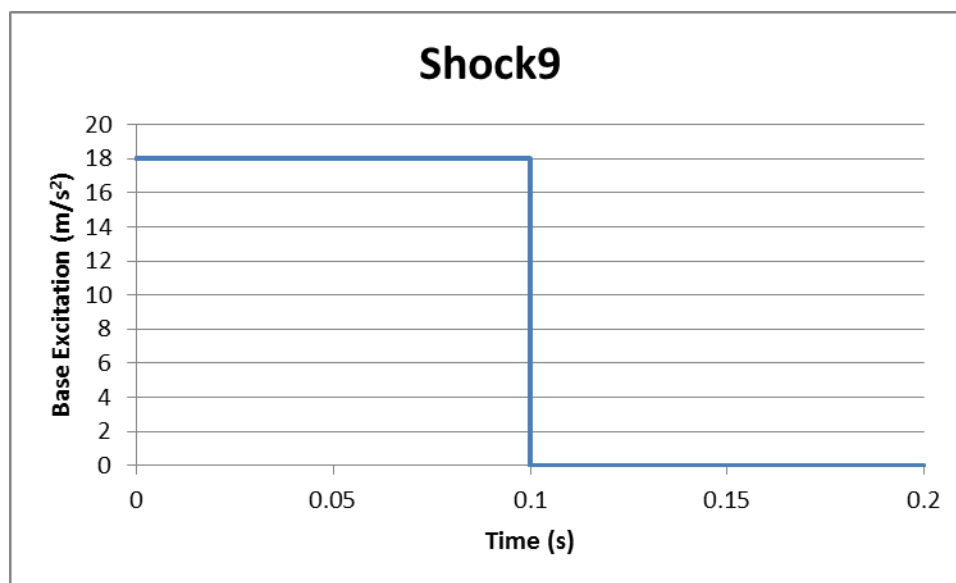


Figure A.5. Shock9, Acceleration Time History

These results show that the character of the shock loading will have a significant influence on the performance of the fuel assembly. The shock loading is not in a range where major damage to the fuel assembly is expected, but permanent deformation of the grid spacers is a possibility. The models predict that the impact forces on the grids could be enough to initiate grid buckling, and start to demonstrate the racking phenomenon. Racking is a term used in grid strength testing, referring to the sideways shifting of all the cells in a grid spacer row. This commonly happens when impact forces exceed the grid's instability limit, and the grid deflection character changes from linear elastic compression to a nonlinear, non-recoverable change in shape. This change in shape can alter the relative spacing of the fuel rods. Figure A.6 shows the model predictions of racking. This is an important threshold to watch for in testing, as it can have a significant effect on the grid's impact behavior if the grid buckling limit is exceeded. It is also important to determine if the PNNL grid model is an adequate predictor of this phenomenon. The next section will describe the fuel assembly shock response results in more detail.

A-4. Fuel Assembly Shock Load Results

The shock loading history that can be expected during the shaker table testing is not yet precisely defined. After test data have been collected, a more precise set of analyses can be conducted, with predicted results compared to actual physical results. This report attempts to anticipate the loading and the range of response with three distinct shock load cases. The random nature of the loading means that precisely predicting the excitation time history beforehand is impossible, so the concern of this study is to anticipate the range of shock response and identify major common trends.

Shock6 is the most damaging of the cases. One of the most striking predictions of the model is significant racking of some of the spacer grids. This is visible in Figure A.6, which shows the locations of plastic strain in the grids, and Figure A.7, which shows a cutaway view of the fuel assembly deformations in the basket at the last time step of the analysis. The deformation of the grids in Figure A.7

is mostly permanent, but the cladding and other fuel assembly components are still in motion and have not yet settled to a final static state. The Shock6 analysis also predicts plastic strain in a number of cladding tubes in the vicinity of spacer grids. Figure A.8 shows the plastic strain in the cladding, in the magnitude range of up to 7 percent. The bottom end of the cladding is not included because it shows plastic strains above 20 percent that appear to be artificial. Major plastic strain in the cladding ends and in the nearby guide tubes occurs before any significant impact occurs, which suggests it is purely artificial. It also occurs in all three cases at the same time steps. This is something that needs to be resolved in the follow-up work, but is not believed to affect results away from the bottom end. Figure A.9 shows what is considered to be credible plastic strains in the guide tubes, and occurs at the second grid spacer from the top end. It only occurs on the side nearest the floor side of the fuel basket. The figure also shows significant instantaneous elastic deflection of the guide tube array at 25 ms. The plastic strain in the guide tube is permanent, but the elastic deflection settles back to the original dimensions over time.

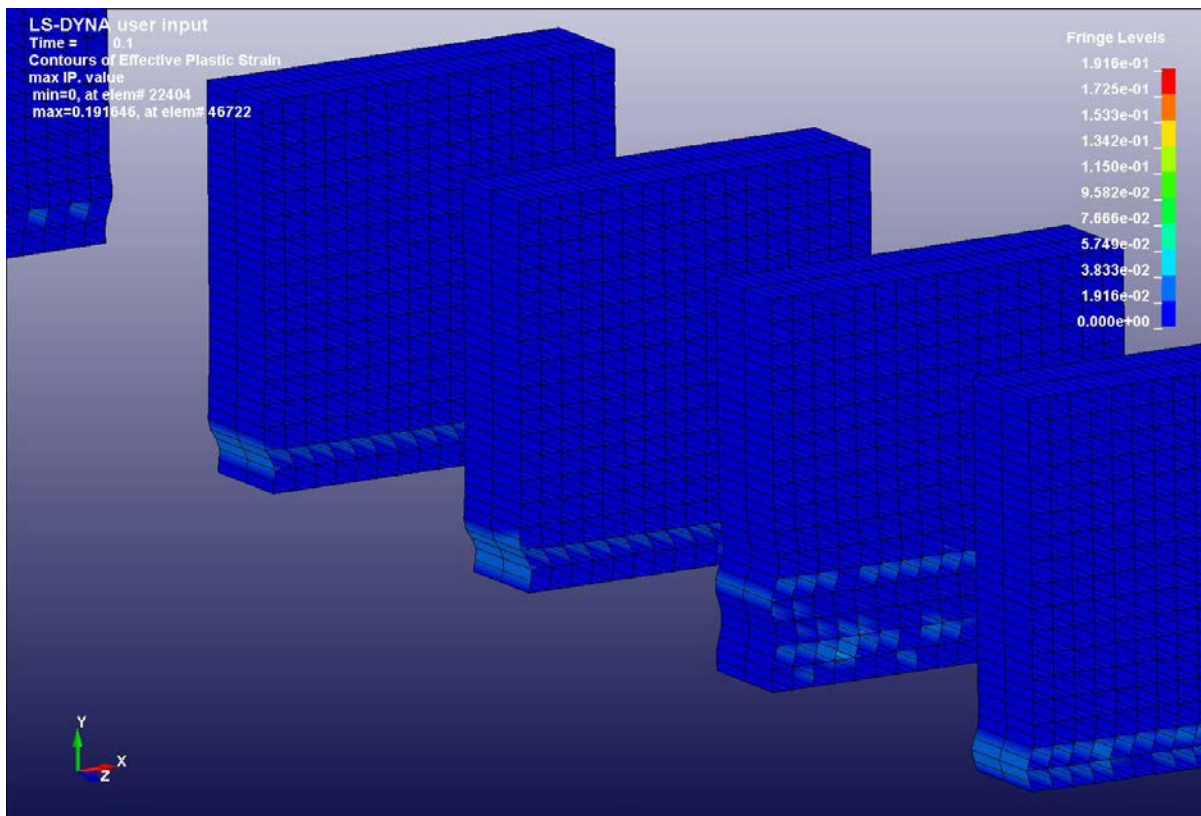


Figure A.6. Shock6, Plastic Strain in Grids

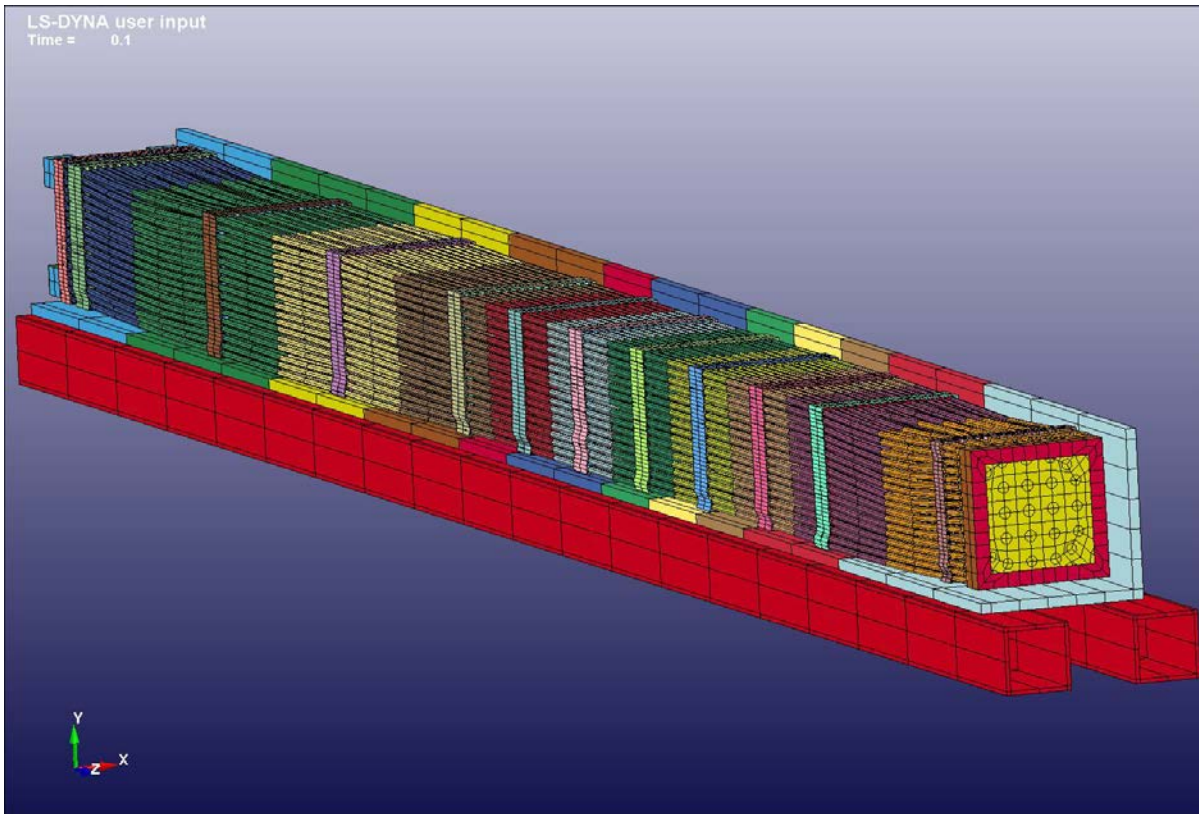


Figure A.7. Shock6, Cutaway View of Fuel Assembly in Basket

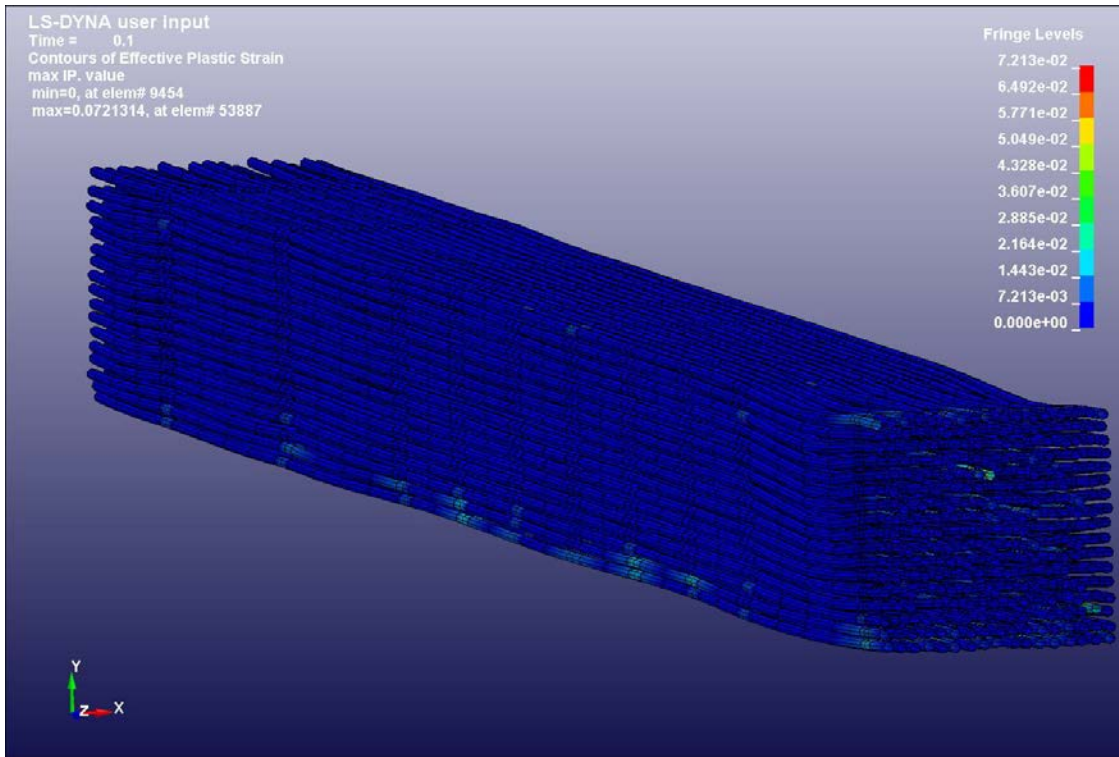


Figure A.8. Shock6, Plastic Strain in Cladding

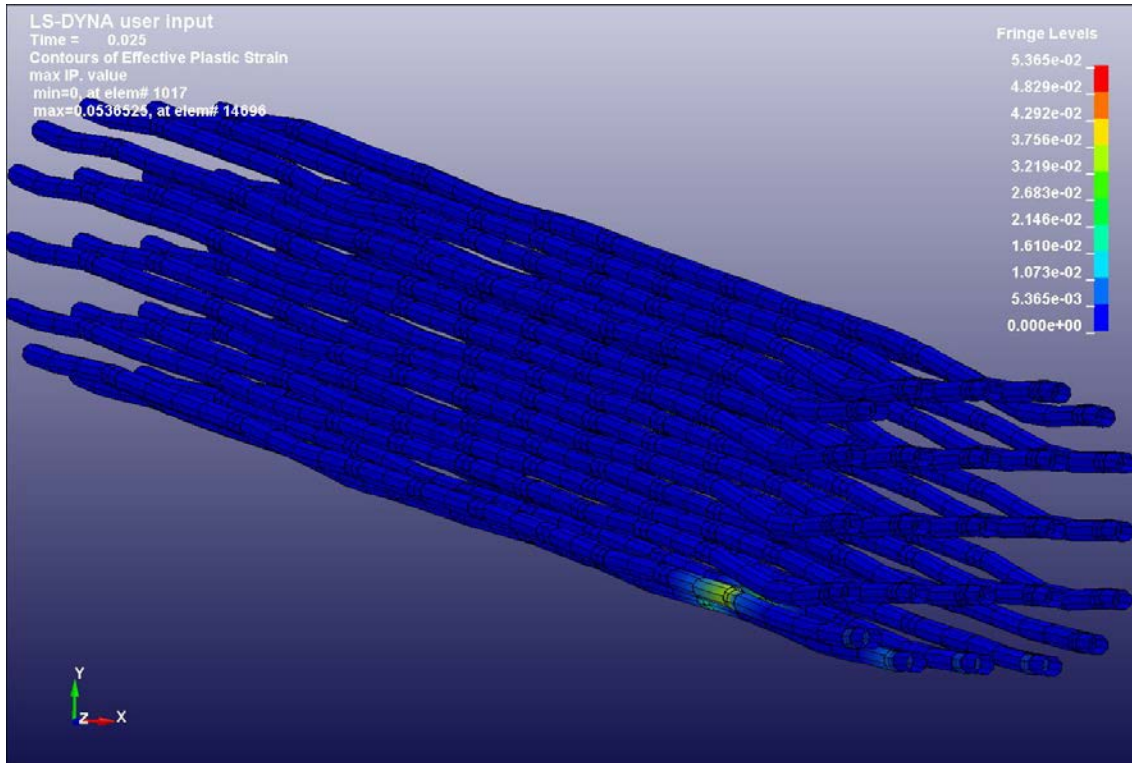


Figure A.9. Shock6, Plastic Strain in Guide Tubes

Shock7 is the least damaging of the cases, and does not predict any plastic deformation of the grid spacers. In this case the impact response of the grids to the basket remains perfectly elastic. Since the Shock7 frequency response spectra are above the target at all frequency control points, this case could be representative of the shaker table loading. If it is, we may not see any racking of the grid spacers during testing. This case predicted some plastic strain in a number of cladding tubes at grid locations. Figure A.10 shows the plastic cladding strain locations, but note that the visible contour levels are near 0.001 equivalent plastic strain, or 0.1 percent. This is for the annealed copper tubing wall case, which has a relatively low yield threshold (69 MPa or 10 ksi) and a long elongation range until the ultimate strength is reached. The bottom end of the cladding is not plotted because the local plastic strains there are thought to be purely artificial.

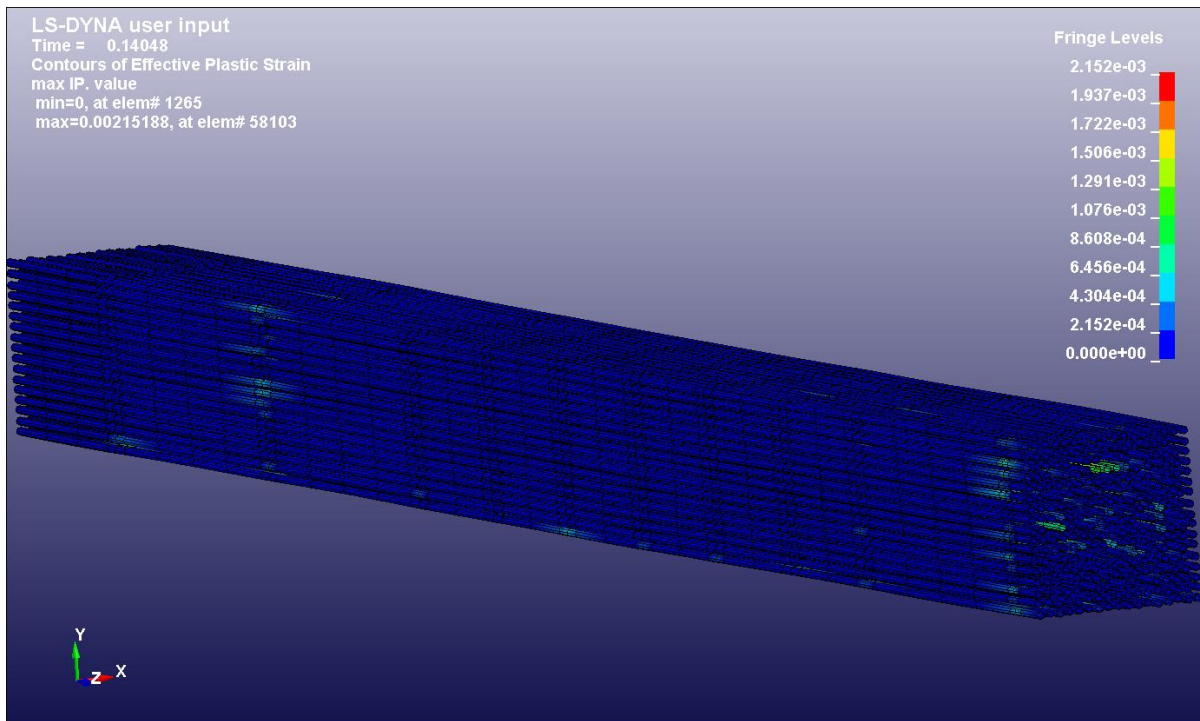


Figure A.10. Shock7, Plastic Strain in Cladding Locations

Shock9 was the middle case in terms of damage to the fuel assembly. It predicts some racking of the grids and plastic strain in the cladding at various locations, but no credible plastic deformation of the guide tubes. Figure A.11 shows plastic strains in one of the grids, localized in the two cell rows closest to the bottom of the figure. Note that the coordinate system axis is shifted in this plot, and the racking occurs on the side of the grid that impacts the “ceiling” surface of the basket. Overall there was much more racking in Shock6 than Shock9. Like both other cases, some plastic strain in the cladding is predicted at various locations near the grids. Figure A.12 shows plastic strain in the cladding, in the range of 1 to 2 percent, which is more deeply into the plastic range than the Shock7 case. Since this material is copper tubing, it is not clear that the stronger Zircaloy-4 would experience the same, or any, plastic strain in the cladding.

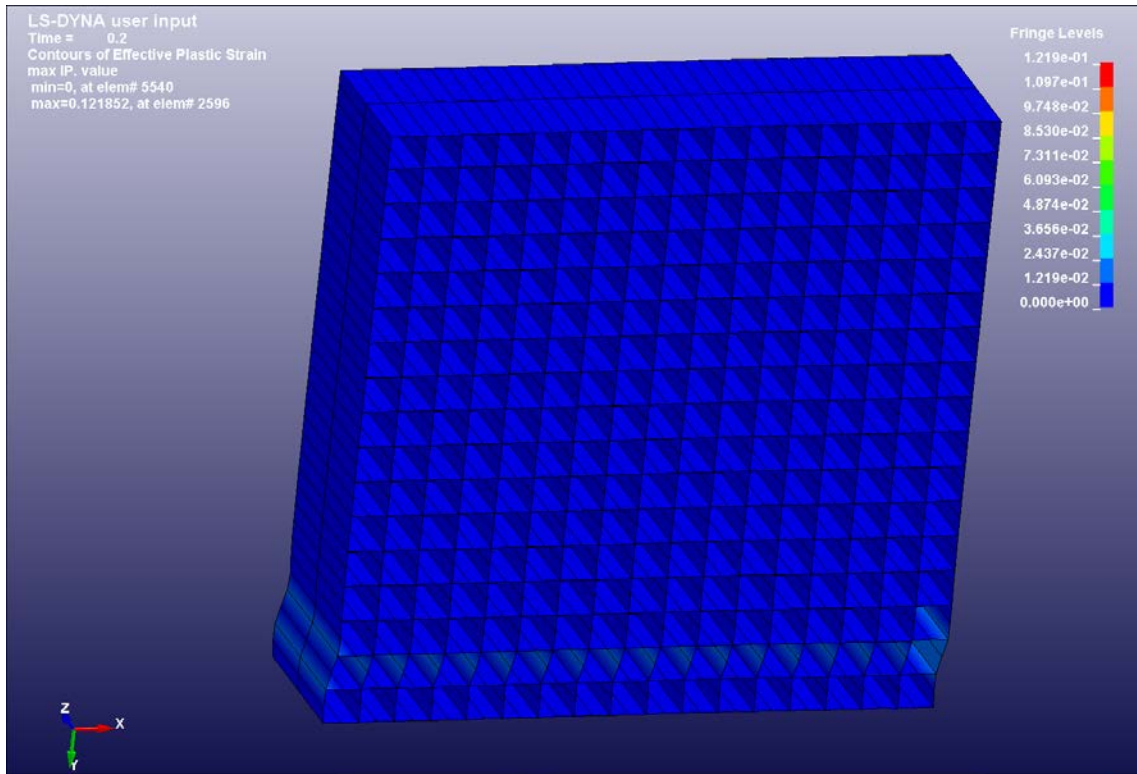


Figure A.11. Shock9, Plastic Strain in Grid

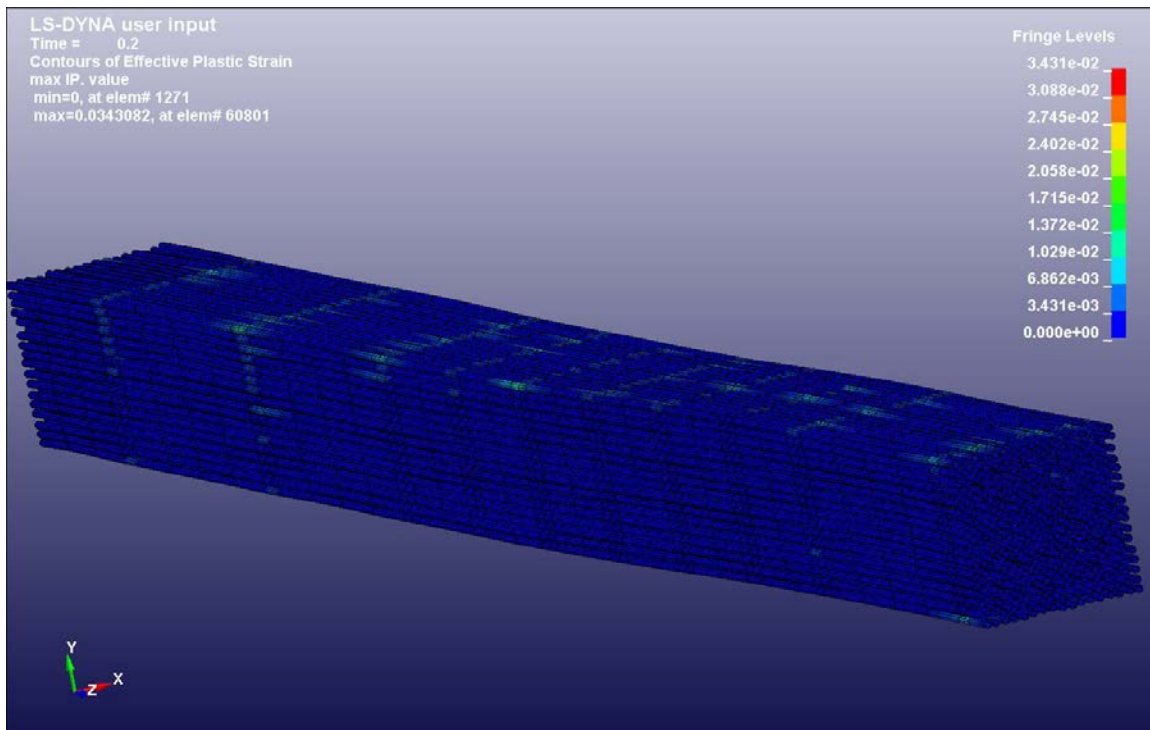


Figure A.12. Shock9, Cladding Plastic Strain

One modeling issue recognized in all three cases is a problem with the interaction between the ends of the cladding and the bottom tie plate. This appears to be an issue with the contact definition between beam ends and shells, or potentially an issue with small element sizing, leading to unrealistically high plastic strains in the end cladding elements. The nearby guide tubes also experience plastic straining that is only attributable to this problem because it happens identically in all three cases before the first fuel assembly impact with the basket occurs. Whatever the source of the problem, this is dealt with by removing highly strained elements from the model. This includes some elements at the ends of the cladding, but does not include the guide tubes, which maintain their integrity throughout every load case. The effect of removing cladding end elements is localized and would not affect the results far removed from the location. This is an issue that we would like to correct in the follow-up work, by modifying the finite element primitives and composition.

The one common result in all three cases is plastic strain predicted at various cladding locations. All incidents of cladding plastic strain occur at or near grid spacers, but aside from that there is no other distinguishing trend to identify where strain gauges should be placed. In Shock6 the strains occurred most frequently in the two rows closest to the “floor” of the basket. In Shock9 the strains were most frequent near the “ceiling” of the basket. This suggests that the major impact could occur when the fuel assembly makes contact with either basket surface, depending on the particulars of the shock excitation. The current version of the model uses copper cladding throughout the fuel assembly, with a yield strength that is based on annealed copper tubing. The Shock7 case had very little plastic strain, and when the stiffness contribution of the lead wire is considered, there is a potential the plastic strain would disappear. Depending on the amount of actual cold work in the cladding, there may not be any permanent cladding deformation in the actual shaker table experiments. Strain gauges would at least be helpful in determining how closely the cladding gets to the yield threshold.

The three sets of case results suggest there is a potential for grid racking. Grid racking would be apparent from visual inspection, but accelerometers could be placed in the guide tubes at grid elevations to record the impact response of the grids. Accelerometer data would help capture the time history response that directly affects the grid response, whether it leads to racking (buckling or instability) or not (remains elastic).

In the most damaging case, plastic deformation of the guide tubes occur away from the questionable bottom tie plate region. Since this only happened in the most damaging case, this may not be representative of what can be expected in the shaker testing.

These analyses provide insight into the shock load testing and the range of potential fuel assembly response. Some of the uncertainty in the range of results could be removed by additional information from the shaker table, such as a sample acceleration time history data set. None of the results predict gross structural failure of any of the fuel assembly components. The anticipated range of response to shock loading is in the high-elastic or low-plastic deformation structural range for this testing initiative.

A-5. Recommendations for Instrumentation

The first recommendation for instrumentation is to put a string of accelerometers inside the guide tubes at all spacer grid locations. These are needed to capture the gross deflection and motion of the fuel assembly throughout its response, along its full length. There are 12 spacer grids and 25 guide tubes. The grids and tubes form the major skeleton structure of the assembly. If four accelerometers can be placed at the four corner guide tube locations of all 12 grid elevations, the gross dynamic behavior of the fuel assembly will be well recorded. Each set of four accelerometers can be averaged to determine the average motion of the section. Taken individually, each accelerometer will give insight into the impact behavior (with the floor and ceiling of the basket) throughout the grid. The collected data will help us understand the dynamic grid impact forces and why the grid does or does not rack. This recommendation is a total of 48 small accelerometers. If this number is not feasible, a minimum of three accelerometers placed down the central tube at the bottom, middle, and top spacer grid elevations are recommended. In this type of testing, more accelerometers are preferred because sometimes individual accelerometers can malfunction, or their data can become corrupted or lost.

Because of the geometry and design of spacer grids, cladding strains are expected to be highest at their contact points in the vicinity of the grids. This is where bending moments are at a maximum. Because of the uncertainty and variability of the shock loads, the modeling does not identify a best location to put strain gauges on the cladding. However, some suggestions can be made. For reference, with the fuel assembly resting horizontally on the shaker table, “top” refers to the row of cladding that is closest to the basket ceiling, while “bottom” is resting on the basket floor. Based on the results, it is suggested to place strain gages on fuel cladding on the top and bottom, close to the edge of a grid spacer. The local cladding may not happen to exceed the elastic limit, but the strain history from a few random locations (on both top and bottom surfaces) should record typical bending behavior and provide insight throughout the assembly. These data would be highly valuable for model validation, even if they do not record plastic strains. Strain gauges should not be placed on the sides of the cladding circumference to avoid the bending neutral axis. To measure strain in the cladding of a top location, the strain gauge should be on the top outside surface, unless this will bring the gauge into contact with the basket wall. Shifting the gauge circumferentially up to 45 degrees to avoid contact should still be a reasonable option, as would be moving the gauge to the next cladding row in the assembly.

The limited number of Zircaloy-4 rods should be placed on the four corners of the array, because it is not guaranteed that the worst impact will occur at the side closest to the shaker table or farther away from it. The shaker shock impulse could be strong enough to hurl the assembly against the basket “ceiling” instead of the “floor”. Spreading them around the assembly will help deal with the uncertainty of the loading conditions until a better loading time history can be assembled.

SNL staff discussed the possibility of testing the shaker table without the fuel assembly on it to capture an actual shock time history. It would be even better to collect these types of data for the whole test fixture and basket assembly prior to fuel assembly testing. This would be ideal to refine the model results and better approximate the actual test conditions beforehand. If this can be done, the time history can be used directly in the model. SNL may need to include a dummy mass to represent the fuel assembly on the

shaker table to make sure the accelerometer data are representative—it would be best to discuss this with SNL’s expert in testing methodology prior to commencing testing.

A-6. Follow-up Work

SNL recently asked for all the cladding in the model to represent Zircaloy-4 instead of copper. This change has not yet been made because of time constraints. In order to meet SNL’s request, the cladding model needs to be modified to make it all Zircaloy-4 instead of the copper that it is now. This is a minor change to the input file, but it needs to be done with care, so no errors are introduced. In preparing this progress report, most of the effort was devoted to evaluating the loading conditions and how the various cases compared to the target load spectrum. The models take approximately 24 hours to solve.

The current models did not adjust the copper cladding modulus to reflect the stiffness contribution of the lead wire. The effect on the results should be evaluated to determine how much of a difference it makes. It is not anticipated to make a large difference in terms of grid racking or guide tube strains, but it may affect cladding strains or have an unexpected effect on the gross dynamic response of the assembly.

The three load cases discussed in this report are intended to represent the range of potential response in the shock loading conditions. The spectral evaluation shows the three cases are not perfectly aligned with the target spectrum, and additional time history construction techniques could be employed to define an excitation curve that is a closer match to the target. Alternatively, SNL may be able to provide additional information to guide the excitation curve construction, including actual time history acceleration data collected from the shaker. As it stands now, two cases out of three predict grid spacer racking, but it is not clear which of the three cases most closely represents the actual test conditions. It would be desirable to generate at least one more excitation history, whose frequency response spectrum closely matches the target spectrum to represent the best estimate load case.

As mentioned in the Fuel Assembly Shock Load Results section, a modeling issue is apparent near the bottom end of the cladding and the bottom tie plate. This appears to be a localized numerical problem that can be resolved through adjustments to the finite element model. This issue is not expected to be a major concern, but it could potentially affect the recommendation to instrument the guide tubes with strain gauges. It may also point to other instrumentation recommendations.

A-7. Conclusions

Significant progress has been made in modeling the shaker table experiment and predicting the range of response. Some uncertainty in the loading still exists and the model has a couple issues that need to be resolved before the study can be considered final, but the results seem to paint a reasonable picture of the anticipated fuel assembly response. Grid deformation appears to be a possibility, and instrumenting the fuel assembly to capture this behavior would be extremely valuable.

Appendix B: Modal and Static Analysis of the Detailed Fuel Assembly Model

B-1. Modal Analysis

Modal analyses of the WE 17×17 assembly were performed to determine the natural frequencies and mode shapes of the assembly. Modal analyses are generally quicker than a full dynamic analysis and can be used to determine the sensitivity of the dynamic response of the assembly to different input parameters or modeling choices. Modal analyses were performed first on the Rev 1 model (described in Section 2.2 of this report) and then on the Rev 2 model (described in Section 2.3 of this report).

To create the modal analyses models, the ANSYS LS-DYNA assembly macros used in the full shaker table runs (first for Rev 1 and later for Rev 2) were modified to work in the ANSYS implicit simulation environment. The element types in the macros were each switched from the explicit element types to corresponding implicit element types. Spot welds between the guide tubes and the spacer grids were replaced with coupling all six degrees of freedom (3 translational + 3 rotational) at each of these spot weld locations. Additionally, all rods were restricted from rotating about their longitudinal axis to prevent each rod from being allowed to making the free body motion of “barrel rolling.”

Extensive sensitivity studies were run on the Rev 1 version. The Rev 1 sensitivity studies are presented in Table B.1. Later, a smaller set of modal analysis were run on the Rev 2 version of the model; these are presented in Table B.2.

Three main categories of parameters were studied: the boundary conditions, the rod material, and the spacer-grid-to-rod connections. The boundary conditions parameters refer to whether the assembly end caps were left free to deform (denoted as Free-Free) or were fixed in all six degrees of freedom at both ends (denoted as Fixed-Fixed). Most of the cases were run for both Free-Free and Fixed-Fixed boundary conditions.

The rod material category refers to what material the rods were and how they were modeled; these include: variations the use of overlapping beams versus adjusted density beams; the use of copper rods, Zircaloy-4 rods, or a combination thereof; the use of increase modulus Zircaloy-4; or the use of Zircaloy-4 exposed to high temperature. Cases 1, 2, 15, and 16 have all the rods modeled as copper using beam elements that have the same outer diameter (OD) and inner diameter (ID) as the copper rods but the density is adjusted to account for the weight of the lead inside the copper rods. The material properties used in these density-adjusted nominal copper rod cases are summarized in Table B.3. Cases 11 and 12 have all the rods modeled as copper with the same OD and ID as the copper rod without the density adjustment for the lead. Instead, a set of overlapping beam elements with same OD as the lead and lead material properties are added to this model. These overlapping beam elements share the same nodes, and thus the same degrees of freedom, as the copper rod elements. Cases 5, 6, 13, 14, and 17-20 use all nominal Zircaloy-4 cladding rods where the beam elements have the same OD and ID as the fuel cladding and the density adjusted for the weight of the fuel inside the cladding. The material properties of this density-adjusted nominal Zircaloy-4 rod are summarized in Table B.3. Cases 7 and 8 use the same density adjusted Zircaloy-4 beam elements, but the modulus of the Zircaloy-4 is increased by 10 percent.

Cases 9 and 10 use the same density adjusted Zircaloy-4 beam elements but the properties (see Table B.3) are adjusted for a high temperature.

Finally, the connection between the spacer-grid-shell elements and the fuel-rod-beam elements was run with several different modifications to determine the sensitivity of the dynamic response to this connection. Cases 1-12 use nominal axial springs and no rotational springs to connect the rod-beam element to the spacer-grid-shell elements. For each rod that passes through the spacer grid, there are four springs attaching the rod to the four sides of the closest spacer-grid-shell elements. The nominal axial springs are the springs that were in the existing assembly model that was modified to create the shaker table specific assembly model. The stiffness of this nominal axial spring is listed in Table B.3. Cases 13 and 14 use an increased axial spring stiffness of 100 times the nominal value. Cases 15-20 use the nominal axial spring in combination with rotational springs. The rotational stiffness of these springs, which are listed in Table B.1, vary from 1 N-m/radian to 10,000 N-m/radian. Two rotational springs are included for every axial spring (there are four axial springs for each rod at each spacer grid, see Figure 2.2); one rotational spring resisting rotation about each of the two transverse directions. As stated previously, rotational in the third direction, the longitudinal direction has been fixed to prevent the rods from barrel rolling.

A smaller set of modal analysis were run on the Rev 2 version of the model. These cases, Cases 21-24 are presented in Table B.2. These include Free-Free and Fixed-Fixed versions of an all nominal Zircaloy-4 assembly (Cases 21 and 22) and a mostly copper assembly with 3 Zircaloy-4 rods (Cases 23 and 24). These final two cases match the Rev 2 version used in the full dynamic shaker table analyses.

Table B.1. Modal Analysis Sensitivity Study Cases for Rev 1 Model

Modal Case Number	Boundary Conditions	Rod Material	Spacer Grid - Rod Connection
Case 1	Free-Free	All Cu - ρ adjusted for Pb	Nominal axial springs; no rotational springs
Case 2	Fixed-Fixed		
Case 3	Free-Free	Most Cu - ρ adjusted for Pb; 3 Nominal T Zirc	
Case 4	Fixed-Fixed		
Case 5	Free-Free	All Nominal T Zirc	
Case 6	Fixed-Fixed		
Case 7	Free-Free	All Nominal T Zirc 10% increase in modulus	
Case 8	Fixed-Fixed		
Case 9	Free-Free	All Hot T Zirc (only fuel rods and guide tubes modified)	
Case 10	Fixed-Fixed		
Case 11	Free-Free	All Cu - Overlap beams for Pb	
Case 12	Fixed-Fixed		

Table B.1. (contd)

Modal Case Number	Boundary Conditions	Rod Material	Spacer Grid - Rod Connection
Case 13	Free-Free	All Nominal T Zirc	100×Stiffness of nominal axial springs; no rotational springs
Case 14	Fixed-Fixed		
Case 15	Free-Free	All Cu - ρ adjusted for Pb	Nominal axial springs & 10,000 N*m/rad Rotational Springs
Case 16	Fixed-Fixed		Nominal axial springs & 10,000 N*m/rad Rotational Springs
Case 17	Free-Free	All Nominal T Zirc	Nominal axial springs & 1 N*m/rad Rotational Springs
Case 18			Nominal axial springs & 100 N*m/rad Rotational Springs
Case 19			Nominal axial springs & 10,000 N*m/rad Rotational Springs
Case 20			Fixed-Fixed

Table B.2. Modal Analysis Sensitivity Study Cases for Rev 2 Model

Modal Case Number	Boundary Conditions	Rod Material	Spacer Grid - Rod Connection
Case 21	Free-Free	All Nominal T Zirc	Nominal axial springs; no rotational springs
Case 22	Fixed-Fixed		
Case 23	Fixed-Fixed	Most Cu - ρ adjusted for Pb; 3 Nominal T Zirc	Nominal axial springs; no rotational springs
Case 24	Free-Free		

Table B.3. Nominal Material Properties

	Density [kg/m³]	Young's Modulus [Pa]	Poisson's Ratio	Notes
Nominal Zircaloy-4 Rod	4.73E+04	8.04E+10	0.3390	density adjusted for presence of fuel
High Temperature Zircaloy-4 Rod	4.73E+04	7.29E+10	0.3527	density adjusted for presence of fuel
Copper Rod	2.32E+04	1.15E+11	0.3200	density adjusted for presence of lead
Spacer Grid	8.41E+03	8.05E+10	0.3250	
Guide Tubes	8.41E+03	9.35E+10	0.3470	
High Temperature Guide Tubes	8.41E+03	7.23E+10	0.3527	
	Stiffness [N/m]			
Nominal axial spring	663.39			stiffness used in previous assembly models

For each of the cases listed in Tables B.1 and B. 2, a modal analysis was performed to search for modes between 0.1 Hz and 150.0 Hz. The lower bound was set to a small non-zero value, 0.1 Hz, to avoid the repeated rigid body modes that would be present at 0.0 Hz. The upper bound was cutoff at 150.0 Hz based on preliminary runs of the shaker table assembly model. As expected in a WE 17×17 assembly with many rods of the same properties, there are many repeated insignificant modes present in all the cases run. Each case returned between 6000 and 10,000 modes. The many insignificant mode shapes typically consist of one or several rods moving independent from the rest of the assembly.

To separate the important modes from the insignificant modes, the modes were ranked by their participation factor in the vertical direction. The choice was made to rank these modes by participation in the vertical direction, as opposed to any of the other five directions and rotations, since the shaker table input motion is in the vertical direction only. Additionally, the change in vertical cumulative mass fraction is also used to identify the important modes. The vertical mass fraction of a mode shape identifies how much mass of the assembly is involved in the excitation of a certain mode shape. The cumulative mass fraction starts at zero before any modes are found. As each natural frequency is reached, the fraction of the effective mass engaged by each mode shape is added to the cumulative mass fraction. Eventually the cumulative mass fraction will reach unity. The significant modes can be distinguished by large jumps in the cumulative mass fraction. The cumulative mass fraction provides the same information as the scaled participation factor; those modes with the greatest participation factor will also have the largest jump in cumulative mass fraction. However, it is sometimes easier to distinguish the important modes in a plot of cumulative mass fraction rather than a plot of participation factors.

Because the purpose of the Rev 1 modal analysis runs is to compare the effect that various model parameters have on the dynamic behavior of the assembly, not all cases in Table B.1 are presented.

Instead, comparisons between the results of various cases are made to determine the effect of each of the parameters studied. These effects are summarized after all of the comparisons are presented. Finally, Rev 2 modal analyses results from the cases in Table B.2 are presented to show the expected natural frequencies and mode shapes of an actual used fuel assembly and the actual shaker table assembly.

B-1.1 Full Shaker Table Runs: Rev 1 – Cases 3 and 4

The full shaker table runs using the Rev 1 model, presented in Section 2.2 of this report, use the same assembly properties as used in Cases 3 and 4 described in Table B.1. Cases 3 and 4 have three density-adjusted nominal Zircaloy-4 clad rods. The rest of the rods are density-adjusted nominal copper rods. These cases have the nominal axial springs connecting the rods to the spacer grids and no rotational springs in this connection. Case 3 has Free-Free boundary conditions while Case 4 has Fixed-Fixed boundary conditions.

Figure B.1 shows the scaled vertical participation factor of all modes found from 0.1 to 150 Hz for Case 3 and Case 4. The participation factors were scaled such that the largest participation factor is set to unity. The participation factors indicate that there are several significant modes from 0 to 5 Hz for Case 3. Greater than 5 Hz, Case 3 shows that there are only two other frequencies that have any significant mode shapes, 11.4 Hz and 56.8 Hz. Case 4 has significant modes spread out all the way up to nearly 150 Hz, but the most significant modes are from 0 to 26 Hz.

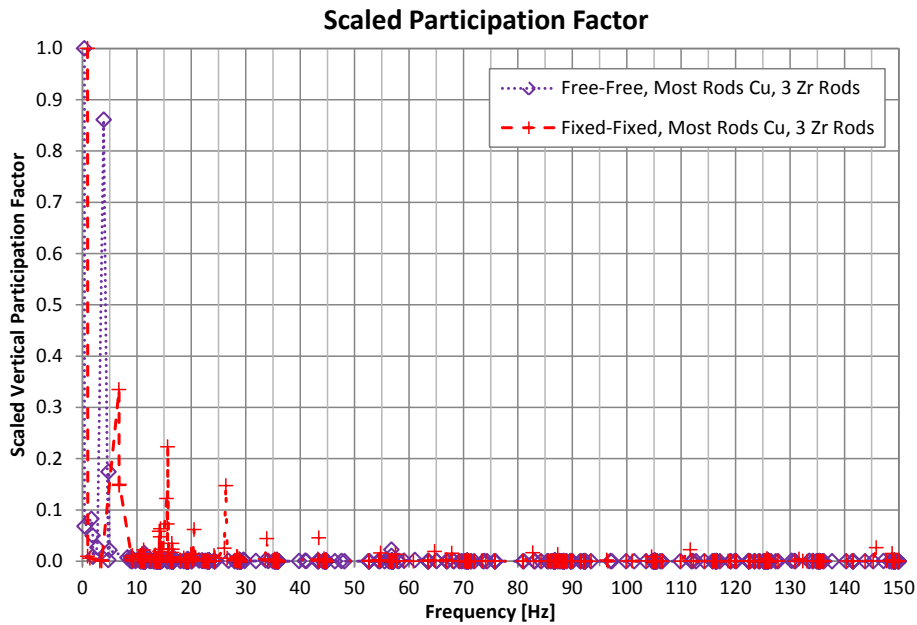


Figure B.1. Scaled Vertical Participation Factor for Cases 3 and 4, Rev 1

Another way to identify which mode shapes are important is to observe the vertical cumulative mass fraction. Figure B.2 shows the vertical cumulative mass fraction from 0.1 to 150 Hz for Case 3 and Case 4. The largest increases in the cumulative mass fraction occur at frequencies below 5 Hz for Case 3 and below 16 Hz for Case 4.

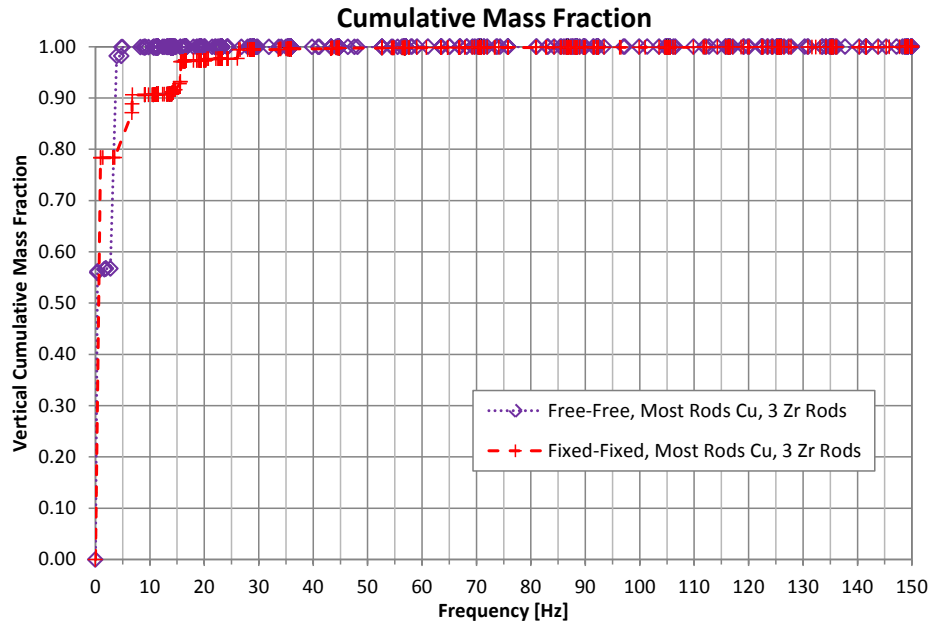


Figure B.2. Vertical Cumulative Mass Fraction for Case 3 and Case 4, Rev 1

Figure B.3 shows the Case 3 mode shapes for the six most significant modes (i.e., the modes with the largest vertical participation factor) from an isometric view point. The contours represent the vertical deformation with red being the highest and blue being the lowest. The actual values of the contours do not matter for mode shapes since the displacements are arbitrarily scaled. Only the relative deformation of one part of the assembly to another part of the assembly matters for modal analysis. The mode shapes are numbered 1 to 6 in order of their significance. The first-, third-, and sixth-most-important modes show vertical deformation of the entire assembly. The second-most-important mode shows shear deformation in the longitudinal direction. The fourth and fifth most important modes show torsional deformation.

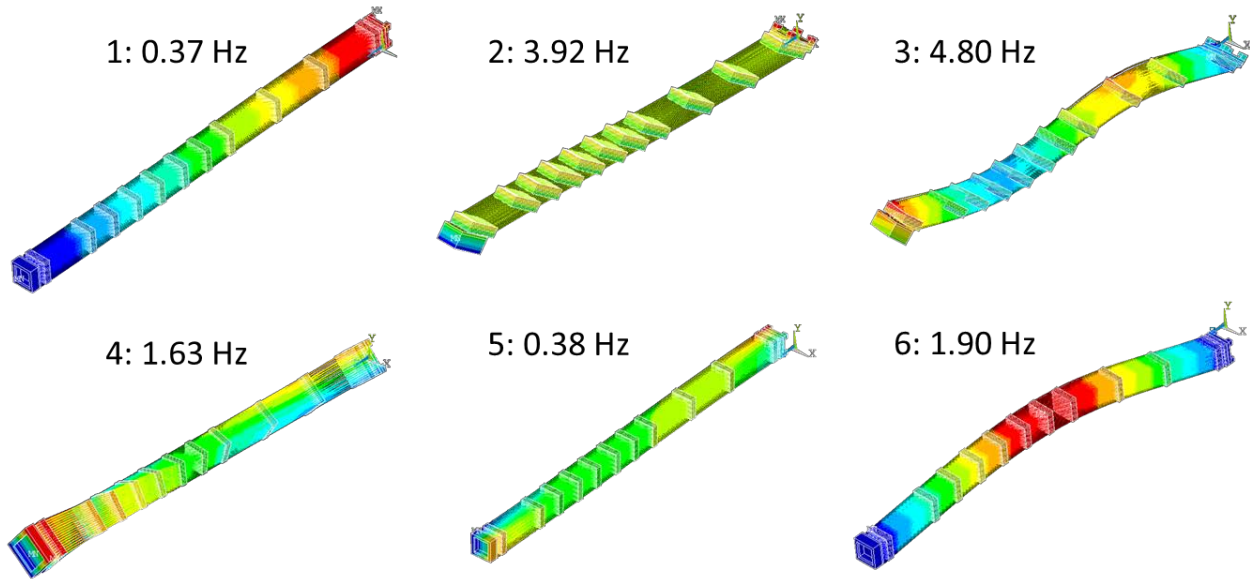


Figure B.3. The Six Modes Shapes with the Largest Vertical Participation Factor for Case 3, Rev 1

Figure B.4 shows the Case 4 mode shapes for the six most significant modes. The mode shapes are numbered 1 to 6 in order of their significance. The first and sixth most important modes show vertical deformation of the entire assembly. The second, fourth, and fifth most important modes show torsion of the assembly. The third most important mode shape shows the three Zircaloy-4 rods moving independently of rest of the assembly.

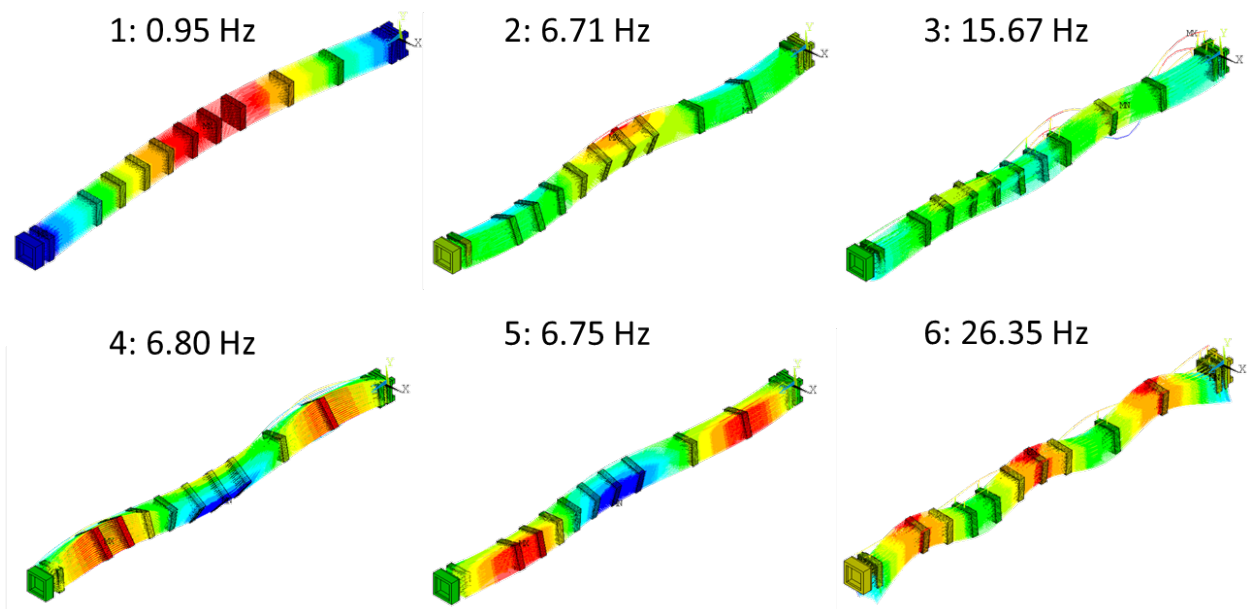


Figure B.4. The Six Modes Shapes with the Largest Vertical Participation Factor for Case 4, Rev 1

B-1.2 Influence of Boundary Conditions: Rev 1 – Case 1 vs. Case 2

The assembly will be resting inside a mock basket on the shaker table. The assembly itself is not physically connected to the basket. During loading, parts of the assembly may lift off from the basket while other parts may not. Because of the uncertainty in the boundary conditions during the shaker table, experiment cases were run with both Free-Free and Fixed-Fixed boundary conditions. Any of the pairs of Free-Free and Fixed-Fixed cases in Table B.1 or B.2 may be used to examine the effect of boundary conditions but Case 1 and Case 2 will be used as an example. Case 1 and Case 2 both have all copper rods with the density adjusted for the lead as well as the nominal axial spring connection. The only difference between Case 1 and Case 2 are the boundary conditions. Case 1 is free while Case 2 is fixed at the end caps. This difference leads to significant differences in the natural frequencies and mode shapes.

Figure B.5 and Figure B.6 present the scaled vertical participation factor and the vertical cumulative mass fraction for both Cases 1 and 2. It is seen that Case 1 has the majority of its important mode shapes below 5 Hz, with one more important mode shape at 14 Hz. The important mode shapes for Case 2 are spread out throughout the frequency range with the most significant shapes below 30 Hz. Some semi-significant shapes still appear all the way up to 150 Hz.

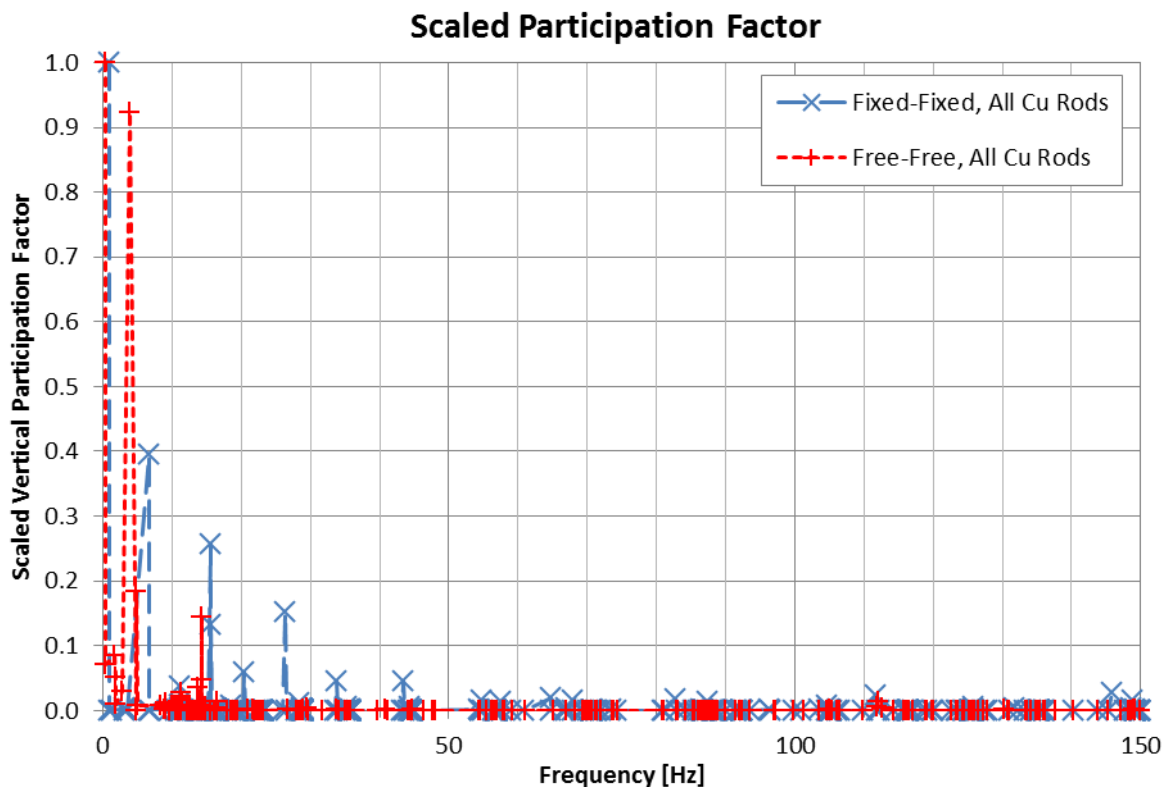


Figure B.5. Scaled Vertical Participation Factor for Cases 1 and 2, Rev 1

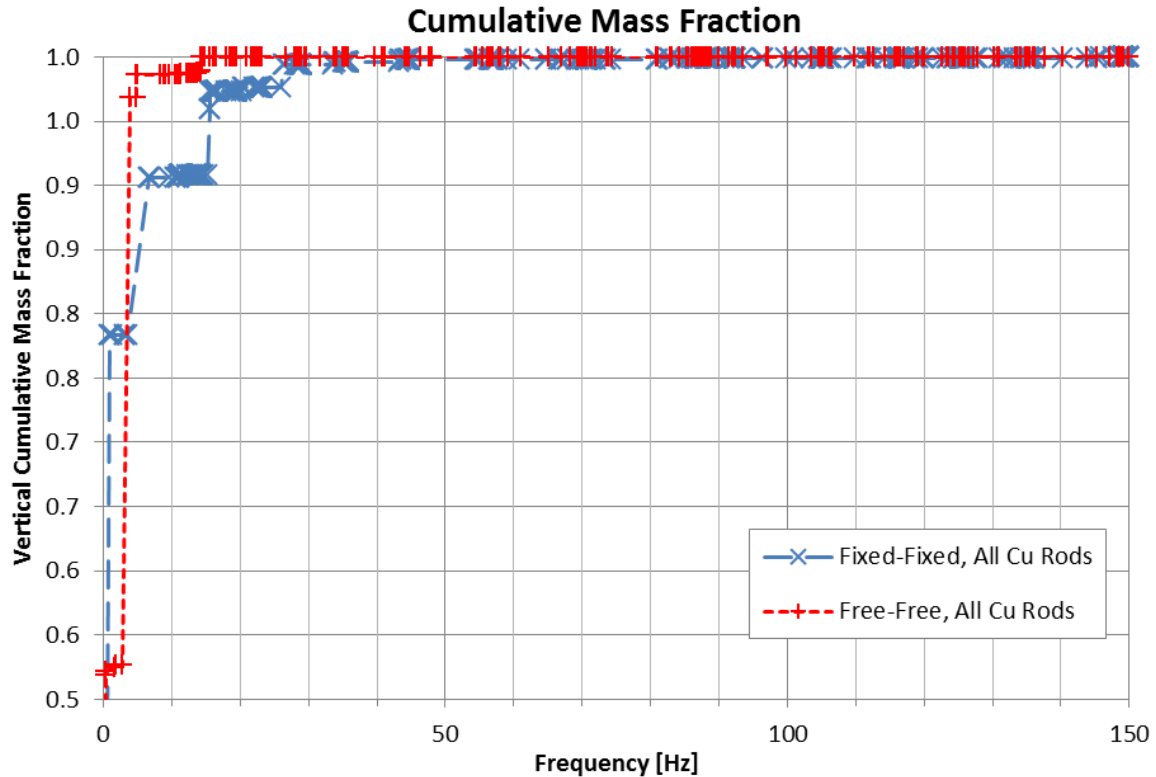


Figure B.6. Vertical Cumulative Mass Fraction for Cases 1 and 2, Rev 1

Figure B.7 and Figure B.8 show the top six mode shapes and frequencies for Case 1 and Case 2 respectively. Case 1 mode shapes are very similar to Case 3 mode shapes shown in Figure B.3 with the exception of a rod expansion mode shape at 14.22 Hz which bumps one of the vertical mode shapes out of the top six. Case 2 shows a significant change in the mode shapes. By fixing the end caps of the assembly the torsional and shearing mode shapes have been eliminated. The top six mode shapes are all mode shapes that involve significant vertical motion of the entire assembly. In some cases all of the rods are moving in unison but in others a subset of the rods will move independently of the rest of the assembly.

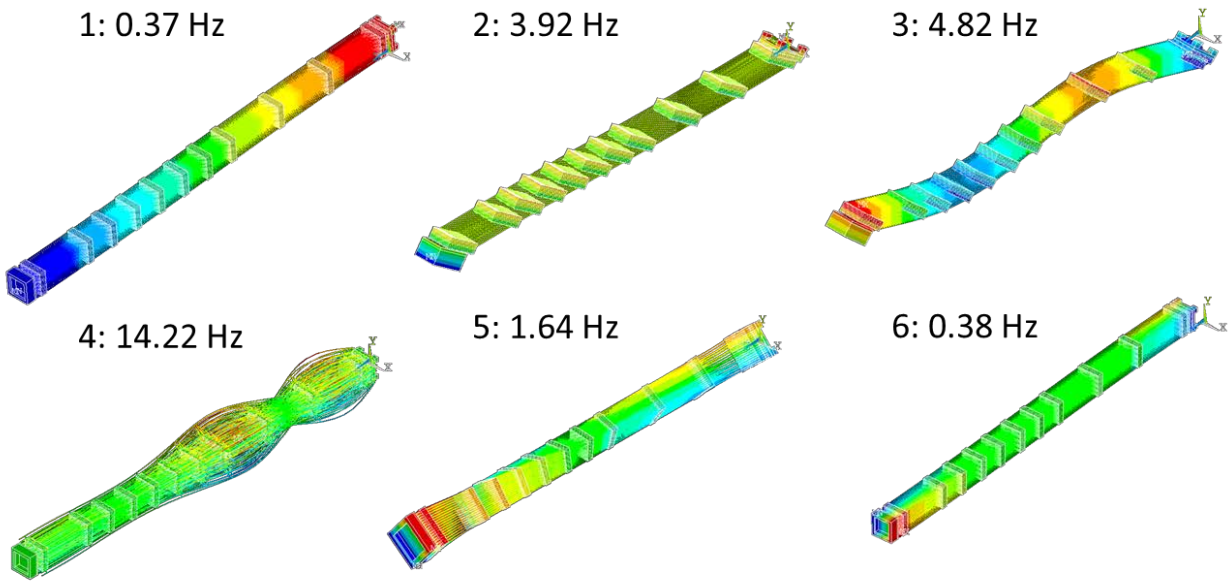


Figure B.7. The Six Modes Shapes with the Largest Vertical Participation Factor for Case 1, Rev 1

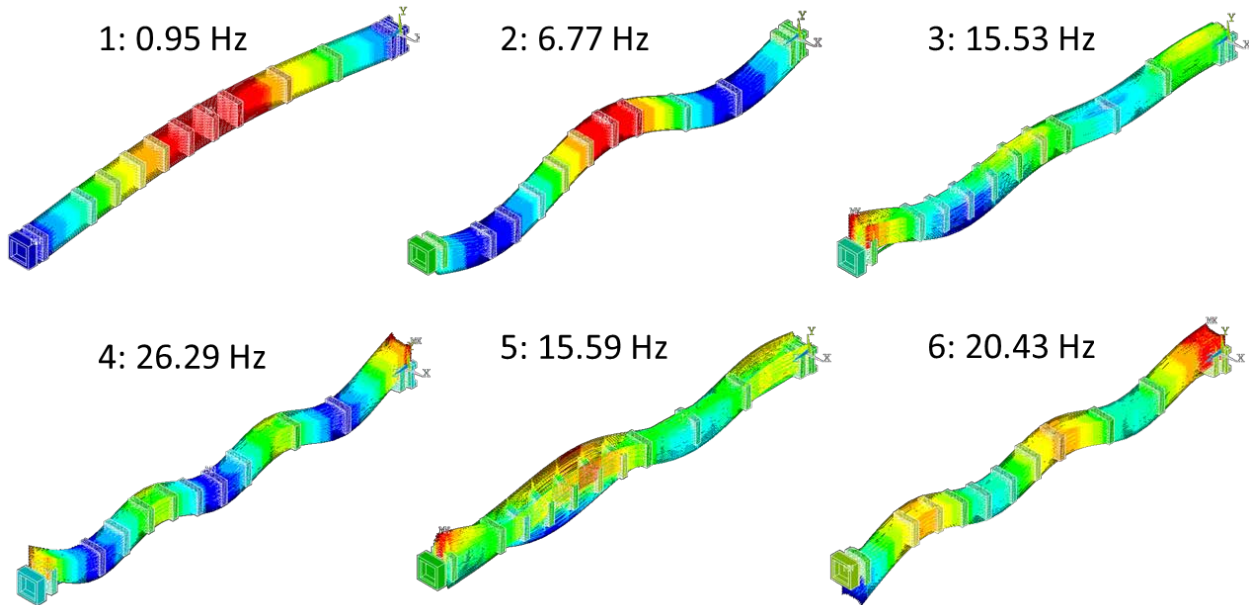


Figure B.8. The Six Mode Shapes with the Largest Vertical Participation Factor for Case 2, Rev 1

B-1.3 Rod Material: Rev 1 – Cases 1, 3, 5, 7, and 9

The rod material may play an important role in the dynamic response of the assembly. To understand this role better, Cases 1 (all copper rods with density adjusted), 3 (mostly copper rods with three Zircaloy-4 rods all with density adjustment), 5 (all Zircaloy-4 rods with density adjusted), 7 (all Zircaloy-4 rods with 10 percent increase in modulus and density adjusted), and 9 (all Zircaloy-4 rods with high temperature properties) are all compared on the same axes. These five cases all use the same nominal axial spring properties with no rotational springs and Free-Free boundary conditions.

Figure B.9 and Figure B.10 show the scaled vertical participation factor and the vertical cumulative mass fraction respectively for Cases 1, 3, 5, 7, and 9 only up to 30 Hz. Beyond 30 Hz there are no significant modes for these cases. Generally speaking, it is seen that the most significant modes are all below 5 Hz regardless of the material used for the rods. Some smaller significance modes do show up between 11 and 15 Hz for some of the cases.

Figures B.11, B.12, and B.13 show the six mode shapes with the highest vertical participation factor for Cases 5, 7, and 9 respectively. The six significant mode shapes are very similar to each other and those for Case 3 presented in Figure B.3. They are also very similar to the mode shapes for Case 1 presented in Figure B.6, except for the lack of the expansion mode shape near 14 Hz.

Based on these results, whether the rods are copper or Zircaloy-4, a combination of the two materials, 10 percent stiffer zirconium alloy, or high-temperature Zircaloy-4, the significant frequencies and modes are very similar. Generally, the material of the rods has a minor influence on the most significant natural frequencies and mode shapes of the assembly.

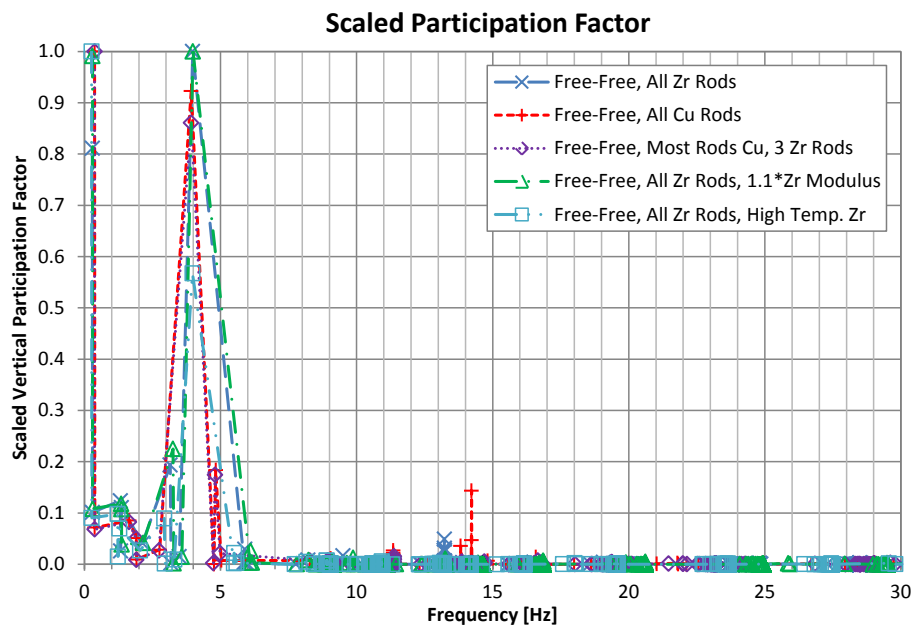


Figure B.9. Scaled Vertical Participation Factor for Cases 1, 3, 5, and 7, Rev 1

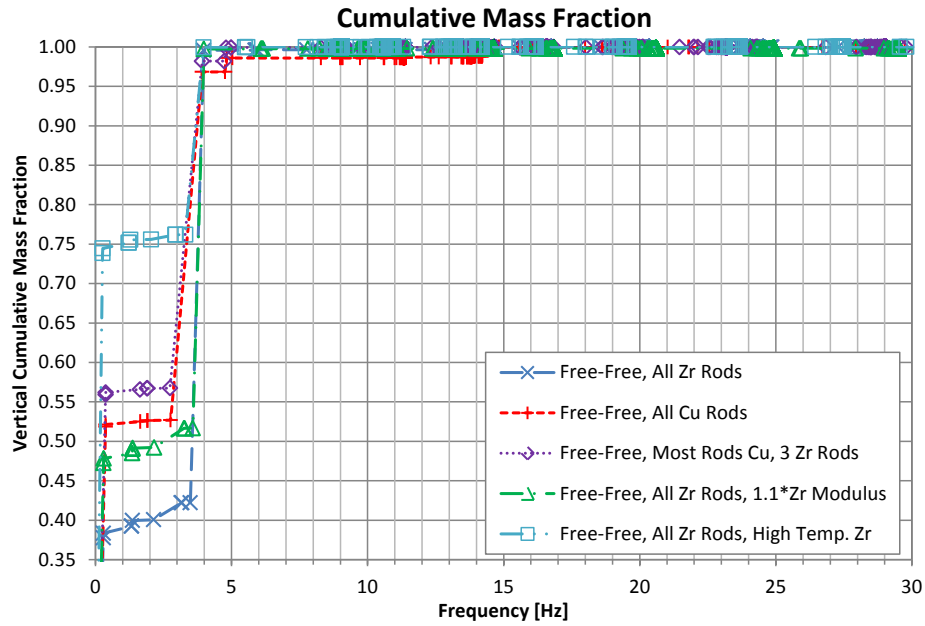


Figure B.10. Vertical Cumulative Mass Fraction for Cases 1, 3, 5, and 7, Rev 1

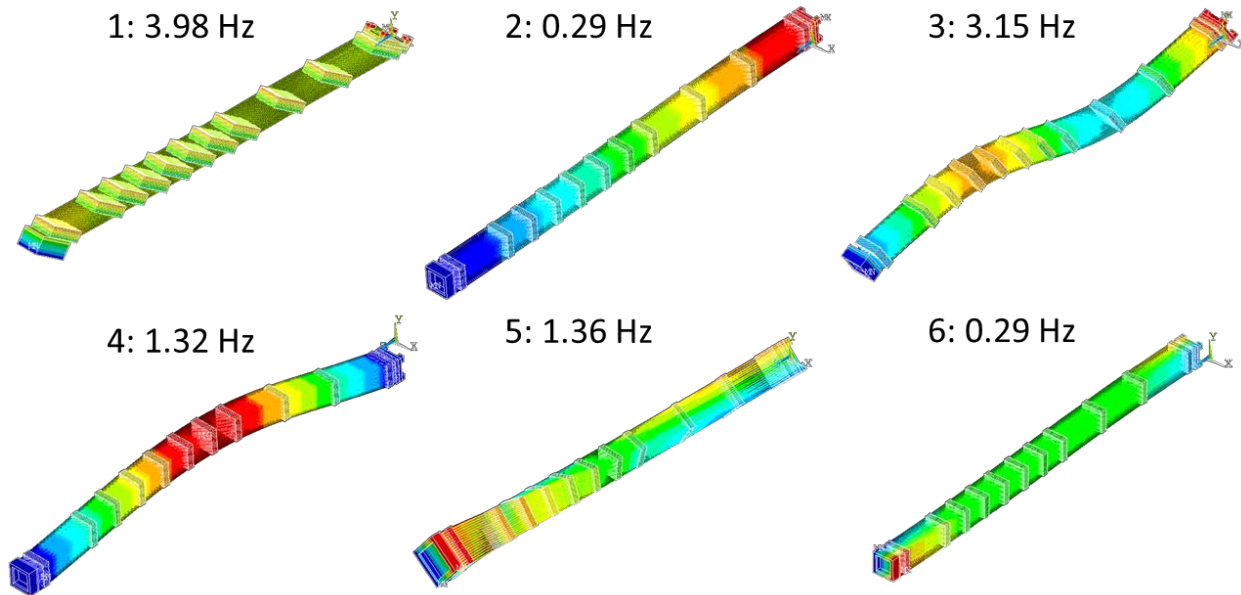


Figure B.11. The Six Mode Shapes with the Largest Vertical Participation Factor for Case 5, Rev 1

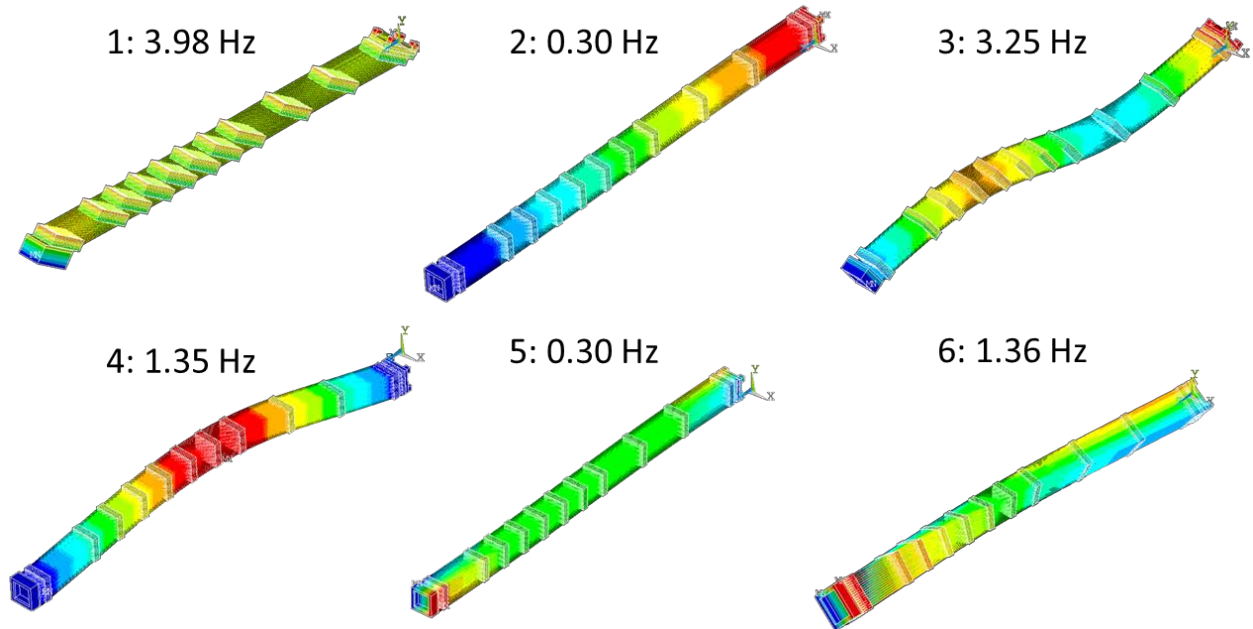


Figure B.12. The Six Mode Shapes with the Largest Vertical Participation Factor for Case 7, Rev 1

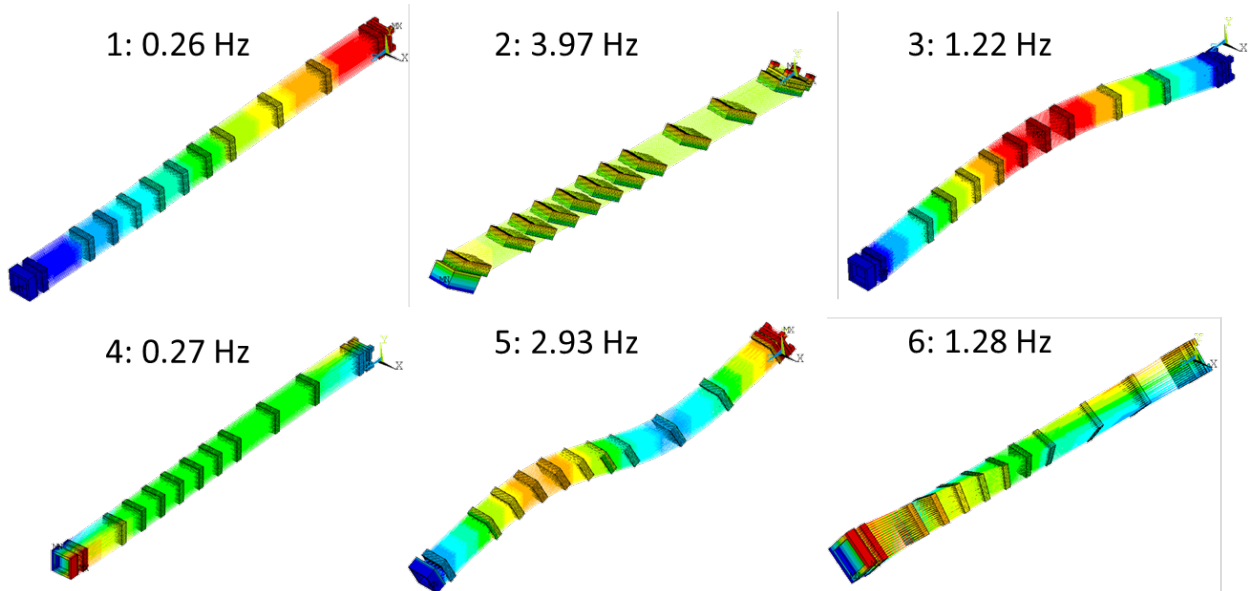


Figure B.13. The Six Mode Shapes with the Largest Vertical Participation Factor for Case 9, Rev 1

B-1.4 Modeling of Rod Material Elements: Rev 1 – Case 1 vs. Case 11

Another modeling choice that could alter the dynamic behavior of the assembly is the use of a single layer of beam elements for each rod with a density adjustment or the use of overlapping beam elements for each rod with no density adjustment. The latter case would have a stiffer overall rod while still having the correct overall rod weight. The overlapping beams share degrees of freedom so the model does not get significantly bigger; the number of equations to solve remains the same but there are more element calculations. To evaluate the effect of this modeling choice Case 1 (single layer of beam elements) and Case 11 (overlapping beam elements) are compared.

Figure B.14 and Figure B.15 show the scaled vertical participation factor and the vertical cumulative mass fraction respectively, for Cases 1 and 11. The figures focus on 0 Hz to 30 Hz since there are no significant modes beyond 30 Hz for these cases. These figures show that there is a difference between the two modeling choices but the effect is relatively minor, particularly below 5 Hz. The most significant modes for both Case 1 and Case 11 all are below 5 Hz. Case 1 and Case 11 both show some less significant modes between 10 Hz and 15 Hz.

Figure B.16 shows the six mode shapes with the largest vertical participation factor for Case 11. These mode shapes are very similar to those shown in Figure B.7 for Case 1 with the exception of a lack of the expansion mode shape found for Case 1.

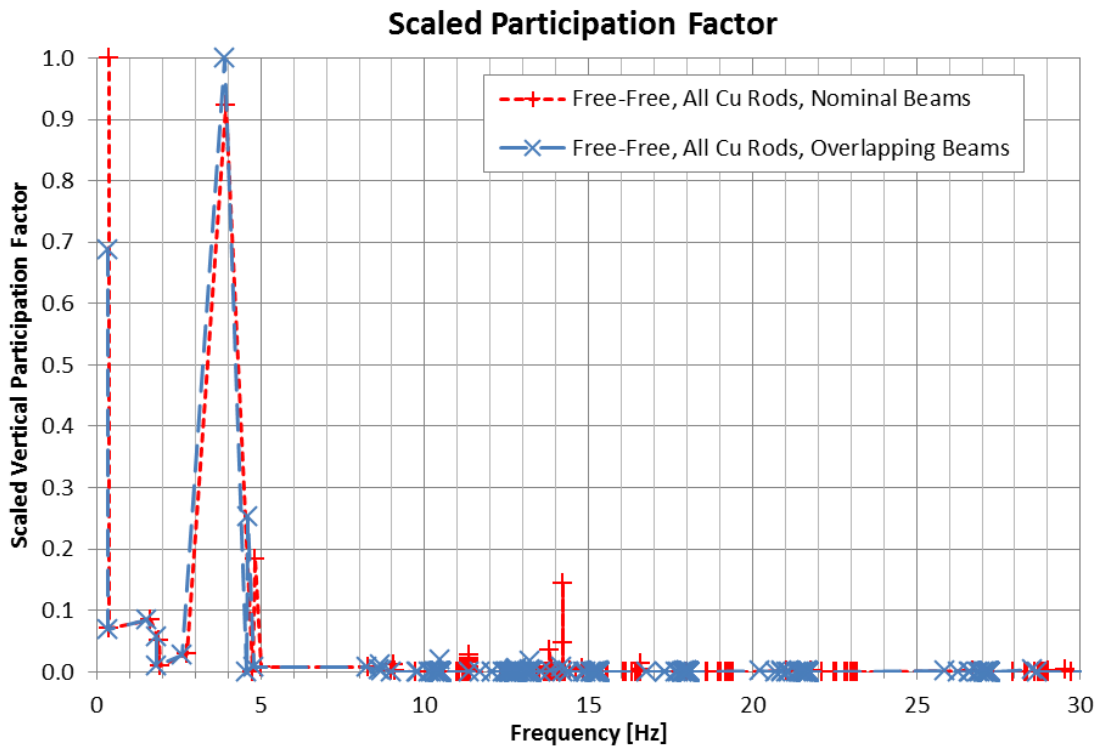


Figure B.14. Scaled Vertical Participation Factor for Cases 1 and 11, Rev 1

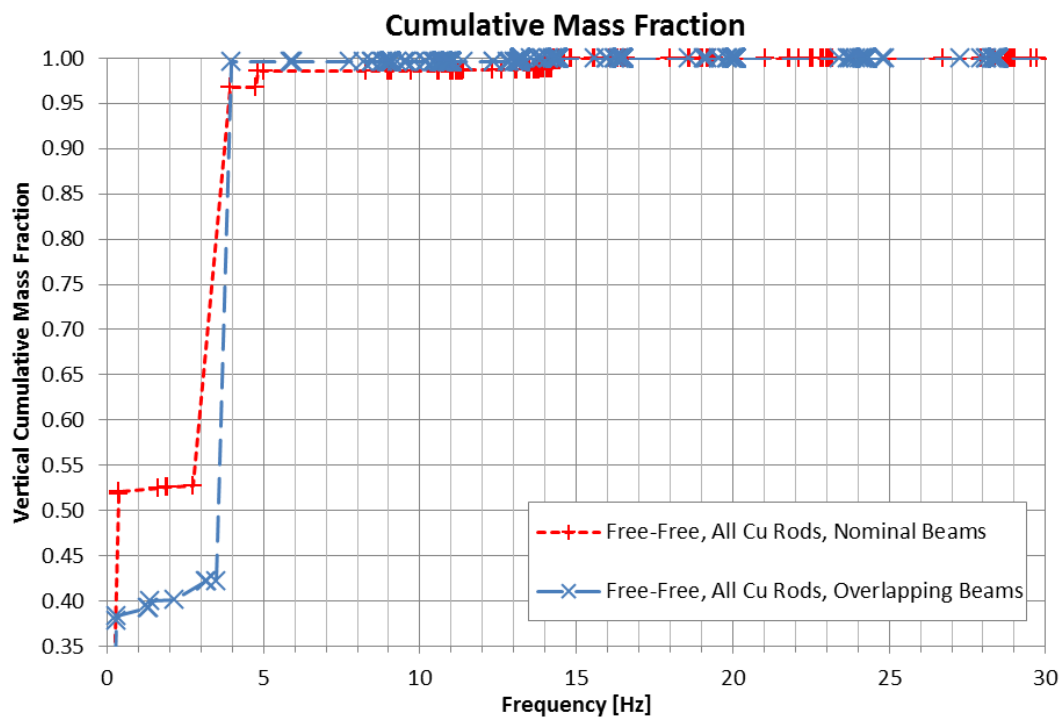


Figure B.15. Vertical Cumulative Mass Fraction for Cases 1 and 11, Rev 1

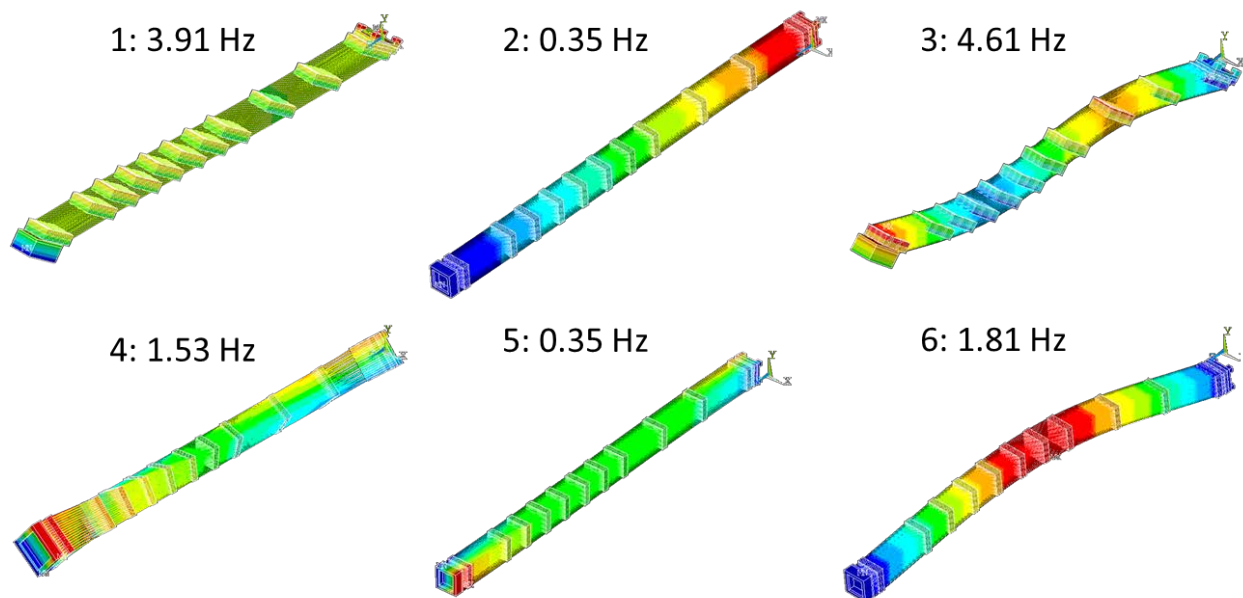


Figure B.16. The Six Mode Shapes with the largest Vertical Participation Factor for Case 11, Rev 1

B-1.5 Axial Spring Sensitivity: Rev 1 – Cases 5, 6, 13, and 14

The axial springs that connect the fuel rods to the spacer grids may alter the dynamic response. To determine the effect the spring stiffness has on the natural frequencies and mode shapes, the results of Cases 5, 6, 13, and 14 are compared. Case 5 is all Zircaloy-4 rods with free boundary conditions and nominal axial springs. Case 13 is all Zircaloy-4 rods with free boundary conditions and axial springs that are 100 times stiffer than the nominal case; Case 13 is best compared to Case 5. Case 6 is all Zircaloy-4 rods with fixed boundary conditions and nominal axial springs. Case 14 is all Zircaloy-4 rods with fixed boundary conditions and axial springs that are 100 times stiffer than the nominal case; Case 6 is best compared to Case 14.

Figure B.17 and Figure B.18 show the scaled vertical participation factors and the vertical cumulative mass fractions respectively for Cases 5, 6, 13 and 14. In comparing Case 5 and Case 13 it can be seen that the axial spring stiffness has a minor effect on the natural frequencies and mode shapes that are important. Figure B.19 presents the six mode shapes with the largest vertical participation factor for Case 13. These shapes are very similar to those for Case 5 presented in Figure B.11.

In comparing Case 6 and Case 14 from Figure B.20 and Figure B.21, it is seen that the stiffer springs has a significant influence on the frequencies and mode shapes. Case 14, which has the 100 time stiffer axial springs, shows that there are significant mode shapes out to nearly 130 Hz. While Case 6 has significant mode shapes out near 150 Hz, their relative importance is less. It is apparent that the stiffer axial springs in the Fixed-Fixed case tends to create more significant modes at higher frequencies and decrease the significance of lower frequency modes. Figures B.20 and B.21 show the six most significant mode shapes for Case 6 and Case 14 respectively.

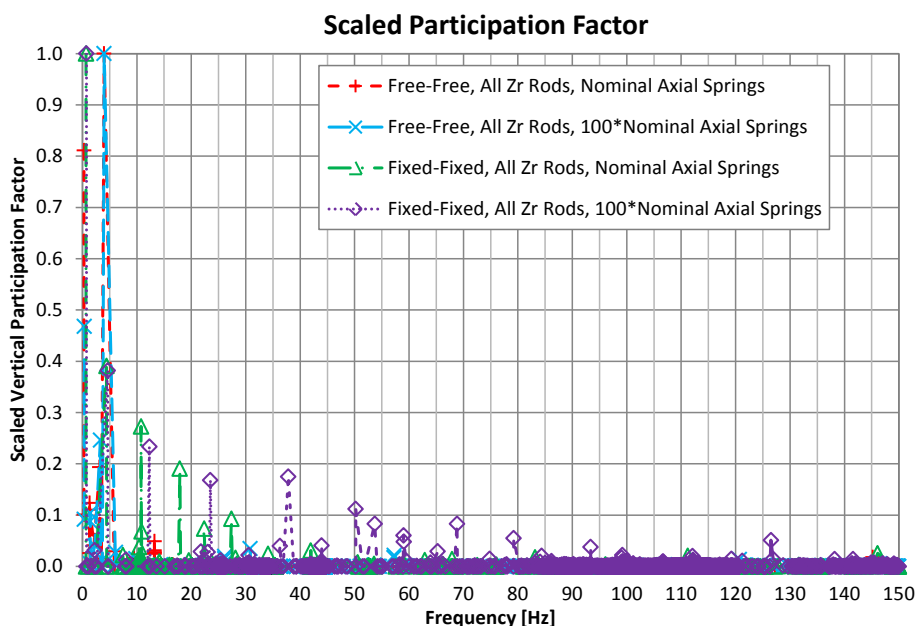


Figure B.17. Scaled Vertical Participation Factor for Cases 5, 6, 13, and 14, Rev 1

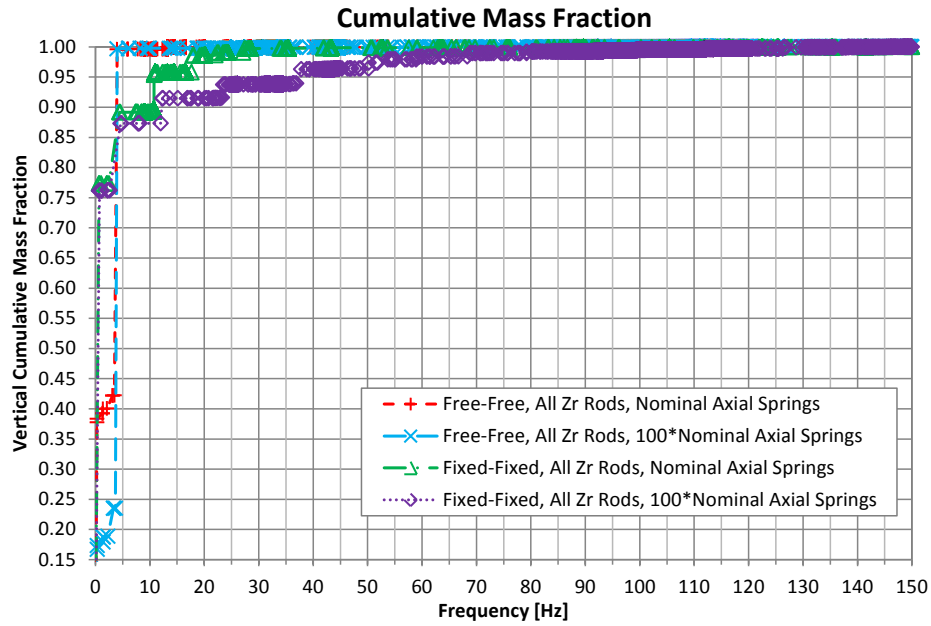


Figure B.18. Vertical Cumulative Mass Fraction for Cases 5, 6, 13, and 14, Rev 1

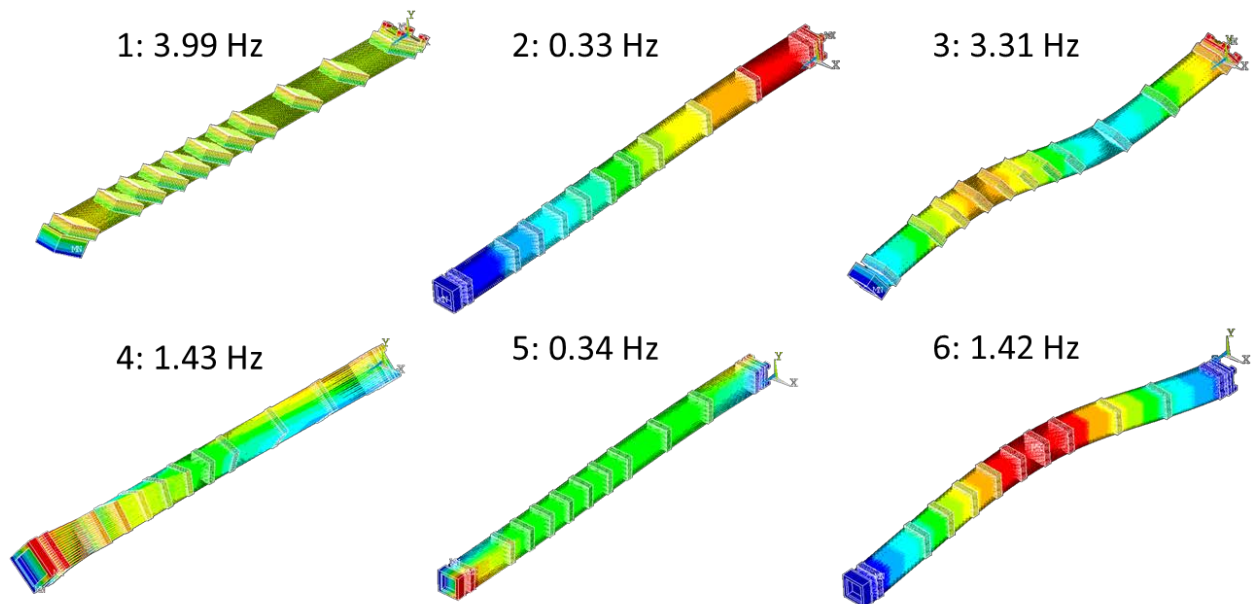


Figure B.19. The Six Mode Shapes with the Largest Vertical Participation Factor for Case 13, Rev 1

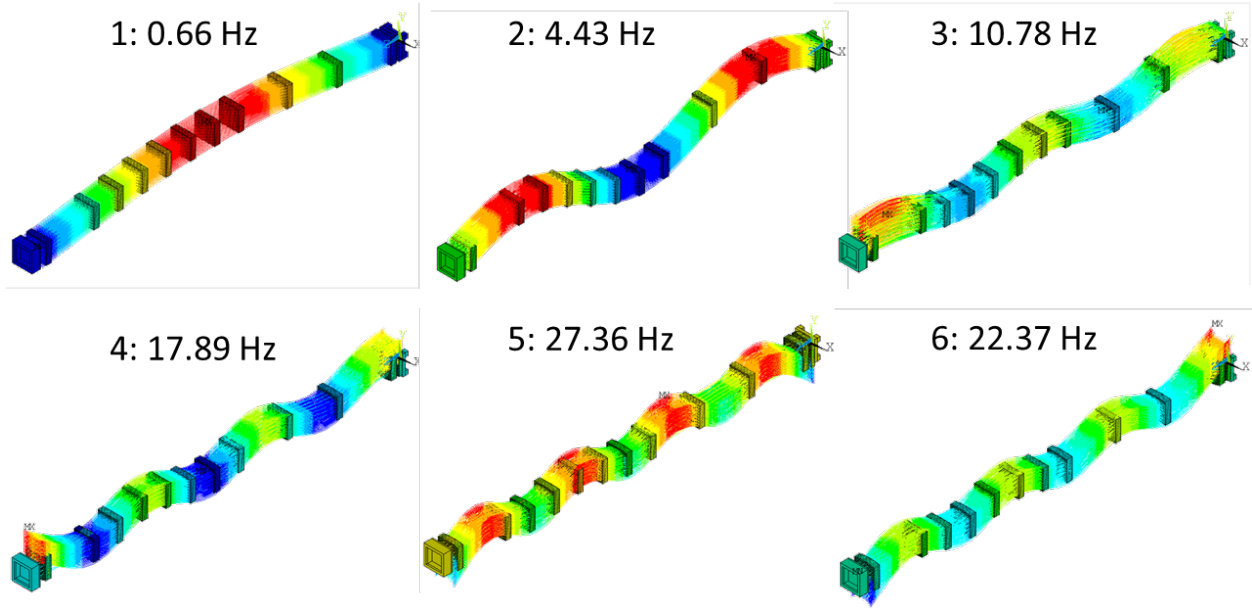


Figure B.20. The Six Mode Shapes with the Largest Vertical Participation Factor for Case 6, Rev 1

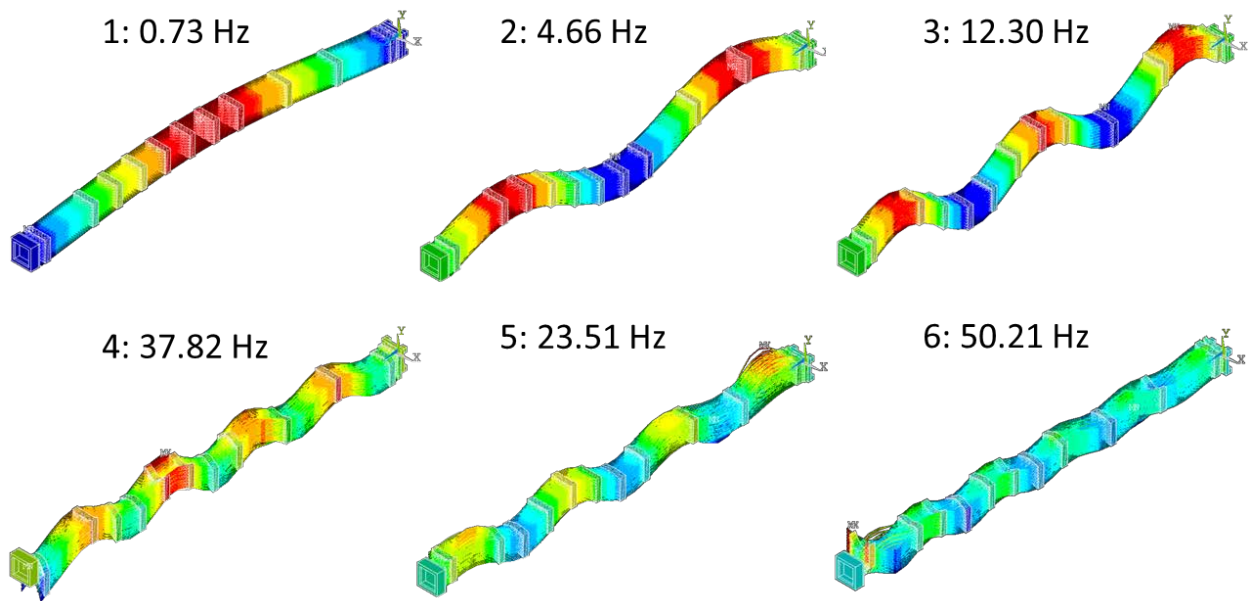


Figure B.21. The Six Mode Shapes with the Largest Vertical Participation Factor for Case 14, Rev 1

B-1.6 Rotational Spring Sensitivity on Copper Rods: Rev 1 – Case 1 vs. Case 15

The presence of rotational springs in addition to the axial springs may alter the dynamic behavior of the assembly. Case 1 and Case 15 are compared below. Case 1 is an assembly with all copper rods, free boundary conditions, and nominal axial springs only. Case 15 is the same as Case 1 with the exception that rotational springs were added in the two transverse directions. The rotational springs were assigned a rotational stiffness of 10,000 N-m/radian.

Figure B.22 and Figure B.23 show the scaled vertical participation factor and the vertical cumulative mass fractions respectively for Cases 1 and 15. These figures show that there is a significant change when the rotational springs are added to the model. Significant mode shapes are found near 64 Hz when the rotational springs are included. Figure B.24 shows the six mode shapes with the largest vertical participation factors for Case 15. Three of the mode shapes have not been seen previously. These mode shapes are all near 64 Hz and some subset of the rods moving in one direction while another subset of the rods moves in another direction. Comparing these mode shapes to those for Case 1 found in Figure B.7 it is seen that these three new mode shapes have replaced a torsional, shear, and expansion mode shape as some of the six most important mode shapes.

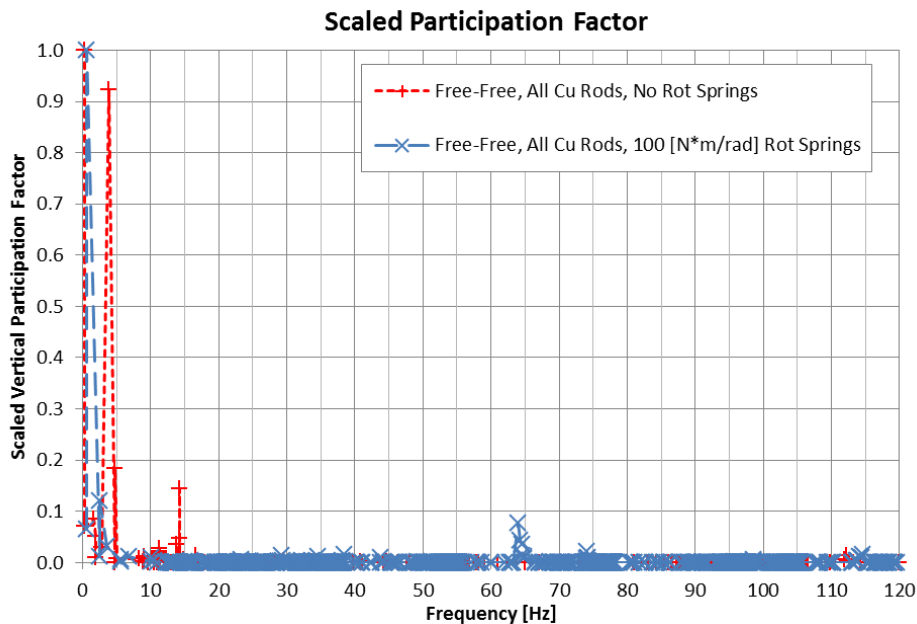


Figure B.22. Scaled Vertical Participation Factor for Cases 1 and 15, Rev 1

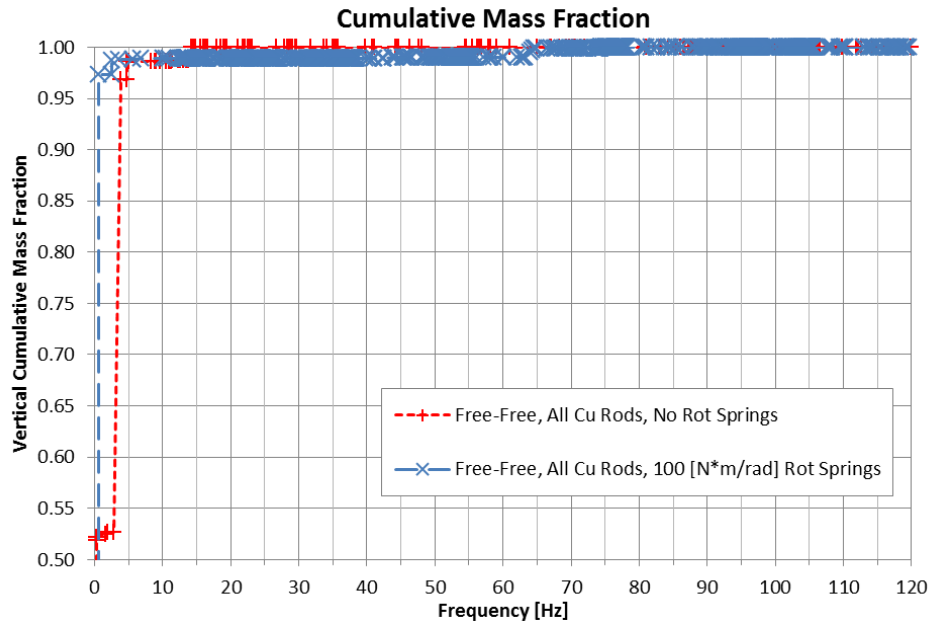


Figure B.23. Vertical Cumulative Mass Fraction for Cases 1 and 15, Rev 1

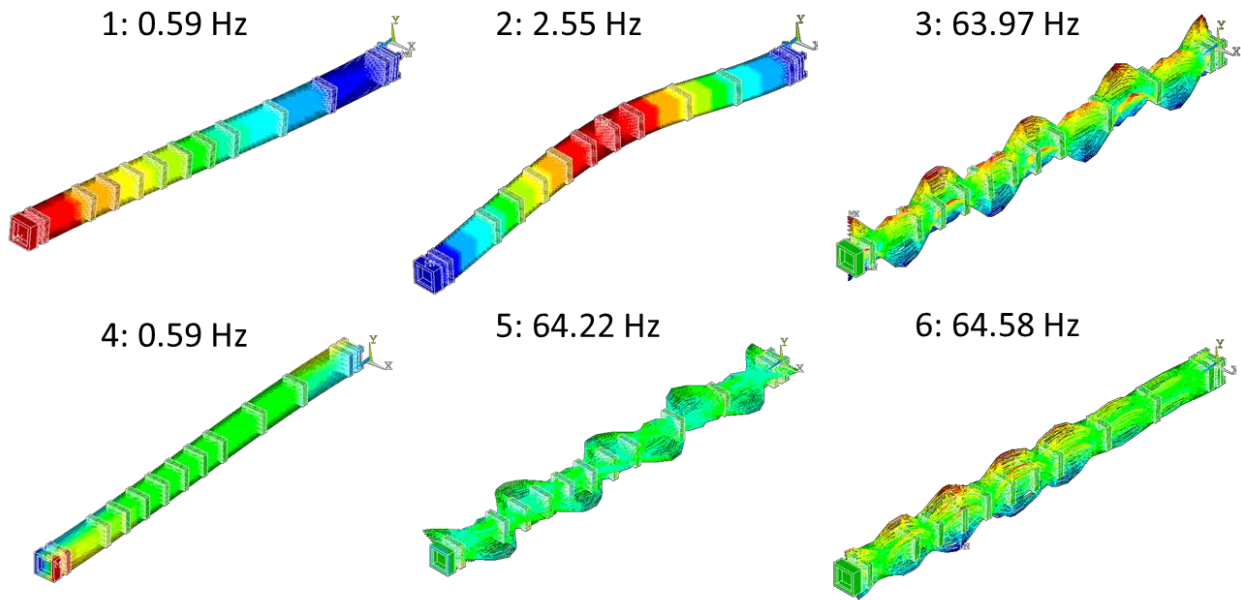


Figure B.24. The Six Mode Shapes with the Largest Vertical Participation Factor for Case 15, Rev 1

B-1.7 Rotational Spring Sensitivity on Zircaloy-4 Rods: Rev 1 – Cases 5, 17, 18, and 19

The effect of the rotational springs is also studied on the Zircaloy-4 rod assemblies. Case 5 consists of an all Zircaloy-4 rod assembly with free boundary conditions and nominal axial springs. Cases 17, 18, and 19 added two rotational springs in the transverse directions at each axial spring. The stiffnesses of the rotational springs were 1 N-m/radian, 100 N-m/radian, and 10,000 N-m/radian for Cases 17, 18, and 19 respectively.

Figure B.25 and Figure B.26 present the scaled vertical participation factors and the vertical cumulative mass fractions respectively for Cases 5, 17, 18, and 19. The presence of the rotational springs alone alters the dynamic response of the assembly. Case 17, with the lowest value of rotational stiffness shows that the rotational springs eliminated a significant mode found around 4 Hz in Case 5. Increasing the rotational springs from 1 N-m/radian (Case 17) to 10 N-m/radian (Case 18) has very little effect on the assembly response. Figure B.27 and Figure B.28 show the six mode shapes with the largest vertical participation factor for Case 17 and 18 respectively. The first five most important mode shapes are nearly identical but the sixth most important mode shape changes from an expansion mode near 9 Hz to a mode with subsets of rods moving in different directions near 35 Hz. Both Case 17 and Case 18 show some same and some different mode shapes than Case 5 (Figure B.11). However, increasing the rotational stiffness to 10,000 N-m/radian (Case 19) makes a significant difference in the natural frequencies and mode shapes of the assembly. Figure B.25 and Figure B.26 indicate that a significant mode is introduced around 10.5 Hz and a less significant mode is introduced around 15.5 Hz. Figure B.29 shows the six mode shapes with the largest vertical participation factors. The second most significant mode shape at 10.48 Hz is markedly different than any previously observed mode shapes.

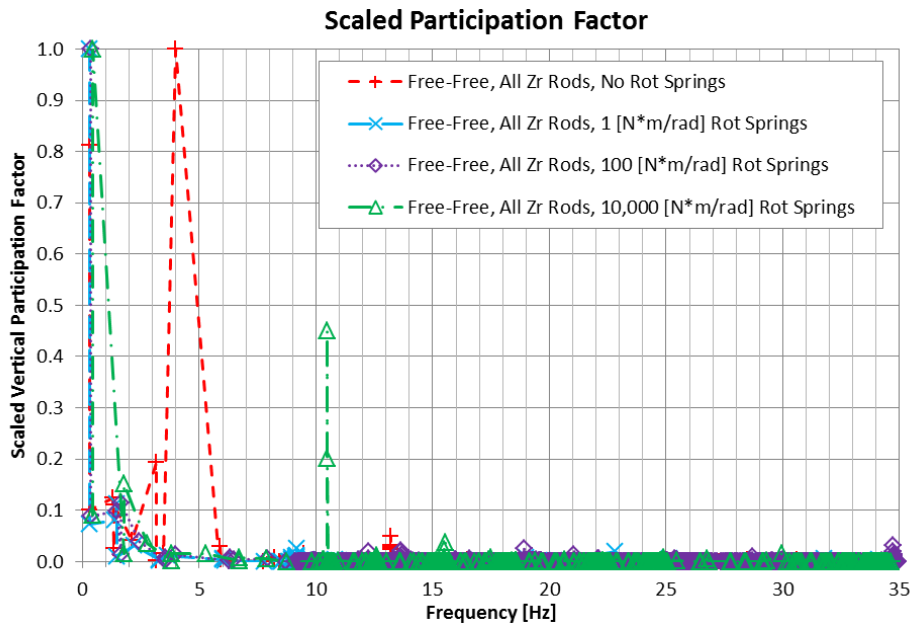


Figure B.25. Scaled Vertical Participation Factor for Cases 5, 17, 18, and 19, Rev 1

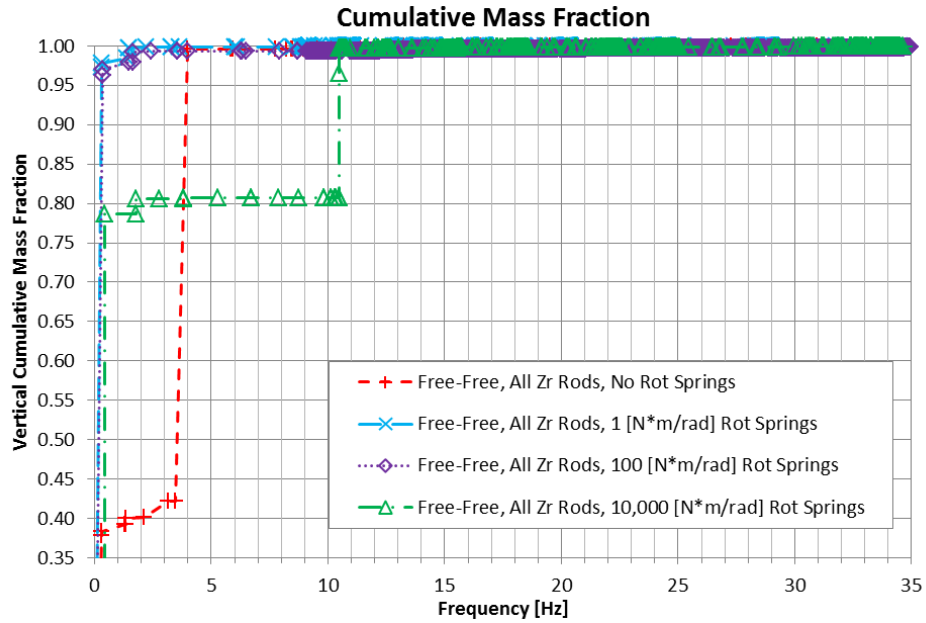


Figure B.26. Vertical Cumulative Mass Fraction for Cases 5, 17, 18, and 19, Rev 1

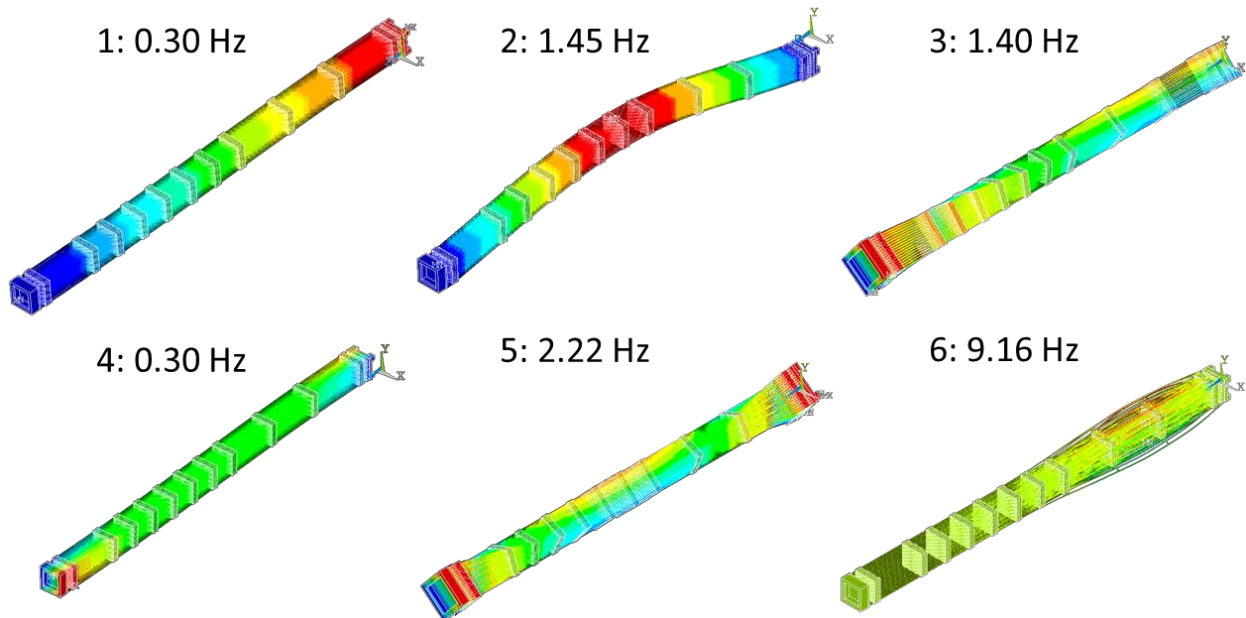


Figure B.27. The Six Mode Shapes with the Largest Vertical Participation Factor for Case 17, Rev 1

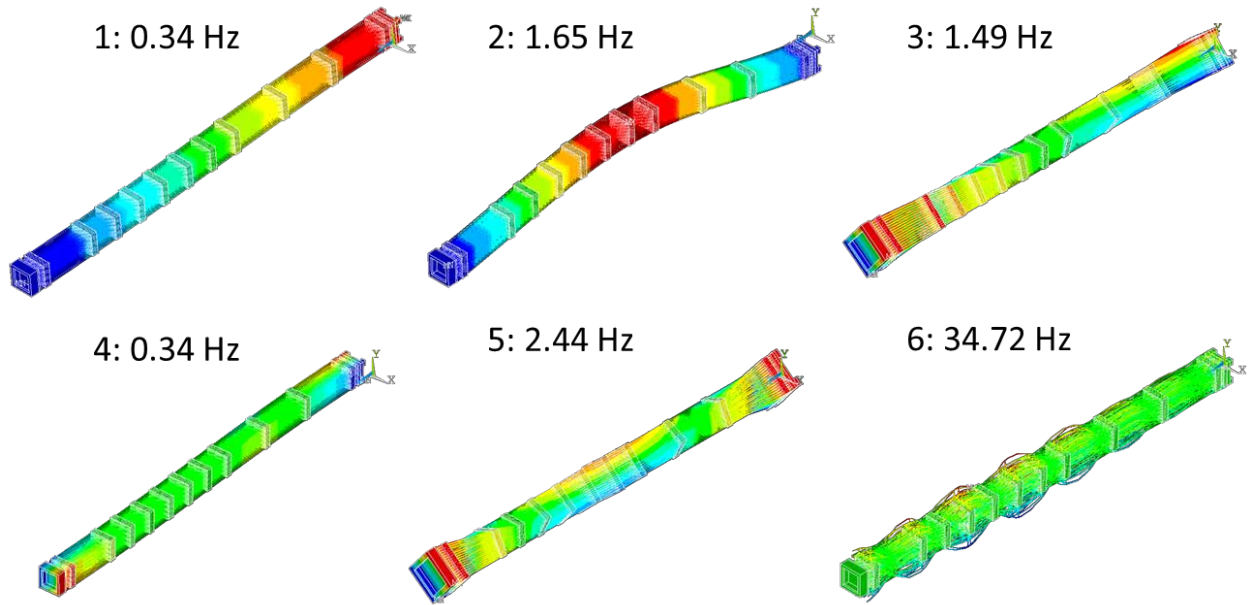


Figure B.28. The Six Mode Shapes with the Largest Vertical Participation Factor for Case 18, Rev 1

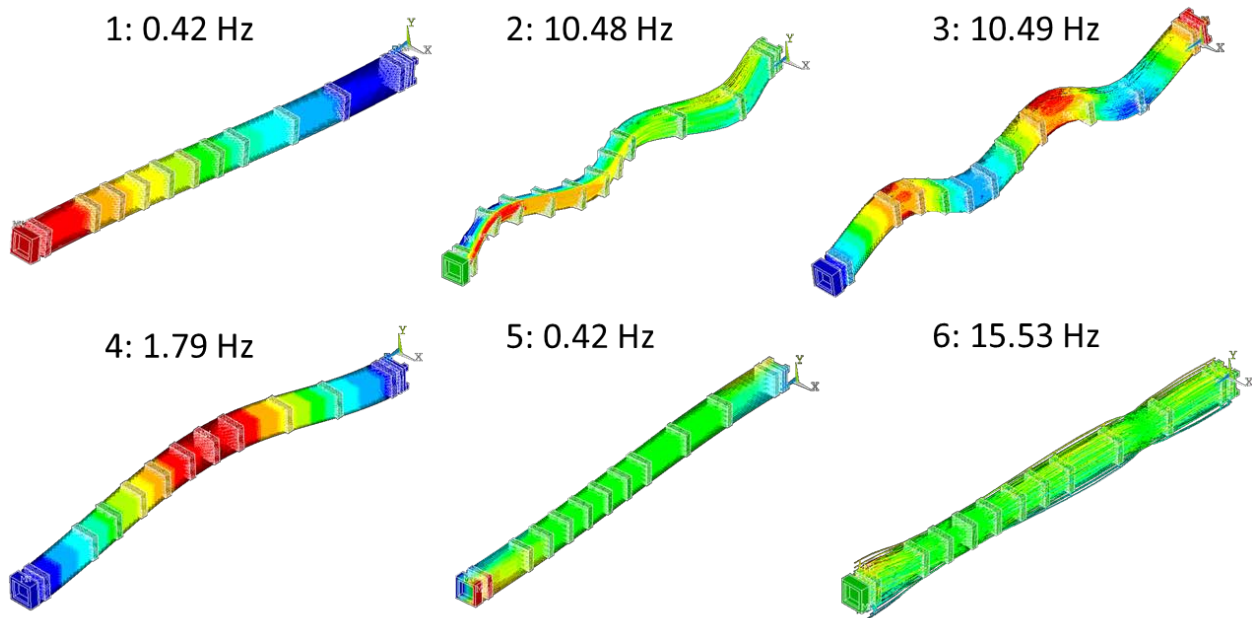


Figure B.29. The Six Mode Shapes with the Largest Vertical Participation Factor for Case 19, Rev 1

B-1.8 Fixed and Free Boundary Conditions with Rotational Springs: Rev 1 – Cases 5, 18, and 20

The response of the assembly because of changing the boundary conditions with rotational springs as well is studied by comparing Cases 18 and 20. Case 18 is an all Zircaloy-4 assembly with nominal axial springs and 100 N-m/radian rotational springs with Free-Free boundary conditions. Case 20 is an all Zircaloy-4 assembly with nominal axial springs and 100 N-m/radian rotational springs with Fixed-Fixed boundary conditions. Case 5 is included in this comparison as a reference for the Free-Free boundary condition Zircaloy-4 assembly without rotational springs.

Figure B.30 and Figure B.31 show the scaled vertical participation factors and the vertical cumulative mass fraction respectively for Cases 5, 18, and 20. Though Cases 18 and 20 have the same rotational springs, they differ significantly because of the difference in boundary conditions. This illustrates that the boundary conditions are a more important parameter than the rotational springs, at least at a rotational stiffness value of 100 N-m/radians. As demonstrated in the other Fixed-Fixed cases, Case 20 shows significant mode shaped intermittently out to around 43 Hz. Figure B.32 shows the six mode shapes with the largest vertical participation factors for Case 20.

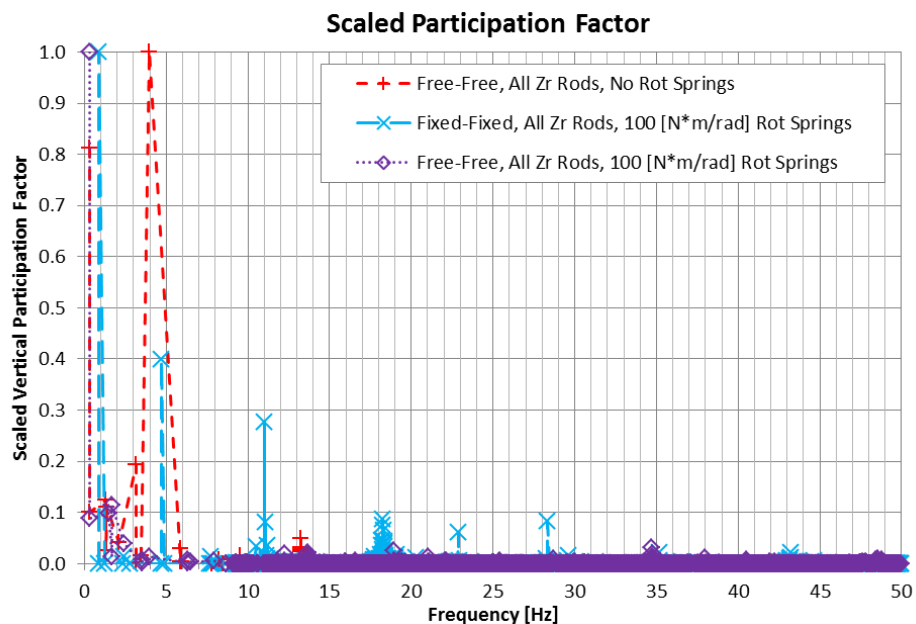


Figure B.30. Scaled Vertical Participation Factor for Cases 5, 18, and 20, Rev 1

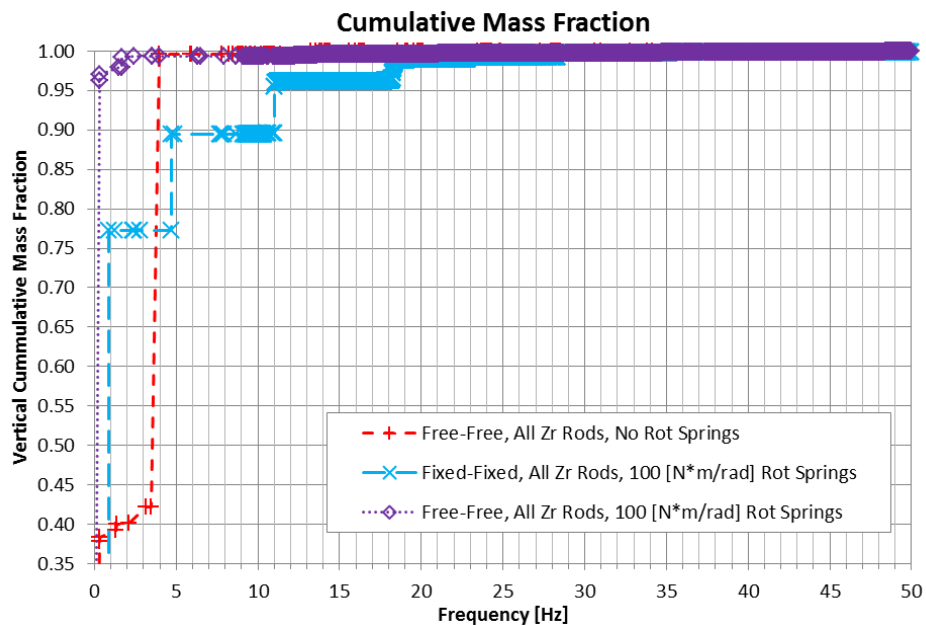


Figure B.31. Vertical Cumulative Mass Fraction for Cases 5, 18, and 20, Rev 1

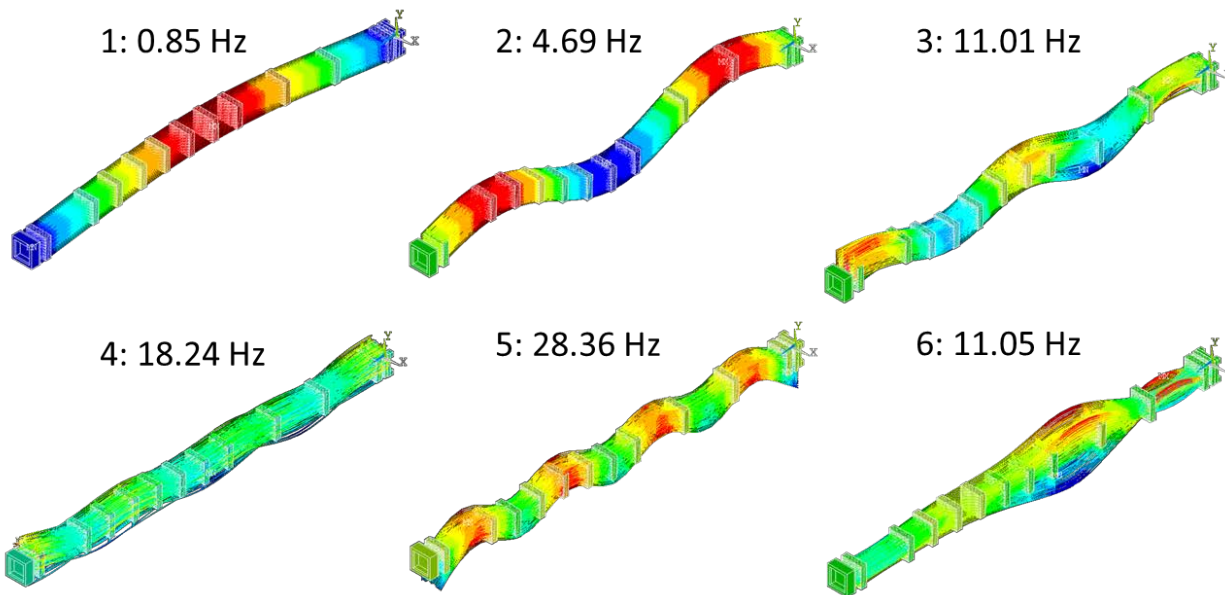


Figure B.32. The Six Mode Shapes with the Largest Vertical Participation Factor for Case 20, Rev 1

B-1.9 Conclusion from the Rev 1 Modal Analysis Sensitivity Studies

Based on the comparisons of the Rev 1 Cases listed in Table B.1, the following conclusions are reached from the modal analysis of the assembly:

- All cases showed that significant mode shapes occur below 5 Hz.
- The boundary conditions significantly affect the natural frequencies and mode shapes. The assembly on the shaker table configuration is neither Fixed-Fixed nor Free-Free as analyzed here, but will come in and out of contact with the basket at various locations throughout the assembly depending on the loading and response.
- Generally, the material of the rods has a minor influence on the most significant natural frequencies and mode shapes of the assembly.
- The choice to model the rod as a single beam with density adjusted or overlapping beams has relatively minor effect, particularly below 5 Hz. At higher frequencies the difference is greater but the relative importance of these frequencies is less.
- It is apparent that the stiffer axial springs in the Fixed-Fixed case tends to create more significant modes at higher frequencies and decrease the significance of lower-frequency modes.
- There is a significant change when the rotational springs are added to the model. Significant mode shapes are found clustered at a higher frequency.
- The presence of the rotational springs alone alters the dynamic response of the assembly. The response is not very sensitive to rotational spring stiffness changes in the range from 1 to 100 N-m/radians, but is very sensitive to stiffness changes in the range from 100 N-m/radians to 10,000 N-m/radians.

The boundary conditions are a more important parameter than the rotational springs, at least at a rotational stiffness value of 100 N-m/radians.

B-2. Rev 2 Modal Analyses

Modifications were made to the Rev 1 assembly model to bring the static behavior more in line with existing experimental data. These modifications include changing the spot welds between the guide tubes and the spacer grids and extending the guide tubes into the end cap plates to increase the rotational stiffness. The modifications are described in Section 2.3 in the body of this report. Since Rev 2 is the final configuration used for the full dynamic shaker table runs four more modal analysis cases were run to see the dynamic behavior of this configuration. Table B.2 lists these four cases (Cases 21-24).

Cases 21 (Free-Free) and Case 22 (Fixed-Fixed) are the Rev 2 model with all nominal Zircaloy-4 rods. Cases 23 (Fixed-Fixed) and 24 (Free-Free) are the Rev 2 model with most copper rods and three Zircaloy-4 rods—the actual shaker table configuration. Figures B.33 and B.34 present the scaled vertical participation factors and the vertical cumulative mass fractions, respectively, for these four cases. These figures show that unlike the Rev 1 model, the Free-Free cases have some significant modes out to nearly 150 Hz. However, the most significant modes are in the range from 0 Hz to 21 Hz. The cumulative mass fractions show that there still exists a significant difference between the Free-Free cases and the Fixed-

Fixed cases. Additionally, the switch from all Zircaloy-4 rods to mostly copper rods has a small effect on the natural frequencies, though not as great as the boundary conditions.

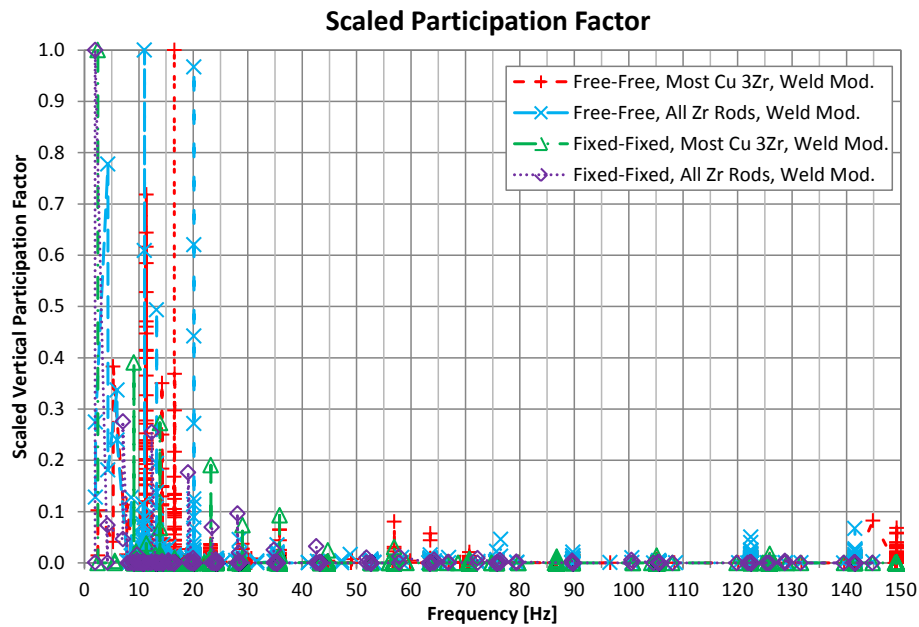


Figure B.33. Scaled Vertical Participation Factor for Cases 21, 22, 23, and 24, Rev 2

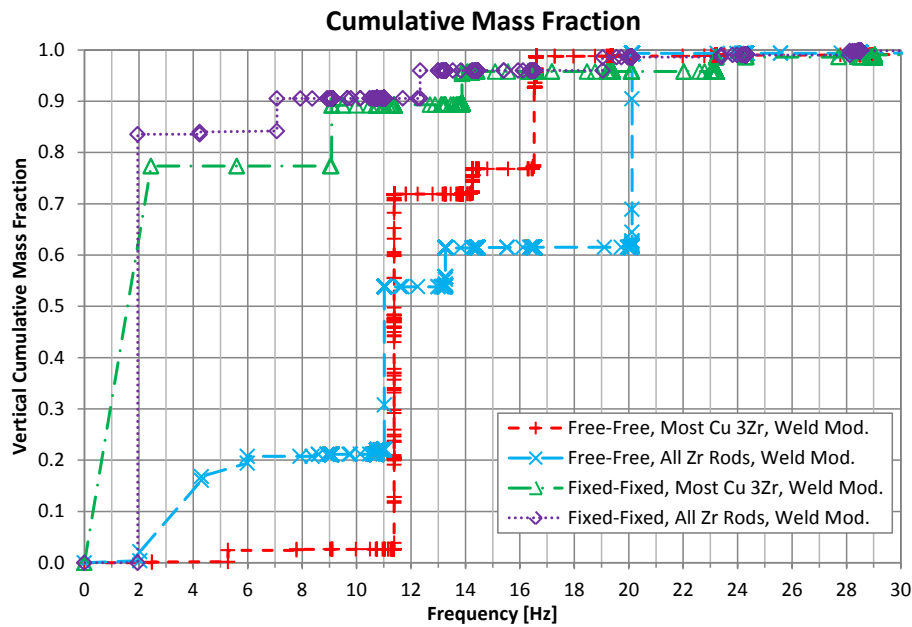


Figure B.34. Vertical Cumulative Mass Fraction for Cases 21, 22, 23, and 24, Rev 2

Figures B.35, B.36, and B.37 show the six modes shapes with the largest vertical participation factor for Cases 21, 22, and 23 respectively. Figure B.38 shows some of the first twelve mode shapes with the largest vertical participation factor for Case 24; there are several repeating mode shapes at 11.38 Hz with large participation factors that are not shown here. The most significant finding from all four of these cases is that they have shifted the frequency of the mode shape in which there is vertical deformation of the entire assembly with one peak in the middle (i.e., the third mode shape shown in Figure B.35).

For example, Figure B.38 shows that for Case 24 (Rev 2, Free-Free with mostly copper rods) this mode is at 5.28 Hz. In Case 3 (Rev 1, Free-Free with mostly copper rods) this mode is at 1.90 Hz as shown in Figure B.3. Another is example is a comparison of Case 23 (Rev 2, Fixed-Fixed with mostly copper rods) and Case 4 (Rev 1, Fixed-Fixed with mostly copper rods). This mode is at 2.45 Hz for Case 23 as shown in Figure B.37 and at 0.95 Hz for Case 4 as shown in Figure B.4. While this shift shows a fundamental difference between the Rev 1 and Rev 2 models, the Rev 2 cases still show that there are important modes between 0 and 5 Hz that must be considered.

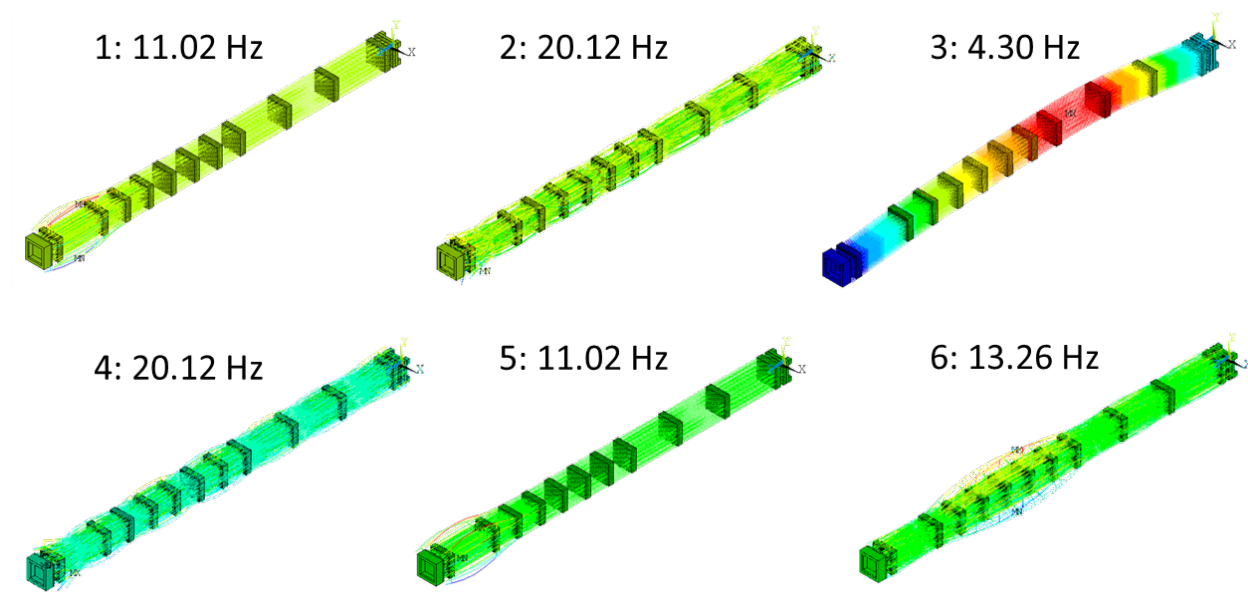


Figure B.35. The Six Mode Shapes with the Largest Vertical Participation Factor for Case 21, Rev 2

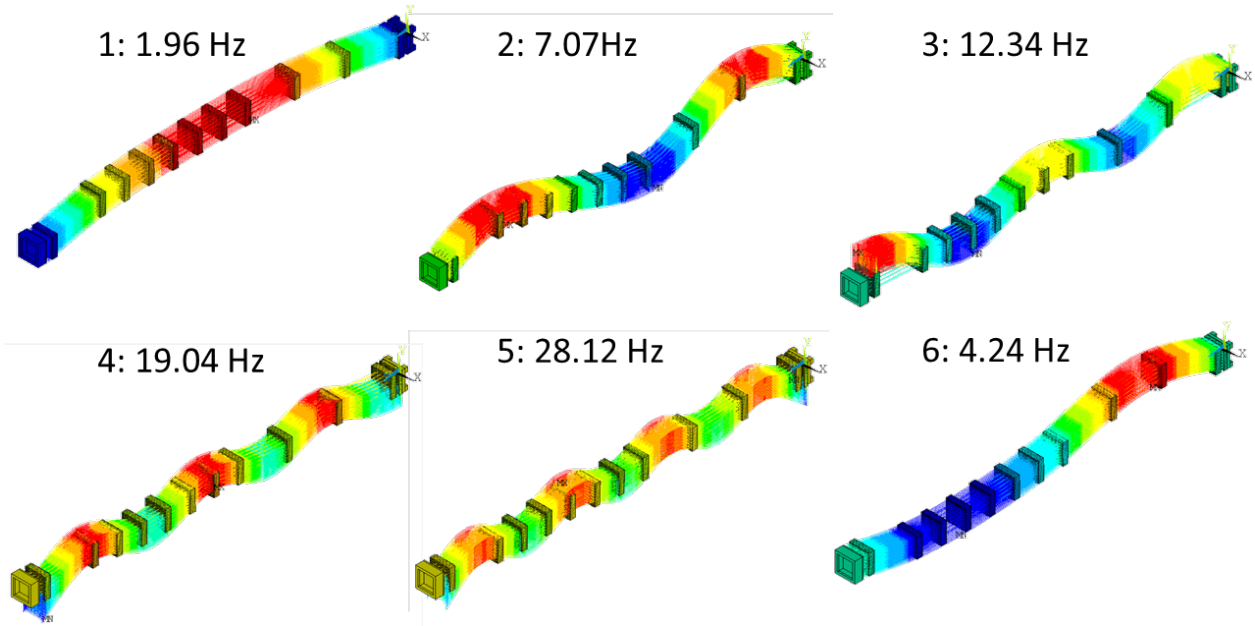


Figure B.36. The Six Mode Shapes with the Largest Vertical Participation Factor for Case 22, Rev 2

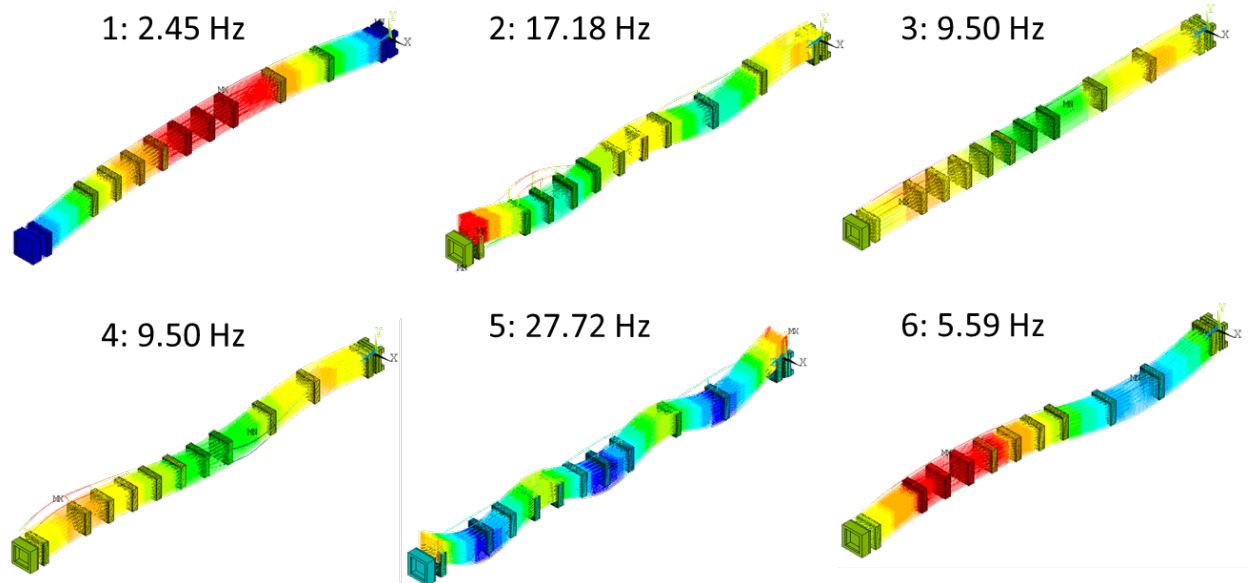


Figure B.37. The Six Mode Shapes with the Largest Vertical Participation Factor for Case 23, Rev 2

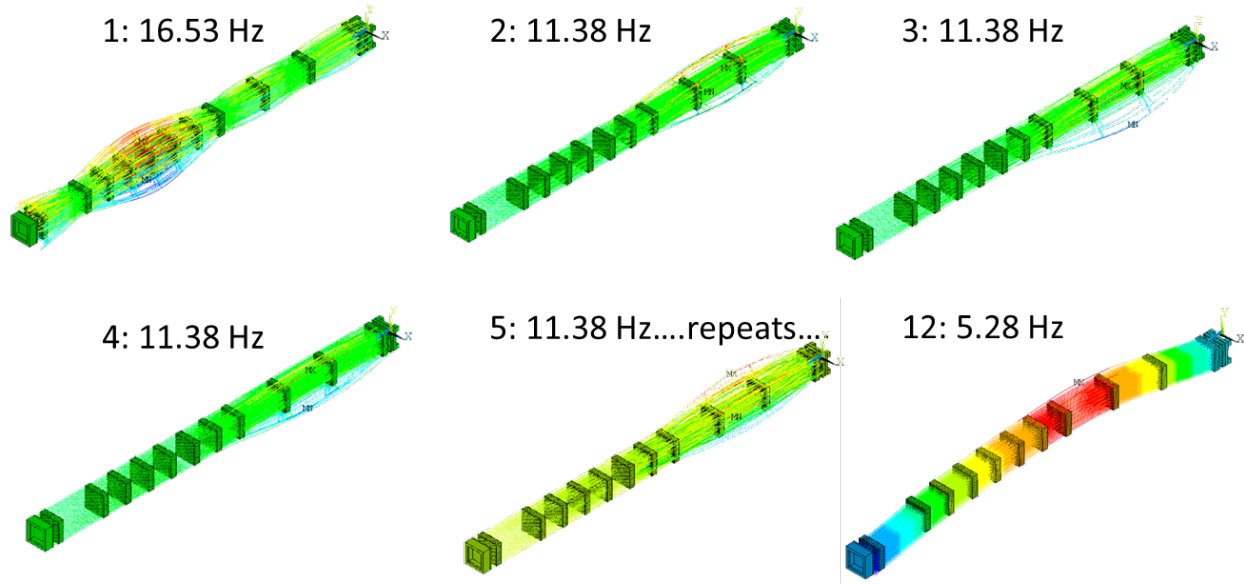


Figure B.38. Some of the Mode Shapes with the Largest Vertical Participation Factor for Case 24, Rev 2

B-3. Static Behavior

The static response of the assembly was evaluated using the implicit ANSYS model created for the modal analyses presented above. The ends of the assembly, at the edges of the end caps, were fixed in all six degrees of freedom. A 30 kgf load was applied as a pressure distributed on one external face of the sixth grid from the bottom (see Figure B.39). This configuration was evaluated using static analysis in the ANSYS implicit environment. No contact was included in this analysis so the results only hold for infinitesimal deformations; the resulting deformations were small so the lack of contact is not an issue.

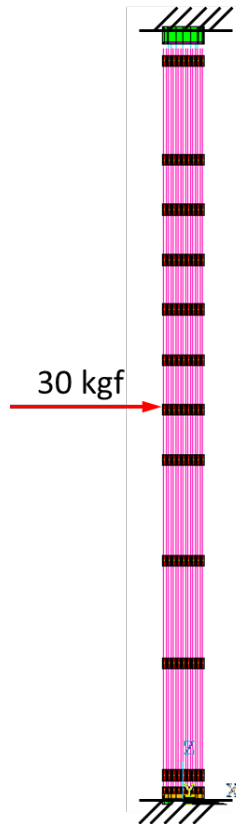


Figure B.39. Static Assembly Test Boundary Conditions

As with the modal analysis, the static response was checked under different materials (copper and Zircaloy-4, different modeling choices for the beams (adjusted density and overlapping beams), and different combinations of axial and rotational spring stiffness that connect the rods to the spacer grids. Each case present always has the same spacer grids, end caps, and control rod materials. The results of the various cases are presented as the displacements measured at the end caps and spacer grids along the length of the assembly.

B-1.10 Rev 1 Static Results

Figure B.40 shows the displacements (x-axis) along the length of the assembly (z-axis) for: 1) an assembly consisting of all-copper rods with the density adjusted to account for the lead; 2) an assembly consisting of all-copper rods with the lead modeled as overlapping beams; and 3) an assembly consisting of all-Zircaloy-4 rods with the density adjusted for the fuel. It can be seen, as expected the displacement is greatest where the 30 kgf is applied. Additionally, the Zircaloy-4 assembly is the least stiff of all these cases with a peak displacement of 27.2 cm. The copper rods with overlapping beams case is slightly stiffer than the density adjusted copper rods case as expected; this is much less than the change in stiffness because of switching to Zircaloy-4 rods from copper rods. The peak displacements of these cases are 23.5 cm for the density adjusted case, and 23.0 cm for the overlapping case.

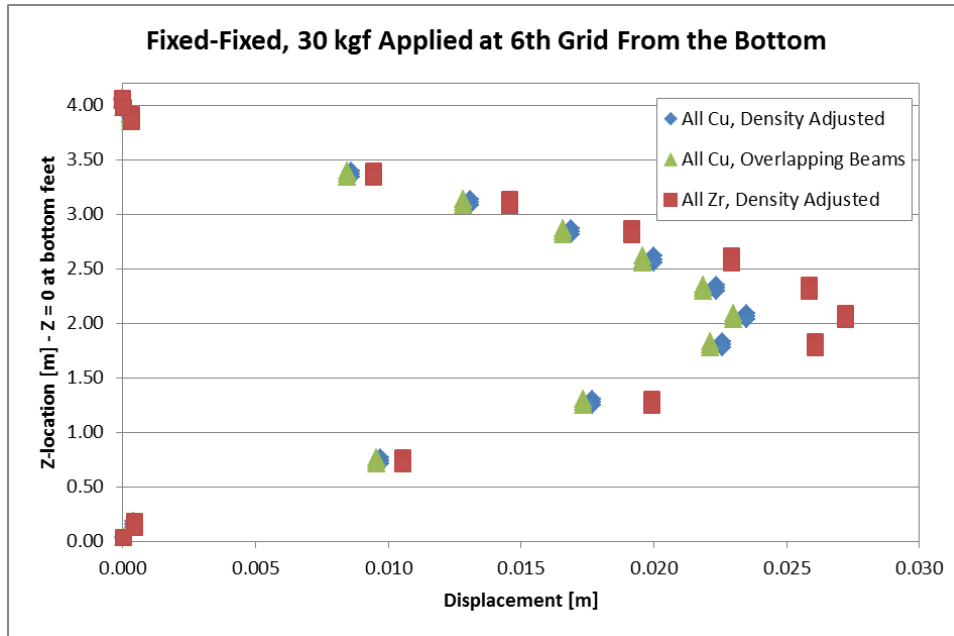


Figure B.40. Displacement Along the Length of the Assembly for the Static Load Tests of all Copper with Density Adjusted, all Copper with Overlapping Beams, and all Zircaloy-4 with the Density Adjusted

Figure B.41 compares the static assembly response for Zircaloy-4 rods with: 1) nominal axial springs only; 2) nominal axial springs and 1 N-m/radian stiff rotational springs; 3) nominal axial springs and 100 N-m/radian stiff rotational springs; and 4) nominal axial springs and 10,000 N-m/radian stiff rotational springs. It is found that increasing the rotational spring stiffness monotonically increases the stiffness of the assembly. In the most compliant case, no rotational springs, the peak displacement is 27.2 cm. In the stiffest case, rotational spring stiffness of 10,000 N-m/radian, the peak displacement is 20.4 cm.

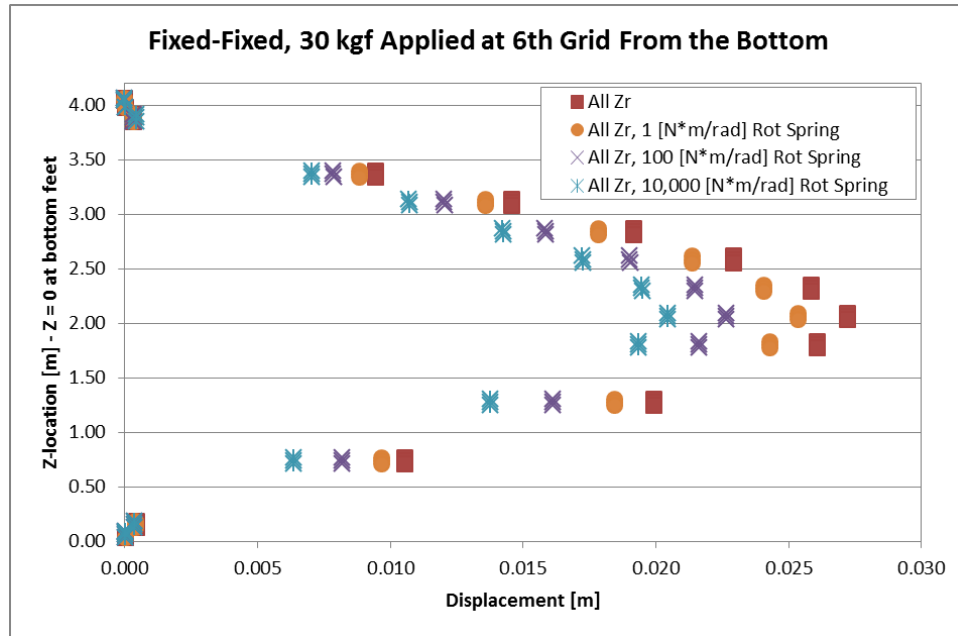


Figure B.41. Displacement Along the Length of the Assembly for the Static Load Test Varying the Rotational Spring Stiffness for a Zircaloy-4 Assembly

Finally, it was noted that compared to an assembly model and experiments studied by Preumont et al. (1982), this model was an order of magnitude softer than their data (near 2 mm instead of the 2 cm found here). Several more sensitivity studies were run, with various combinations of rotational and axial spring stiffnesses to determine if the peak displacements could be brought into the 2 mm range.

Figure B.42 shows the assembly displacements for various combinations of the rotational and axial spring stiffness values. All Zircaloy-4 rods are used. The all-Zircaloy-4 case with nominal axial springs is shown for comparison. The four other cases shown are: 1) 100 [N-m/radian] stiff rotational springs with 100 times the nominal axial spring stiffness; 2) 100 [N-m/radian] stiff rotational springs with 10^6 times the nominal axial spring stiffness; 3) 10^6 [N-m/radian] stiff rotational springs with 100 times the nominal axial spring stiffness; and 4) 10^9 [N-m/radian] stiff rotational springs with 100 times the nominal axial spring stiffness. It appears that increase the stiffness of the rotational springs and/or the axial springs leads to a limiting peak displacement of 19.9 cm.

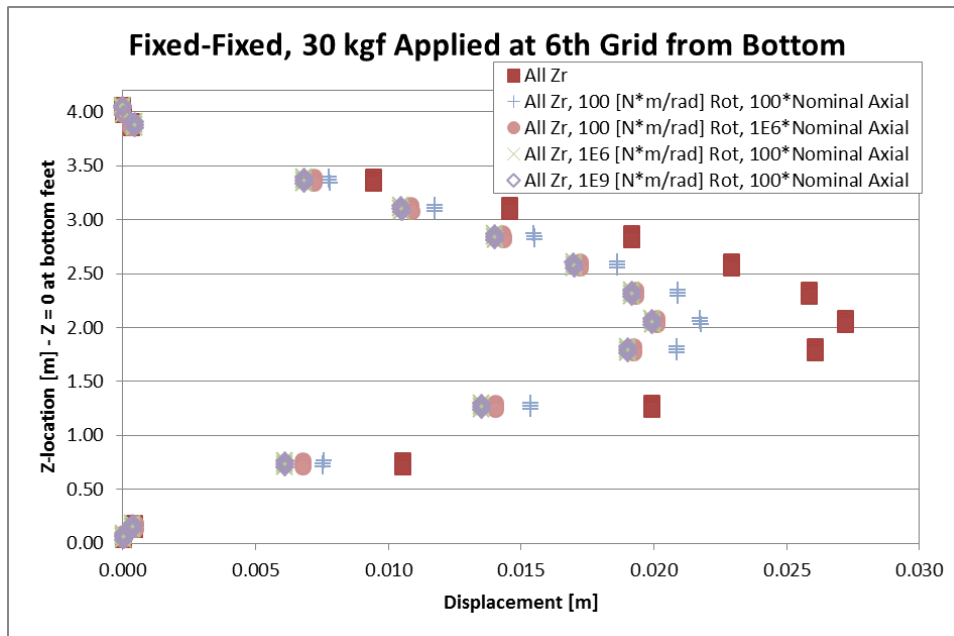


Figure B.42. Displacement along the Length of the Assembly for the Static Load Test Varying the Rotational Spring Stiffness and Axial Spring Stiffness for a Zircaloy-4 Assembly

Evidentially, increasing the stiffness properties of the axial and/or rotational springs connecting the fuel rods to the spacer grids will never bring the static deflection of the assembly into the range of experimental data. This prompted a modification to the connections between the guide tubes and the spacer grids and the guide tubes and the end caps. These modifications were the basis for the Rev 2 assembly model.

B-1.11 Rev 2 Static Results

Based on the Rev 1 static model results (presented above) it was determined that increasing the stiffness properties of the axial and/or rotational springs linking the fuel rods to the spacer grids would never increase the overall assembly stiffness enough to bring the static behavior in the range of experimental results. Examination of the deformed shape of the static model indicated that the connections between the guide tubes and the spacer grids and the guide tube and the end caps were likely allowing too much rotation. For each guide tube at each spacer grid, the Rev 1 model only had a single node to single node spot weld. The Rev 2 model changed this spot weld to group the four nodes on each side of the guide tube for each of the three rows of nodes per spacer grid; i.e., a total of 12 spacer grid nodes were welded to a total of 3 guide tube nodes. In addition to this spot-weld modification, the guide tubes were also extended into the end cap plates to overcome the lack of rotational resistance at the guide tube-end cap connection. This extended portion of the guide tubes shared nodes with the plate meaning, that however the end cap plates rotated the guide tubes would essentially rotate the same.

After these Rev 2 modifications were made, the static load test was performed on an all nominal Zircaloy-4 assembly. The maximum displacement was found to be about 4.5 mm, which is in the range of the experimental data presented in Preumont et al. (1982). Next, a sensitivity study was performed on this all Zircaloy-4 assembly to determine the sensitivity of the displacements to the number elements used

to mesh the fuel rods. It was found that increasing number of elements per rod from 56, to 84, and then to 134 had a minor effect on the displacement (maximum displacements were 4.5 mm, 4.7 mm, and 4.8 mm respectively) while significantly increasing the run times. Finally, static analysis was rerun with the Rev 2 model using the same assembly setup as the shaker table experiment, most copper rods with three Zircaloy-4 rods. As expected, the slightly stiffer copper resulted in maximum displacements slightly less than those of the all Zircaloy-4 assemblies. The maximum displacement was about 4.3 mm. Figure B.43 shows the displacement profile along the length of the assembly for all four of these Rev 2 static analyses.

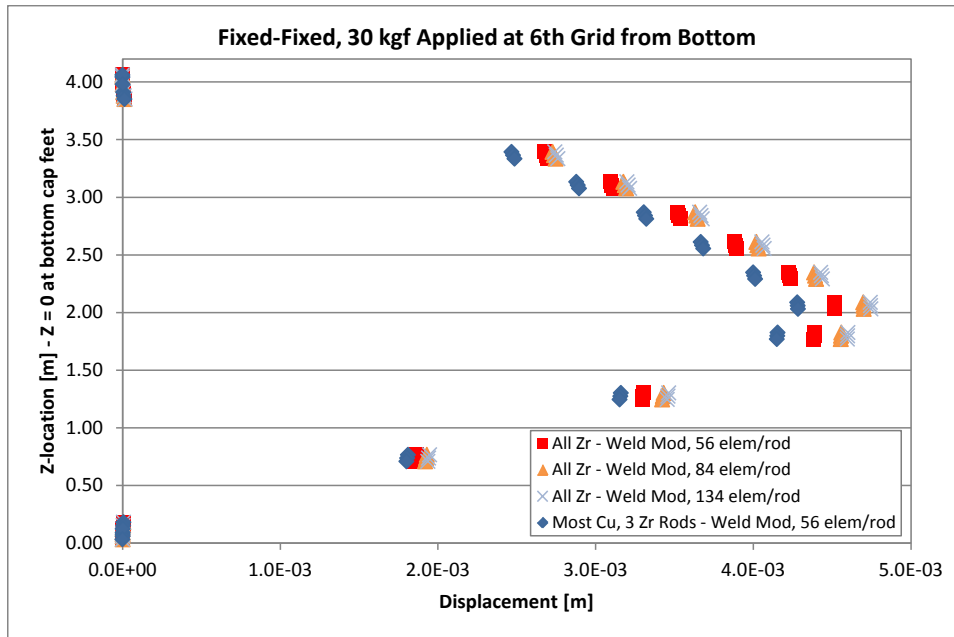


Figure B.43. Displacement along the Length of the Assembly for the Static Load Tests with the Rev 2 Modifications